

**A Study of Two-photon Excitation in Turbid
Media
– Possibilities in Photodynamic Therapy**

Master's Thesis
by
Daniel Karlsson
and
Henrik Nilsson

Lund Reports on Atomic Physics, LRAP-277
Lund September 2001

Abstract

The possibilities and limitations of using two-photon excitation (TPE) in photodynamic therapy (PDT) have been studied. The study has been both theoretical and experimental, with special focus on the behaviour of two-photon excitation in turbid media. Parts of the two-photon absorption (TPA) theory, as well as that of PDT are given. In an experiment, the axial distribution of two-photon induced fluorescence in tissue phantom has been investigated. A considerable amount of publications in the area have also been reviewed. Various aspects of the topic is thoroughly discussed. The conclusions, based on the experiment as well as on the results of others, are that TPE PDT has an advantage of higher selectivity over single-photon excitation (SPE) photodynamic therapy, but that the possibilities to treat thick or deeply localised lesions are very limited for TPE PDT.

Contents

1. Introduction.....	1
2. The theory of two-photon excitation.....	3
2.1. History of two-photon absorption.....	3
2.2. Different types of multi-photon processes.....	4
2.2.1. <i>Stepwise one-photon excitation</i>	4
2.2.2. <i>Raman scattering</i>	5
2.2.3. <i>Simultaneous multi-photon absorption</i>	5
2.2.4. <i>Two-photon emission</i>	6
2.2.5. <i>The two-photon excitation rate</i>	6
3. Photodynamic therapy	11
3.1. Photosensitisers	11
3.1.1. <i>Porphyrins and chlorine</i>	11
3.1.2. <i>Aminolevulinic acid and protoporphyrin</i>	12
3.2. The photochemical reaction.....	13
3.3. Photobleaching and photoproduct formation.....	14
3.3.1. <i>Bleaching process</i>	14
3.4. Two-photon excitation in photodynamic therapy.....	15
4. The path of the light in a TPE PDT system.....	19
4.1. The laser source.....	19
4.2. The optical system.....	19
4.2.1. <i>Dispersion</i>	20
4.2.2. <i>The numerical aperture</i>	22
4.3. Light interaction with tissue	23
4.3.1. <i>Scattering in tissue</i>	23
4.3.2. <i>Absorption in tissue</i>	25
4.3.3. <i>Pulse-length dependence of photodamage</i>	26
5. Experiments	29
5.1. A study of the variation of two-photon induced fluorescence as a function of depth in tissue phantoms	29
5.1.1. <i>Setup and materials</i>	30
5.1.2. <i>Tissue phantom preparation</i>	32
5.1.3. <i>Measurement procedure</i>	32
5.1.4. <i>Results</i>	33
5.2. A study of the variation of single-photon induced fluorescence as a function of depth in tissue phantoms	34
5.2.1. <i>Experimental setup</i>	34
5.2.2. <i>Measurement procedure</i>	34
5.2.3. <i>Results</i>	34
5.3. Measurement of optical constants in the tissue phantom mixtures	35
5.4. Experimental analysis and discussion.....	36
5.4.1. <i>Analysis of the two-photon excitation induced curve</i>	36
5.4.2. <i>Analysis of the one-photon excitation curve</i>	42
5.4.3. <i>Measurement errors</i>	44
5.4.4. <i>Experimental improvements</i>	45
5.5. Theoretical calculation of the TPE in turbid media.....	46
5.5.1. <i>Variations of the scattering coefficient</i>	47
5.5.2. <i>Variations of the numerical aperture</i>	49
6. Discussion and conclusion.....	51
6.1. Two-photon excitation in turbid media	51
6.1.1. <i>Ballistic versus non-ballistic photons in TPE</i>	51

6.1.2.	<i>The g-factor influence on scattered photons in TPE</i>	51
6.1.3.	<i>The dependence of polarization for TPE in turbid media</i>	52
6.1.4.	<i>The significance of the numerical aperture in TPE PDT</i>	52
6.1.5.	<i>Gaussian beam of ballistic photons</i>	53
6.2.	Photodamage.....	54
6.3.	Two-photon excitation in photodynamic therapy.....	56
6.4.	Conclusion.....	57
7.	Acknowledgements	59
8.	References	61

Appendix 1 – Theoretical derivations of two-photon properties

Appendix 2 – Tissue optics

Appendix 3 – Spectra of Rhodamine B

Appendix 4 – Basics on Monte Carlo simulations

1. Introduction

One of the main limitations of photodynamic therapy is the low penetration in tissue of the wavelengths used in treatments today. Therefore it is interesting to study the possibilities to use light in the tissue optical window. However, because of the lack of available photosensitisers absorbing light at these wavelengths, one could use non-linear excitation in the photodynamic process.

Photodynamic therapy is a method to treat for example cancer. The active substance in the therapy is a photosensitiser – a molecule that absorbs light, and in turn, induces a chemical reaction, leading to local cell death. The major drawback of this technique is that tissue has strong absorption for the wavelengths used to excite the photosensitisers, which limits the penetration depth of the light. Therefore photodynamic therapy is restricted to treatment of superficial lesions, or to the use of interstitial light delivery. However, tissue has an optical window in the far red and near infrared region, where the absorption is significantly lower. The problem is that most molecules have no absorption bands in this wavelength region, and at present, no photosensitiser is available with absorption in this region.

In order to take advantage of the tissue optical window, the presently used photosensitisers must be excited in a non-linear process, where the energy of two- or more photons are combined to excite one molecule. These non-linear excitation processes depend on the intensity to the power of n , where n is the number of photons involved in the excitation process. Hence, the two-photon excitation process depends on the intensity squared. The probability for a non-linear process to occur is very low, and thus very high peak intensity is required. This is obtained by strongly focusing a pulsed laser beam. The non-linear intensity dependence together with the high intensity required confine the multiphoton excitation processes within the focal region, which makes it possible to selectively excite molecules in three dimensions.

Tissue is, however, a turbid medium, which degrades the focusing; consequently also the yield of two-photon absorption.

At present a number of articles have been published in the field of two-photon excitation for photodynamic therapy but it is still not clear how good this method is. Therefore we have, experimentally and theoretically, studied the proposed advantage of this technique, like better penetration depth and higher selectivity. We have not performed any clinical experiments, but in the discussion section we elaborate on possible clinical applications of two-photon excitation in photodynamic therapy.

2. The theory of two-photon excitation

In a normal absorption process, one photon excites one atom. This process is linear and the probability of the process is proportional to the intensity. The energy of the photon corresponds to the energy needed to excite the atom. This energy, required to excite the molecule, can also be achieved by combining the energy of two or more photons. If the photon in the single-photon absorption (SPA) process has the energy corresponding to the wavelength, I_{SPA} , and if the two-photons have the wavelength, I_{TPA} , the latter wavelength has to be twice as long to preserve the amount of energy, hence $I_{TPA} = 2I_{SPA}$. For example, two photons with the wavelength of 810 nm can simultaneously excite a molecule that absorbs one photon at 405 nm. In this way it will be possible to excite molecules that have strong absorption in the UV and visible light with near-infrared (NIR) light. The probability of these multiphoton absorption (MPA) processes are, however, very low and depends on the intensity to the power of the number of photons, involved in the process. For the case of two-photon absorption (TPA), the probability* will thus depend on the intensity squared (around 10^{-50} cm⁴s/photon compared to 10^{-20} cm²s/photon for a linear single-photon absorption process). The process therefore requires very high peak intensity, which can be achieved in the focal region of a lens. Together with the nonlinear dependence of the TPA, and the high intensity required confines the TPA process to within the focal region (approximately 80% of all TPA) [1], which makes it possible to selectively excite volumes of the order of μm^3 , in three dimensions.

The theory behind the general expressions of the transition probabilities and transition probability rates for two- and multi-photon absorption is very extensive and not of critical importance for this report. Those with special theoretical interest are therefore referred to any textbook specialised in nonlinear optics (for example reference [2]). However, in appendix 1 there is a derivation (of transition probability, transition probability rates and absorption cross section) for the special case of two-photon absorption in a monochromatic radiation field.

2.1. History of two-photon absorption

The theory of two-photon absorption where first developed by the German physicist Maria Göppert-Mayer, who published her results in 1931 [3]. She used the quantum-mechanical approach of time-dependent perturbation theory to the second order, in order to treat this nonlinear process.

The first experimental reports on observed two-photon absorption, where published in 1950 by Hughes and Grabner at Columbia University, New York [4]. They worked with strong radiofrequency fields in a study of the spectrum of Rb⁸⁵F, when weak unexpected lines showed up at exactly half the wavelength of some of the studied lines. After excluding other causes, the best remaining explanation to the lines, where that it actually was fluorescence from two-photon

* The two-photon absorption cross section is commonly denoted by \mathbf{d} which has the dimension of area squared, times time, per photon. See appendix 1, section *Two-photon absorption cross section*, for further reading.

absorption they had observed. However, no experimental confirmation that there in fact was TPA was obtained.

Confirmation of the phenomenon did wait until the laser had been innovated. Kaiser and Garrett focused the red light ($\lambda = 694.3 \text{ nm}$) of a ruby laser into $\text{CaF}_2 : \text{Eu}^{2+}$ crystals, and investigated the thereby generated blue fluorescence light, which showed the characteristically (see above) squared intensity dependency on the excitation light [5].

During the last four decades, following the evolution of laser technology (especially that of pulsed lasers) examinations of several multiples of multi-photon absorption have been performed, and useful spectroscopic techniques such as *Doppler-free two-photon spectroscopy* has been developed (see for example references [6, 7, 8]).

2.2. Different types of multi-photon processes

There exist some different kinds of multi-photon processes. Below, four types of two-photon processes are briefly described. All of them are schematically shown in figure 2.1 below.

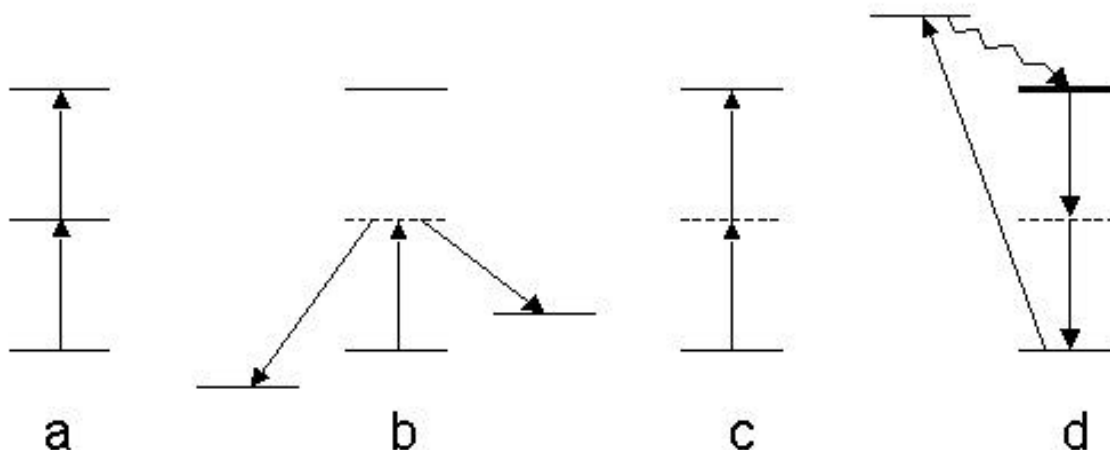


Figure 2.1 Different types of two-photon processes. The horizontal lines represent energy levels; the filled lines show real states, and the dashed lines show virtual states. The arrows represent transitions between states. a) Step-wise two-photon excitation. b) Raman scattering, the left and right “deexcitations” represents the anti-Stoke shift and Stoke shift, respectively. c) Simultaneous two-photon excitation. d) Two-photon emission. The wave formed arrow symbolises fluorescence; the thick line denotes a metastable state.

2.2.1. Stepwise one-photon excitation

By absorbing a photon, an atom (or molecule) can be excited, from *e.g.* the ground state to an allowed configuration with higher internal energy (a real state). If a consecutive absorption, by another photon, occur *before* the deexcitation from that real state, there will be a process called *stepwise* (two steps) *one-photon excitation/absorption* (figure 2.1a). In the same manner also more than two consecutive absorptions, via intermediate real levels, might be attained.

2.2.2. Raman scattering

In the quantum-mechanical picture of the well-known *Raman scattering* (figure 2.1b) phenomena, the Stokes and anti-Stokes shifts of the scattered field are regarded as photons emitted from a virtual level, which intermediates the scattering process. That is to say, that the Raman scattering is a two-photon process. The field of Raman spectroscopy is indeed interesting, but nothing which will be discussed in this report. For the basics of Raman scattering and some references of interest for that subject, see reference [7].

2.2.3. Simultaneous multi-photon absorption

What is concerned in this report is so called *multi-photon absorption*, especially *two-photon absorption* (abbreviated *TPA*). The equivalent term *two-photon excitation* (TPE) is also frequently used*. *Simultaneous multi-photon absorption* (figure 2.1c) can occur when two or more photons, with a total energy corresponding to the energy difference between two real electronic atomic/molecular energy levels, reaches the atom at almost the same time. (Of course the lower energy level need to be populated before the process is initiated.) The absorption process can be thought of as if the transition is intermediated by virtual energy levels between the real ones. The lifetime of such virtual levels is limited by Heisenberg's uncertainty principle. The energy level of the closest real state cannot be precisely determined if it is observed under a very short period of time. The lifetime of the virtual state is then in the order of 10^{-17} to 10^{-15} seconds. This sets the timescale for simultaneous multi-photon absorption. More precise calculations has been performed, and according to reference [9] are they indicating that the photons must arrive to the atom/molecule within one attosecond (10^{-18} s), which require a high photon flux achieved by a strongly focused laser beam. The short lifetime of the virtual level makes the two-photon absorption cross section very low, and typical values are about $10^{-50} - 10^{-49}$ cm⁴/s/photon [10].

The usual selection rules for electronic dipole transitions, tells us that because the odd parity of photons, one-photon excitation can only take place between electronic levels with opposite parity (in order to preserve the total parity). (See any basic textbook in atomic physics, *e.g.* reference [7] or [11].) In TPE two photons are absorbed, and therefore a two-photon transition takes place between two electronic levels with the same parity, unlike the situation in single-photon excitation (SPE). This can be used in spectroscopic investigations of electronic energy levels, hard to populate by ordinary single photon excitation because of violation of parity rules, but allowed for TPE.

The different parity selection rules of TPE, compared to that of SPE, implies the absorption spectra also differs. When working with fluorophores (*i.e.* fluorescent substances), which is the case in work with *photodynamic therapy* (PDT), as well as in *multiphoton fluorescence microscopy*, there is such a complexity in the molecules to be excited, that one rather speaks of semi-continuous energy bands than of discrete energy levels. Hence there is usually no problem (if the light intensity is high enough) to excite a fluorophore by TPE. However, the absorption spectra might differ more or less. Several experimental comparisons, with many different types of fluorophores, have been performed [9, 10, 12-16]. A common difference is that TPA spectra are much broader than their SPA (single-photon *absorption*) counterparts. Further, there is a trend that the TPA peaks of the spectra often are shifted to the blue, relative the corresponding SPA spectra profiles (the wavelength doubled). (At least the peaks are seldom red-shifted to the corresponding SPA peaks.) Several papers (*e.g.* references [12] and [15]) have also reported that

* One often also sees abbreviations for one-photon excitation: *OPE* or *SPE* ("S" for *single*).

the excitation spectra of non-centrosymmetric molecules show only small differences between single- and two-photon excitation modes. This is opposite to centrosymmetric molecules, which often show great differences. This indicates that for non-centrosymmetric molecules the same excited states are reached, independent of if the excitation is due to absorption of one or two photons. The transition probability of simultaneous two-photon absorption also depends on the mutual polarization of the two photons, see appendix 1.

2.2.4. Two-photon emission

In analogy with two-photon absorption, an opposite process known as *two-photon emission* (figure 2.1d) is also possible. This is possible to happen when an atom in a metastable state, from which deexcitation by usual one-photon emission is parity forbidden, and therefore, relatively seen, very unlikely. However, according to the selection rules for atomic transitions, such a deexcitation is fully allowed for a two-photon process (though very unlikely too).

2.2.5. The two-photon excitation rate

In appendix 1 a detailed theoretical derivation, based on quantum mechanics, of two-photon absorption rate and two-photon absorption cross section is given. In practise more “conceptual” and practicable expressions are needed. In many recent papers, on the topic of two-photon applications, such has been given (*e.g.* references [10, 13, 15, 16, 17]). One of the easiest ways to explain the nonlinear behaviour of the two-photon process is to model the excitation as the rate-limiting step in a chemical reaction [13]. For a photochemical reaction the formula will then be



where N_0 is a molecule in the ground state, being excited to a higher state N_1 , after the interaction with two photons, $2h\nu$. The simultaneous absorption of the two photons makes it possible to describe the interaction as a single-step termolecular chemical reaction*. The rate of production of excited state molecules, N_1 , is then given by,

$$\frac{\partial[N_1]}{\partial t} = k[N_0] \cdot [h\nu]^2, \quad (2.2)$$

where k is the rate coefficient and $[N_0]$, $[N_1]$, and $[h\nu]$ symbolise the concentration of the components involved in the reaction. This expression can be rearranged by defining an interaction volume with the path length, l , and the cross section area of the laser beam, A ; defining a two-photon cross section d ; changing to molar concentration, C ; converting to the light power; and dividing by 2, because two photons are absorbed. The new formula will then give an expression for the rate of production of excited-state molecules, R_{TPE} :

$$R_{\text{TPE}} = \frac{d}{2} \frac{l}{A} C(P(t))^2 \quad (2.3)$$

In equation (2.3) $P(t)$ is the instantaneous power. For a pulsed laser the power P can be approximated by P_{peak} (the peak power in the pulses) times P_{ave} (the average power);

* A termolecular reaction is a chemical reaction involving three molecules interacting simultaneously.

$P_{\text{ave}} = P_{\text{peak}} \cdot t \cdot f$, where t is the pulse width, and f is the pulse repetition frequency. Thus, the rate equation (2.3) may be described as

$$R_{\text{TPE}} \approx \frac{d}{2} \frac{l}{A} C P_{\text{peak}} P_{\text{ave}} = \frac{d}{2} \frac{l}{A} C t f P_{\text{peak}}^2. \quad (2.4)$$

This formula is a rough approximation but gives a rather good picture of the nature of the two-photon excitation process.

A more detailed expression is given by Xu and Webb [15] and the following derivation is based on that one.

Assuming no saturation or photobleaching, and thereby keeping the sample concentration of fluorophores constant, (and supposing no stimulated emission or self-quenching in the sample), the time-averaged two-photon excitation rate, $\langle R(t) \rangle$ (in s^{-1}), can be written as:

$$\langle R(t) \rangle = \frac{1}{2} g^{(2)} C d \langle f_0(t) \rangle^2 \int_V S^2(\vec{r}) dV \quad (2.5)$$

Here $g^{(2)}$ (unitless) is equal to $\langle I_0^2(t) \rangle / \langle I_0(t) \rangle^2$ and describing the *second-order temporal coherence* of the excitation source. The parameter C represents the fluorophore concentration (expressed in number of molecules per unit volume; cm^{-3}), and d its two-photon absorption cross section (in cm^4s). The flux $f_0(t)$ (the number of photons per area and time; $\text{cm}^{-2}\text{s}^{-1}$) is defined as the flux in the geometrical focal point. Finally, $S(\vec{r})$ represents a unitless *spatial distribution function*, describing the spatial distribution of the incident light. Its expression (2.5) $S(\vec{r})$ is integrated over the illumination sample volume. The factor 1/2 arise from that two photons are needed to excite one atom.

Instead of the intensity in the geometrical focal point, it is preferred to use the incident laser power $P(t)$. The relation between those is (see reference [15])

$$I_0(t) = \frac{\mathbf{p}(N.A.)^2}{l^2} P(t), \quad (2.6)$$

where $N.A.$ is the numerical aperture of the focusing lens (and l is the light wavelength); I_0 is the intensity, expressed as the flux times the photon energy ($I_0(t) = \hbar \omega f_0(t)$). Inserting (2.6) in (2.5) gives

$$\langle R(t) \rangle = \frac{\mathbf{p}^2 (N.A.)^4}{2I^4} g^{(2)} C d \left\langle \frac{P(t)}{\hbar \omega} \right\rangle^2 \int_V S^2(\vec{r}) dV = \frac{\mathbf{p}^2 (N.A.)^4}{2\hbar^2 \omega^2 I^4} g^{(2)} C d \langle P(t) \rangle^2 \int_V S^2(\vec{r}) dV \quad (2.7)$$

and a strong dependency on the $N.A.$ shows up.

Xu and Webb [15] then applied the paraxial form of the normalised intensity point-spread function for a diffraction-limited lens, to calculate the integral over the spatial distribution. That integral expression cannot be analytically integrated. If the sample thickness is very big, in relation to the

focal depth (that is to say that the volume, V over which the integral is taken, approaches infinity), numerical calculations results in

$$\int_{V \rightarrow \infty} S^2(\vec{r}) dV \approx \frac{8nI^3}{p^3(N.A.)^4}. \quad (2.8)$$

Here n represents the refractive index of the sample. This result is very interesting. As seen when inserted into (2.7), the strong numerical aperture dependency cancels out:

$$\langle R(t) \rangle \approx \frac{4n}{p\hbar^2 w^2 l} g^{(2)} C d \langle P(t) \rangle^2 \quad (2.9)$$

The relation between the wavelength, l , and the angular frequency, w , is $l = 2pc/nw$, where c is the speed of light in vacuum, and n is again the refractive index of the sample. This can be used to rewrite expression (2.9) as

$$\langle R(t) \rangle \approx \frac{2n^2}{p^2 c \hbar^2 w^2} g^{(2)} C d \langle P(t) \rangle^2. \quad (2.10)$$

This formula gives the two-photon absorption caused by ballistic photons in the entire exposed volume (TPE outside the focus is also included). Lenses with higher $N.A.$ have small focal regions with high intensities, and lenses with low $N.A.$ have larger focal region with lower intensities. The total two-photon absorption will, however, be approximately the same. Note, however, that this is a *theoretical ideal*; in practical experiments, as seen below, the size of the numerical aperture may be important.

The second-order temporal coherence, $g^{(2)}$, is hard to measure experimentally, but can be approximated as

$$g^{(2)} = \frac{g_p}{f t}. \quad (2.11)$$

The parameter, g_p , is dimensionless and depends on the shape of the laser pulse, and of the laser duty cycle. It is defined through the relation between the second-order temporal coherence ($g^{(2)}$) and the laser pulse repetition frequency (f) and pulse width (t). Its numerical value can be calculated for different pulse profiles. For pulses with Gaussian temporal profile it is (approximately) 0.664, and for pulses with hyperbolic-secant square profile it is (about) 0.588. The two parameters in the denominator of (2.11), are the laser pulse repetition frequency (f), and the FWHM of the pulses (t), measured in time. This expression holds for a completely mode-locked (*i.e.* there is no continuous wave featured) laser pulses. Thus, expression (2.9) leads immediately to the final expression for the time-averaged two-photon excitation rate:

$$\langle R(t) \rangle \approx \frac{4n}{p\hbar^2 w^2} g_p C d \frac{\langle P(t) \rangle^2}{f t l} \quad (2.12)$$

Or, alternatively, expression (2.10) gives

$$\langle R(t) \rangle \approx \frac{2n^2}{\mathbf{p}^2 c \hbar^2 \mathbf{w}^2} g_p C d \frac{\langle P(t) \rangle^2}{f \mathbf{t}}. \quad (2.13)$$

Obviously, the TPE depends primarily on the squared photon flux from the laser source (implicitly included in the time-averaged power); but also on the pulse repetition rate of the laser; its pulse width and wavelength/frequency; and on concentration and the two-photon absorption cross section of the fluorophore. From the equation above it can also be seen that the fluorophore with the highest product of the concentration and two-photon absorption cross section contribute to the highest total TPE yield. In expressions (2.12) and (2.13) f and \mathbf{t} appears in the denominator, in contrast to in expression (2.4), where these parameters appears in the nominator. However, if P_{peak} in equation (2.4) is expressed in P_{ave} , the same relation appears:

$$\frac{P_{\text{ave}}}{f \mathbf{t}} = P_{\text{peak}} P_{\text{ave}} = f \mathbf{t} P_{\text{peak}}^2 \quad (2.14)$$

Compared to the single-photon excitation process the main difference is that the TPE process has a quadratic dependence of the photon flux, which makes a pulsed laser source favourable, whereas the SPE depends solely on the time-averaged power. The absorption cross sections also differ between the SPA process and the TPA process. However, the nonlinear dependence for TPA gives different units for the cross sections and makes it is hard to compare the values. A detailed theoretical quantum mechanic description of the TPA cross section is given in appendix 1, and from that it could be seen that the TPA cross section also has a dependence on the direction of polarization of the two incident photons.

3. Photodynamic therapy

Photodynamic therapy (PDT) is a novel approach to treat for example cancer. The therapy is based on a photodynamic reaction, which is a chemical reaction initiated by light irradiation. The reaction can be used to selectively treat diseased cells.

Three components are required to perform PDT; namely, photosensitiser, oxygen, and light. A photosensitiser is a light sensitive molecule, which accumulates to a higher degree in some types of diseased tissue than in normal tissue. This is especially true for malignant tumours. Following administration of the photosensitiser, its concentration becomes 2–5 times higher in the diseased cells than the surrounding tissue. The tissue is then irradiated by light. The light induces a cytotoxic photochemically reaction including the photosensitiser molecules and oxygen molecules, leading to local cell death.

Compared to other oncological treatment modalities, PDT has several advantages, for example; the selective treatment of malignant tumours; the minimal hazardous effects on the patient and/or medical personnel (light in the visible region does not hurt); and relative moderate cost. The main disadvantage of PDT is the limited penetration depth of the treatment light, which restricts this modality to superficial lesions. However, it is possible to overcome this problem by an interstitial delivering of the light, and possibly also by two-photon excitation with near-infrared light, which will be investigated in this paper. Another drawback of PDT is that several photosensitisers cause relatively long elevation in skin photosensitivity.

3.1. Photosensitisers

A photosensitiser (or a PDT agent) is, as mentioned before, a molecule that absorbs light at a specific wavelength (a *chromophore*) thereby starting a photochemical reaction. There are many different photosensitisers, but the induced photochemical reaction is similar for many of them. Presently, Protoporphyrin IX (PpIX) is used in most PDT studies at Lund University Hospital. Hence, it will work as an example in this paper.

3.1.1. Porphyrins and chlorine

The group of molecules, based on a pyrrole ring structure shown to the left in figure 3.1, is called porphyrins. Many of them have photosensitising properties. Porphyrins have their strongest absorption peak at the Soret band at about 400 nm. The most common porphyrin-based photosensitisers are Protoporphyrin IX and Photofrin. The photosensitiser PpIX has besides the Soret band also a minor absorption bands up to about 630 nm.

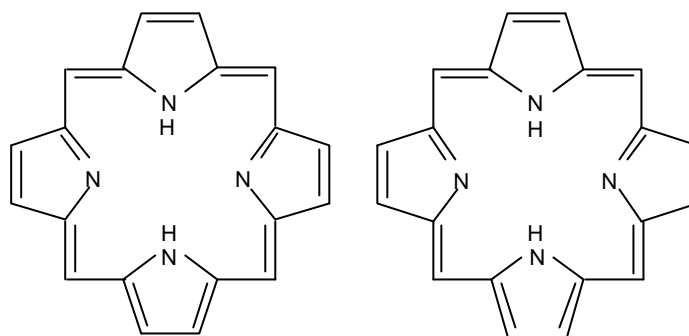


Figure 3.1 The main cores of the porphyrin and chlorine structures, respectively. The difference between them is that for chlorines at least one double bond in the pyrrole rings is reduced to a single bond. (From reference [18].)

Another group of common used photosensitisers is chlorines, which in fact are reduced porphyrins. Porphyrin becomes chlorine, when one or more double bounds in the pyrrole rings are reduced to a single bond. The reduction of a double bond changes the optical properties of the ring so that the strongest absorption peak shifts to the red spectrum (640–700 nm), which gives chlorine a green colour as *e.g.* chlorophyll.

3.1.2. Aminolevulinic acid and protoporphyrin

The photosensitiser prodrug δ -Aminolevulinic acid (ALA) has, over the last few years, started to be widely used in clinical PDT. ALA is a naturally occurring compound, which is converted to Protoporphyrin IX, PpIX, by chemical reactions in the haem-cycle. PpIX is a photodynamically active compound or photosensitiser, which is selectively accumulated in malignant cells due to the higher activity of haem production by cells that grow rapidly. As a porphyrin, PpIX exhibit a dual-peaked fluorescence spectrum, with a major peak at about 635 and a smaller at approximately 705 nm.

There are several advantages of ALA over other photosensitisers; like, low toxicity; easy to deliver; short accumulation time; and the photosensitiser is cleared out within one or two days. The main drawback of ALA is that; PpIX has absorption peaks, where tissue has rather high optical density. Therefore the light used to excite PpIX has low penetration in tissue, which leads to a small treatment depth.

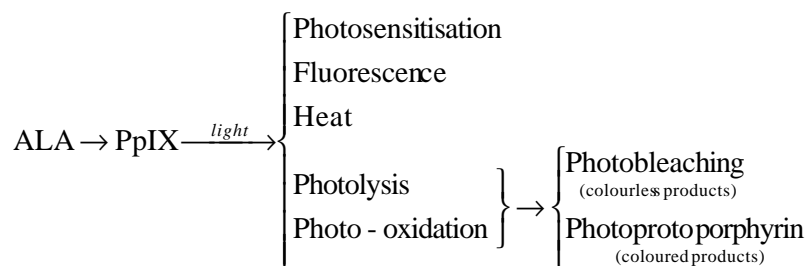


Figure 3.2 Cytotoxic chemical reactions. Possible deactivation pathways for ALA-induced PpIX after photoactivation.

3.2. The photochemical reaction

In order to explain the mechanism of the PDT, the photochemically reaction of PpIX will be taken as an example. When PpIX absorbs light for example at 635 nm, the molecule will be excited to the first excited single state (S_1 in figure 3.3). This energy level or absorption band is called the Q-band. From this state the molecule can be transferred to the lowest triplet state (T_1), even though this inter-system crossing is spin-forbidden. This is possible because the small energy difference between the states makes the quantum yield for the transition high enough. The next relaxation of the molecule from the triplet state to the singlet ground state, S_0 , is also a spin-forbidden inter-system crossing with a low transition probability. Hence, the lifetime of the triplet state is relative long (of the order of milliseconds), which gives the sensitizer time to interact with surrounding molecules.

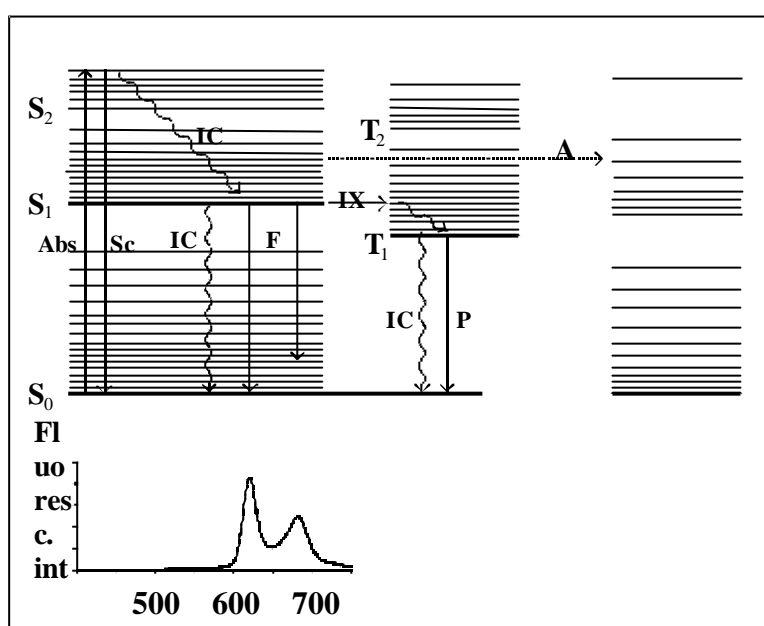


Figure 3.3 A schematic Jablonski diagram showing the various decay paths from an excited state of a molecule. The abbreviations are S_n , singlet states; T_n , triplet states; Abs, absorption; IC, internal conversion; F, fluorescence; IX, Intersystem crossing; P, phosphorescence; A, energy transfer to other molecules. The fluorescence spectrum is also shown in the figure (From reference [18]).

There are two types of PDT reactions. In Type I reactions, a radical is formed, which may directly, or indirectly, induce cell damage. The energy of the excited molecule (the sensitizer) is transferred to another molecule via electron transfer or hydrogen abstraction. In the other type of reactions, called Type II, cell death is caused by the very reactive singlet oxygen. These reactions involve a process where the photosensitizer is relaxed from its triplet state to its singlet ground state, simultaneously as oxygen is excited from its triplet ground state to its singlet state (also a spin-forbidden intersystem crossing). In this way the combination of the two spin-forbidden transitions will be allowed, because the sum of spin quantum numbers, before and after the transitions, is unchanged. Hence, the energy from the photosensitizer is transferred to the very reactive singlet oxygen, which has a diffusion distance in biological tissue of the order of $0.01\mu\text{m}$, and a corresponding lifetime of about $0.001\text{--}0.004\mu\text{s}$ [18]. In other words, single oxygen acts as a

very aggressive oxidant on many target molecules within the cell, such as proteins and nuclei acids, leading to instant cell death. Thus, not only the concentration and subcellular localisation of the sensitiser is important for the cell killing efficiency, but also the oxygen concentration.

3.3. Photobleaching and photoproduct formation

In both types of reactions discussed above, the sensitiser is relaxed to the ground state and the process can be repeated again – the molecule acts as a catalyst. The photosensitiser might, however, itself also be oxidised by the singlet oxygen. This process is called photobleaching or photodegradation. For the PpIX case, König *et al.* [19] have shown that the photochemical process of formation of photoproducts requires oxygen and that singlet oxygen is involved.

When PpIX is photodegraded during PDT, several different photoproducts of PpIX are formed. The main photoproduct *in vivo* is the green photoporphyrin, Ppp, which is formed by the reduction of a double bond in the pyrrole ring, changing the molecule into a chlorine-type molecule [20]. Also other photoproducts are formed, like formyl products, but these exhibit the same optical properties as PpIX, since the ring is unchanged. Therefore, formyl-type products are hard to discriminate from intact PpIX [21] and will not be further studied in this report. Instead we will focus on the chlorine-type photoproducts, because these have the highest yield but also because the chlorine molecules are known to have large two-photon cross section. The two-photon efficiency of Ppp has actually already been found to be large [22].

Ppp consist of two hydroxyaldehyde chlorine-type isomers [23], resulting from a cycloaddition of $^1\text{O}_2$ to one or more vinyl groups and a double bond break of the two PpIX tautomers [24]. Hence, the characteristics of Ppp are chlorine like, for example the strongest absorption for Ppp is at about 670 nm [25] compared to 400 nm for PpIX. The major fluorescence emission peak of Ppp is at about 675 nm [21, 26]. However, when Ppp is excited at 407 nm a slight blueshift has been observed of this peak [27].

Since Ppp is chlorine-type molecule, Ppp is also, like chlorines, a very photosensitive substance and has similar photostability as PpIX [27]. When Ppp is bleached a new photoproduct is formed with a chlorine-type spectrum, where the absorption maximum is at 648 nm [24] and fluorescence peak is at about 654 nm [26].

3.3.1. Bleaching process

Ppp is formed during a bleaching process of PpIX, but is then itself photobleached. Consequently, the concentration of Ppp in the tissue will reach a maximum after a certain amount of photobleaching, and then decrease again. This has been observed during treatment of 5 mW/cm^2 with 514 nm laser, and the maximum of the 675 nm peak is reached after less than 5 J/cm^2 . The fluorescence intensity of Ppp is then approximately 8% of the initial fluorescence intensity of PpIX [28]. Oxygen and production of singlet oxygen are involved in the process, where Ppp is photobleached [28, 29], hence, Ppp also acts as a photosensitiser [20, 24]. However, according to Robinson *et al.*, the concentration of Ppp seems to be as great in normal, as in tumour tissue [28]. If this is true, Ppp has not the selectivity needed to be a good photosensitiser. Any enhancement of the PDT damage due to Ppp has not yet been found [28].

The result of the bleaching process depends on various parameters of the laser beam, like irradiance and power. Lower irradiance causes more efficient bleaching of PpIX and, in turn, more efficient Ppp formation. But lower irradiance also leads to more efficient photoproduct bleaching, which gives a lower net accumulation of Ppp [26, 28, 29]. The fact that photobleaching increases for lower irradiance, supports an oxygen-dependent mechanism of PpIX photobleaching [26]. Due to the variations between the absorption spectra of PpIX and that of Ppp, the relative bleaching rate is wavelength dependent. For example, the bleaching rate of Ppp is faster at 440 nm than 410 nm [27]. The different absorption cross sections and fluorescence quantum yields also make it difficult to quantify the relative concentration of PpIX and Ppp [29].

3.4. Two-photon excitation in photodynamic therapy

One of the disadvantages of PDT is, as mentioned before, the low penetration depth of the laser light used in the treatment. The penetration depth of the light, in the region of 400–700 nm, is limited by the strong absorption of tissue chromophores, *e.g.* haemoglobin, and the scattering that increases with decreasing wavelength (*Appendix 2 – Tissue optics*). Because of these limiting factors the maximum treatment depth of linear PDT (without interstitial light delivery) is only about 3 mm. The penetration of light in tissue is, however, much better for light in the near-infrared (NIR) region between 700–1300 nm (the optical window of tissue), where the absorption is much lower. However, most molecules have no absorption bands in this wavelength region and, at present, there is no photosensitiser that has these wanted properties available. Hence, if the light in this region should be used in PDT a multiphoton absorption process is therefore needed to excite the photosensitisers. As mentioned before, two photons combine their energy to excite one molecule, in a two-photon excitation process. The combined energy of the two-photons should correspond to that of one photon normally used to excite the molecule, which means that photons with wavelengths in the NIR can be used to excite chromophores with absorption bands in the UV and visible region. Then the Soret-band (at 400 nm) could be used, that has a SPA cross section 100 times higher than that of the Q-band (at 630 nm, used in PDT today). The main reasons for using TPE instead of SPE in PDT should then be to get access to the optical window of tissue (leading to larger penetration depth); the possibility to excite the Soret-band; and maybe most important, the selectivity in three dimensions given by the confinement of the excitation in the focal region, due to the non-linear intensity dependence. The very low probability of two-photon absorption can partly be compensated by the higher peak intensities in pulsed laser and the better penetration of NIR light in tissue.

Since the beginning of 1990 the possibilities of two-photon excitation in photodynamic therapy has been studied and the two-photon excitation properties of some photosensitisers have been published. In experiment performed by Fisher *et al.* [13], it was shown that SPE and TPE fluorescence spectra were almost identical for the photosensitisers 8-MOP (8-methoxypsoralen) and AMT (4'-aminomethyl-4,5,8-trimethylpsoralen). This implies that the relaxation process is independent of the excitation process. Both AMT and 8-MOP are non-centrosymmetrical molecules and their two-photon absorption spectra had similar shape to their single-photon absorption spectra [13]. In contrast, the centrosymmetric porphyrine derivative HP-IX has clearly different absorption spectra for TPA compared to SPA. For example, the Soret band at 400 nm appears to be disallowed in the TPA spectra. Another approach in TPE PDT is to first excite a fluorophore with a very large TPA cross section, which then transfer its energy to a

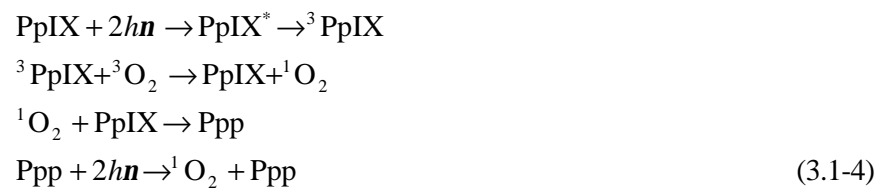
photosensitiser. With this method, Bhawalkar *et al.* [30] could demonstrate the production of singlet oxygen in a sample.

Experiments *in vivo* have also been performed. Wachter *et al.* [31] treated tumours in rats with TPE and MPE PDT. The photosensitisers used in their experiment were the porphyrine based Photofrin and a natural precursor to melanin called DHICA. The result supported the assertion that the fundamental properties of the excited state of photosensitiser, like the photodynamic reaction, will be identical whether excitation occurs via SPE or one of various non-linear excitation processes. For example, a multiphoton excitation of DHICA in a M-3 melanoma tumour ($5.3 \times 5.3 \times 2.8 \text{ mm}^3$) using 1047 nm light ($<250 \text{ fs}$, 250 J/cm^2) resulted in immediate bleaching of tumour followed by necrosis. Then 18 days later the primary tumour was gone, but a secondary tumour was still present (not treated). Moreover, no tissue damage was evident beyond tumour margins for any wavelength examined. Similar results were also achieved for TPE of Photofrin but then as much power as 800 J/cm^2 was used, compared to 150 J/cm^2 for the SPE case. In addition, no detailed description of the method used in the experiments was given, and no further results have yet been published (and some of the authors work at a company...).

Another interesting experiment has been performed by König *et al.* [32]. They studied the photodynamic therapy effects of Photofrin-labelled and PpIX-labelled Chinese hamster ovary (CHO) cells during two-photon excitation. The laser apparatus used was a mode-locked 76 MHz Titanium:Sapphire (Mira model 900-F, Coherent) and the pulse duration at the sample was approximately 200 fs. The laser beam was focused with a high numerical objective lens (PlanNeofluar $40\times/N.A. 1.3$, oil) and scanned over a sample area of $160 \mu\text{m} \times 160 \mu\text{m}$. For a typical cellular area of $700 \mu\text{m}^2$, the cell dwell time was about 400 ms per scan. The result showed that the exposed sensitiser-labelled cells had decreased their cloning efficiency to 50% after 13 scans for Photofrin and 24 scans for PpIX, which corresponds to applied energies of about 10 mJ and 19 mJ per cell, respectively. The cell destruction was accompanied by photobleaching effects.

Porphyrins are centro-symmetrical molecules, and have low two-photon absorption cross sections. This is especially true for PpIX that has a TPA cross section of $0.7 - 2.0 \cdot 10^{50} \text{ cm}^4 \text{ s/photon}$ [22], which caused that the possibilities of using PpIX for TPE PDT not has been studied that much. However, two-photon fluorescence microscopy has been used to study concentration and distribution of PpIX and Ppp [33]. The results from this have indicated that Ppp might have a larger two-photon cross section. If this is true and if the molecule also works as a photosensitiser, suggested by Dickson and Pottier [24], it could be used in TPE PDT applications. The TPE excitation of Ppp is very wavelength dependent and has an excitation maximum around 746 nm, equivalent of 373 nm, placing it into the blue edge of a typical porphyrin Soret spectral feature [22].

In order to understand if Ppp act as photosensitiser or not, the reactions formulas of the photobleaching process of PpIX and Ppp must be roughly known. For single-photon excitation the formation of the Ppp is independent of illumination wavelength. This indicates that the efficiencies of photooxidation reactions are independent of whether the molecule was excited in the first or second excited single state [21]. If this is true also for TPE has to be investigated. In the absence of oxygen, PpIX and its photoproducts are not bleached, indicating that the bleaching process involves oxygen. Hence, the following reaction formulas are suggested [22]:



The oxygen involved in the photobleaching of Ppp implies that Ppp might act as a photosensitiser.

4. The path of the light in a TPE PDT system

The light propagation in the optical system is affected by various phenomena that degrade the two-photon excitation efficiency. In order to explain these phenomena, the light path will be divided into three parts. First the parameters of the laser source will be issued, because the shape of the laser pulse is very crucial to the performance of the components in the optical system. In the second part there will be a brief theory of dispersion and how the components of the optical system affect the shape of the laser pulse and the size of the focal point. Finally, there will be an overview of what happens when the light interacts with tissue and which limitation this sets to excitation intensity of the laser beam.

4.1. The laser source

In principle any laser can be used for two-photon excitation. However, due to the low absorption cross sections depending on the intensity squared, in practise only pulsed lasers are applied to the issue. While high peak intensities are a necessity, the mode-locked laser is the common choice. Because of its high peak intensities, high pulse repetition frequency (PRF), high stability, tuneable wavelength in the near-infrared part of the spectrum, and simplicity to handle, the self-mode-locked Titanium-Sapphire lasers is probably the most used in TPE PDT research (as well as in two-photon fluorescence microscopy). Other types of mode-locked lasers are also in use, for example different kinds of Neodymium lasers (*e.g.* Nd:YAG). The pulse length of the Ti:Sapphire-laser is of the order 100 fs, whereas the pulses from a Neodymium laser can be in the order of picoseconds. Ultra-short pulses like these consist of broad wavelength spectra (it is a real example of the Fourier transform; a shorter pulse in time gives a longer pulse in frequency space). Therefore the pulsed light from a mode-locked laser is described as chromatic rather than monochromatic.

4.2. The optical system

All components in an optical system affect the laser light, to some extent. These effects can degrade the shape of the laser pulse and also decrease the peak intensity in the focal point of the lens. Since TPE has a quadratic dependence on the intensity, it is very crucial to minimise the degrading of the shape of the laser pulse. In order to achieve a highly confined focal point and high peak intensity, the laser beam has to cover the entire back aperture of the focusing lens. Expansion of the beam might be required. This can be accomplished by two lenses, which are called beam expander or condenser. The beam expander and the objective are the main components in the optical system. Other components, like mirrors and fibres, are needed to guide the beam from the laser source to the objective. Further on, in photodynamic therapy the focal point has to be scanned over the entire lesion, which can be accomplished by vibrating mirrors.

The degrading of the laser pulse already starts when the pulse is guided to the lens system, because there are no perfect optical components. Any tiny little defect can deform the pulse shape in such way that the temporal and spatial peak intensity in the focal point decreases. Consequently,

the optical system should only consist of high-performance equipment, and as few components as possible, to avoid unwanted distortion. Then the numbers of mirrors, used to guide the laser beam, must be kept low. This may constitute a problem in a clinical set-up. The alternative, to the use of mirrors, is the guiding through a fibre. Unfortunately, the ultrashort pulse, that has a broad spectrum of wavelengths, is widened, due to chromatic dispersion in fibres.

4.2.1. Dispersion

Chromatic dispersion is broadening of a pulse due to variation of the refractive index with wavelength (or frequency). In other words, different wavelengths travel at different speeds through the medium (since $v = c/n$). The phenomena is the same that occur when white light passes through a prism, and gives the spectrum of the rainbow out of white light, see figure 4.1. The red light with the highest refractive index travel slowest and are bent least, while violet light travel fastest and are bent most. Then it will take shorter time for the violet light than for the red light to travel through the fibre. The time delay between the violet and the red light broaden the laser pulse and this dispersion increase with increasing distance of the fibre, see figure 4.2.

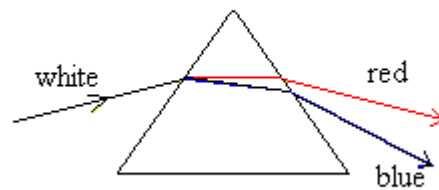


Figure 4.1 Dispersion in a glass prism.

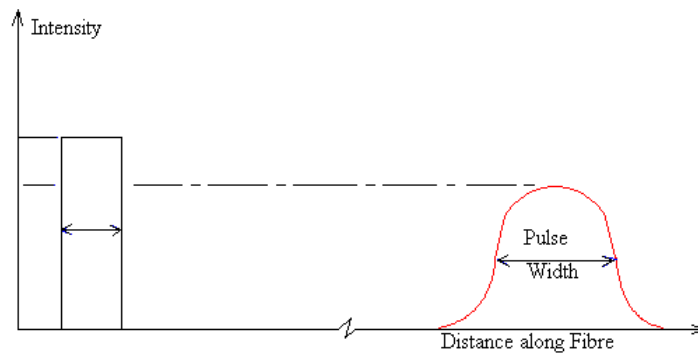


Figure 4.2 Pulse dispersion in an optical fibre.

There is also another phenomenon in the fibre that is called intermodal dispersion, multimodal dispersion, or just modal dispersion, even though it has nothing to do with a wavelength-dependence of refraction. Modal dispersion is caused by the fact that the ray paths or modes, by which light can propagate down the fibre core, depends on the incident angle into the fibre. The lower order modes travel almost parallel to the axis of the fibre and takes the shortest time. Higher angle, or higher order modes rays travel in “zigzag” route, which is longer and takes longer time. Hence, different modes correspond to a slightly different transit times.

The total time delay between the arrival of the axial ray, and the one travelling the longest distance, depends on the refractive index of the fibre. This is due to the fact that the non-axial route is longest when the ray is incident at the critical angle, which, in turn depends on the refractive index. In other words, modal dispersion depends on the refractive index but not on the fact that the refraction index itself is wavelength-dependent. Modal dispersion can be avoided by the use of single mode fibres.

Both chromatic dispersion and modal dispersion have the undesirable effect of smearing out the pulse due to different transit times. As a result, a sharp rectangular pulse (a “boxcar”) gradually gets wider and the peak intensity decreases. The widening due to chromatic dispersion is less for longer pulses since the spectral width of the pulse decreases with increasing pulse length ($1 \leq \Delta t \cdot \Delta f$). Pulses in the range of picoseconds have no dispersion problem to travel through a fibre. In summation, dispersion smears out the pulse in the fibre and the effect increases with increasing distance. In addition the laser beam has to be focused into the fibre, which also causes dispersion.

The optics of lenses is normally explained by Gaussian optics, but there are a few aberrations or image errors that deviate from this theory. In order to explain these phenomena a third-order theory of optics is needed (a third-order term is added to the first order approximation of $\sin \hat{a}$). There are two main types of aberrations: chromatic and monochromatic. Examples of monochromatic aberrations are spherical aberration, coma and astigmatism. These will not be discussed in this paper as the lenses compensate for such aberrations. The chromatic aberrations are, on the other hand, more significant and arise from dispersion effects (refractive index, n , is a function of wavelength, $\tilde{\nu}$). One result of this is that the focal length depends on the colours of the light. This could be seen from the thin-lens equation

$$\frac{1}{f} = (n_1 - 1) \left(\frac{1}{R_1} - \frac{1}{R_2} \right), \quad (4.1)$$

where number of refraction, $n_1(\tilde{\nu})$, decreases with wavelength over the visible region and thus the focal length, $f(\tilde{\nu})$, increases with wavelength (R_1 and R_2 are the radius of the lens curvature). Since a short laser pulse consists of a spectrum of wavelengths, the focal point will smear out in space. When the pulse travel through a lens system or objective, it will also be broaden in time, due to differences in the optical path lengths (in the same way as in the fibre). These effects are called phase distortion and group-velocity dispersion, and can be compensated for by a pulse compressor. A pulse compressor consists of pairs of prism that gives negative dispersion of the pulse, which compensates for the positive dispersion from the objective. Higher numerical aperture gives higher group-velocity dispersion.

4.2.2. The numerical aperture

The numerical aperture ($N.A.$) of a lens determines how tightly the lens is focusing, and therefore the size of the focal volume. Higher $N.A.$ gives more tightly focusing (smaller focal volume), which gives higher intensity in focus. The numerical aperture can be defined as $N.A. = n \cdot \sin a$ and indicates the light acceptance angle of the objective. Further on it determines the light gathering power, the resolving power and the depth of focus:

$$N.A._{obj} = n \cdot \sin a \quad (4.2)$$

Here a is half the objective angular aperture A (see figure 4.3) and n is the refractive index of the medium (air, water, or oil) between the objective and the specimen. A high numerical aperture gives a small diffraction-limited focal point with high intensity. The diffraction pattern in the focal plane has a bright circular disc surrounded by an alternating series of bright and dark higher-order diffraction rings whose intensities decreases as they become further removed from the central disc (see figure 4.3) The central circular disc is called *Airy disc* and determines the size of the focal point. The size, or the radius, of the Airy disc is determined by the numerical aperture of the objective and condenser (beam expander). When the condenser and objective have equivalent numerical apertures, the Airy pattern radius from the central peak to the first minimum is given by the equation:

$$r_{Airy} = 1.22 \frac{\lambda}{2N.A._{obj}} \quad (4.3)$$

Here r_{Airy} is the Airy radius, λ is the wavelength of illuminating light, and $N.A._{obj}$ is the objective numerical aperture.

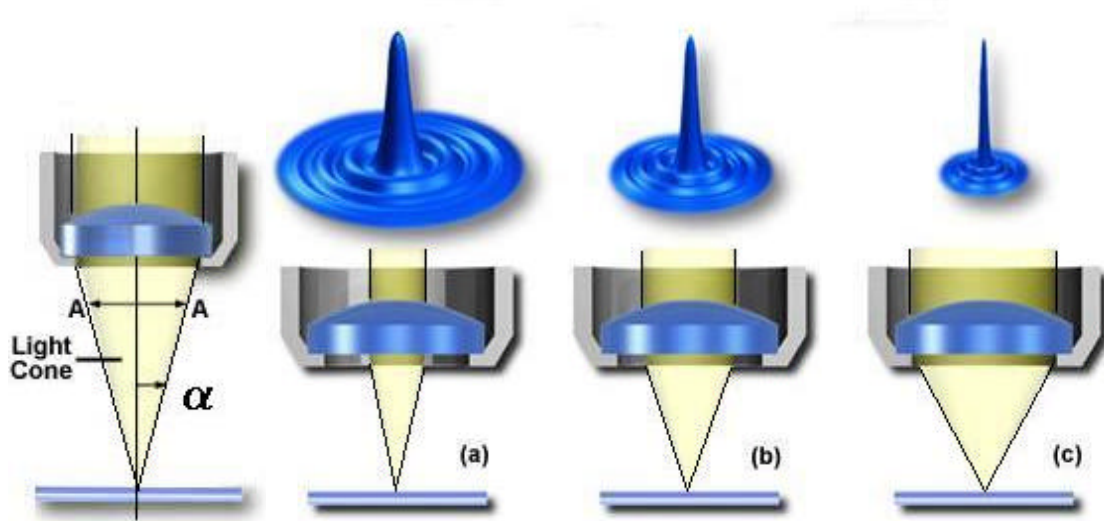


Figure 4.3 To the left: The numerical aperture $N.A.$ is described by $N.A._{obj} = n \cdot \sin a$, where a is half the objective angular aperture A . To the right: The light cone and Airy disc for different $N.A.$; a) $a = 7^\circ$, $N.A. = 0.12$, b) $a = 20^\circ$, $N.A. = 0.34$, c) $a = 60^\circ$, $N.A. = 0.87$.

Instead of the Airy disc, it could sometimes be more appropriate to describe the light distribution of a Gaussian beam, by using the beam radius $w(z)$ (defined as the radial distance from the centre of the beam, to where the intensity has dropped to $1/e^2$, compared to the centre). For a Gaussian beam, the intensity distribution in vacuum can then be expressed as in (cylindrical co-ordinates) (e.g. references [34, 35])

$$I(\mathbf{r}, z) = \frac{2P}{pw^2(z)} \exp\left(-\frac{2\mathbf{r}^2}{w^2(z)}\right), \quad (4.4)$$

where P is the power, and $w^2(z)$ the beam-radius:

$$w^2(z) = \left(\frac{I}{p(N.A.)}\right)^2 \left(1 + \left(\frac{4p(N.A.)^2 z}{I}\right)^2\right) \quad (4.5)$$

The TPE signal is proportional to the intensity squared, and it is easily seen that

$$I^2(\mathbf{r}, z) = \left(\frac{2P}{pw^2(z)}\right)^2 \exp\left(-\frac{4\mathbf{r}^2}{w^2(z)}\right) \Rightarrow I^2(0,0) = \frac{4p^2 P^2 (N.A.)^4}{I^4}. \quad (4.6)$$

Hence, the intensity in the centre of the focal spot shows strong $N.A.$ dependency. (Note the strong wavelength dependency too.)

4.3. Light interaction with tissue

When light propagates through tissue, both scattering and absorption interactions occur (see *Appendix 2 – Tissue optics*). These processes decrease the efficiency of two-photon excitation and limit the excitation intensity that can be used without any biological damage. Phenomena that may cause unwanted cell damages are plasma formation, heating, and multiphoton absorption of chromophores that are not photosensitisers.

4.3.1. Scattering in tissue

The scattering of the light is the main limiting factor for two-photon excitation in turbid media. When the light is scattered, the temporal and spatial coherence is lost, which decrease the peak intensity in the focal point, and in turn the yield of two-photon excitation. The scattering properties of tissue is described by the scattering coefficient, m_s , and the anisotropy factor, g , which give the scattering events per unit length and the average value of the cosine of the scattering angle, respectively. For 800 nm the scattering coefficient of tissues is of the order of 10/mm. Typical values of the g -factor for tissues lies in the range of 0.7–0.95 [36], where $g = 1$ indicates complete forward scattering and $g = 0$ represents isotropic scattering.

The g -factor dependency of the two-photon excitation was studied in Monte Carlo simulations performed by Dunn *et al* [37]. According to their results, the angular deviation of photon path for $g \leq 0.9$ is large enough to prevent the photon from reaching the focal point [37]. In other words, it is mainly the ballistic (meaning non-scattered) photons that enter the focal region and contribute to two-photon excitation. This means that the yield of two-photon excitation is relatively insensitive to g when g is less than 0.9. On the other hand when g is larger than 0.95, photons can reach the focal region after they have been scattered [37]. From this findings Dunn *et al* drew the conclusion that the yield of two-photon excitation is determined by single scattering for $g \leq 0.9$, whereas multiply scattered photons also can contribute to the excitation when g is larger than 0.95. Worth noting about that study, is that it was based on simulation parameters for a focus depth of 200 μm , and $m_s = 10 \text{ mm}^{-1}$ (a typical value for tissue). Thus the photons reaching the focus on average scatter once before reaching the focal volume. For a g -factor of 0.98 they found a peak intensity approximately 3 times higher than for $g = 0.9$.

Experiments of two-photon excitation of fluorophores in scattering media have also been performed by Ying *et al.* [38]. In their experiment they focused the beam from an Nd:YAG laser (1064 nm, 82 MHz, 92 ps pulse duration) approximately 2.5 mm deep inside a scattering sample. They found that two-photon fluorescence (TPF) intensity near the surface remains relative constant whereas the TPF at the focal point decreases exponentially as the scattering strength of the sample media increases. As a result the TPF intensity near the front surface is higher than the TPF intensity at the focal region when the scattering coefficient is larger than 1.4/mm. Ying *et al.* [38] also found that the peak position near the focal point moved slightly toward the surface with increasing scattering of the media. In order to explain their findings they used a mathematical model based on Gaussian optics, where they only included ballistic photons and neglected all absorption. From this approximation they made a calculation for a system, where the focal point was 200 μm deep into the tissue, the focal size was 2 μm , and the scattering coefficient was 20/mm. Under these conditions the total TPF signal generated on the surface would be approximately 1/3 of the signal at the focal spot. The movement of the peak intensity towards the surface could also be explained by this approximation.

The effects of scattering have also been studied by Gu *et al* [39]. They used Monte Carlo simulations (see appendix 4) to see how the number of scattering event (n) before the photons reach focus and numerical aperture ($N.A.$) affect the two-photon yield. Their simulations were run for $g = 0.25$ and a wavelength of 1064 nm (this g -value is not appropriate for tissue but the rate of TPE in focus is pretty independent of g for $g \leq 0.9$, so the results are interesting anyway). The number of scattering events was investigated for the fix value of $N.A. = 0.25$. For weak scattering, when $n \leq 2$ the peak of the two-photon excitation was confined in the focal region. However, for $n \geq 4$ the excitation peak in the focal region decreases and the intensity near the surface increases, which confirmed the results of Ying *et al.* [38]. Finally, for $n = 8$ the intensity near the surface becomes higher than the intensity in the focus. The effect of the numerical aperture was studied for $n = 4$ and the result showed that a higher numerical aperture gives a stronger and more narrow peak in the focal region. The unwanted two-photon excitation near the surface was also decreased by the higher $N.A.$ [39]. However, Monte Carlo simulations, based on Gaussian optics, done by Blanca and Saloma [40], showed that a lower fraction of photons reach the focal spot area for *high* numerical aperture, than for low. The photon *concentration* is anyway higher for larger $N.A.$, due to the smaller focal region.

4.3.2. Absorption in tissue

The absorption of light in tissue is also a limiting factor. Both unwanted one-photon and multiphoton absorption can occur. The one-photon absorption causes heating and depends on the average power, or rather energy. The multiphoton absorption of chromophores can part from heating also cause cell damage. The problem of heating by absorption can be divided into two parts; heating in focus, and heating outside focus. The heating by linear absorption, in the focus of an objective lens, has been investigated by Hell *et al.* [41]. They found that the local temperature increase of water was 0.2 K, when exposed by light with 100 mW of 850 nm for 1 s. From this and other results they came to the conclusion that heating is no limiting factor in standard multiphoton-excitation microscope, either for pulsed nor CW-lasers. However, for a higher average power, optical trapping in the sample cannot be ignored. For pulses in the femtosecond and picosecond ranges the increase of temperature does not depend on the pulse length [41]. In these case heat dissipation becomes too slow to cool off the focal area. Then the temperature increase, caused by absorption in focus, can be predicted by Gaussian models [41] and depends solely on the average power, P_{ave} .

The heating outside focus is, due to its linear behaviour, treated in the same way as in the light dosimetry for photodynamic therapy with single-photon excitation. Here the total light dose is calculated, which depends on the fluence rate, the illumination geometry and treatment time. The total light dose is equal to the total light energy density [Jcm^{-2}], delivered to the irradiated area. This is calculated as the product of the irradiance, or fluence rate [Wcm^{-2}], and the treatment time [s]. This parameter is easily interpreted for monochromatic, or narrow-band, light sources and guilty for superficial lesions, such as skin lesions. For example, in Lund, the standard treatment for non-melanoma malignant skin cancers with ALA-PDT is a total light dose of $60 Jcm^{-2}$ with an average power of $100 mWcm^{-2}$. The heating caused by linear absorption of the NIR light is, however, much smaller than for the case at 630 nm, because the low absorption in the optical window. Hence, it will be possible to deliver a higher light dose using NIR light.

The multiphoton absorption, however, in focus limit the peak intensity that can be used in photodynamic therapy. If other chromophores than photosensitisers are excited, they may cause cell damage outside the lesions and the selectivity of the photodynamic therapy will then degrade. In order to preserve the selectivity the absorption of the photosensitisers must be significantly higher than that of the other chromophores. In other words, the two-photon cross section and the concentration of the photosensitisers must be significantly higher than those for the other chromophores. Because of the unwanted two-photon absorption of some chromophores the use of two-photon excitation in photodynamic therapy is restricted to a certain optical window. The lower limit of this window is determined by at what intensities the photosensitiser needs to be activated. The upper limit is determined by the induced cell damage not caused by the photosensitiser.

Chromophores (or endogenous cellular absorbers) that may be subject to two-photon absorption are, for example, the coenzymes NAD(P)H, flavins, and porphyrins. Excitation of these can result in the formation of destructive oxygen radicals, singlet oxygen or indirect DNA damage [42]. Further on, DNA itself and proteins can be excited by three-photon absorption. Nuclei acids have major absorption band at 260 nm and excitation of this band results in direct DNA damage [42].

At sufficiently high input light intensities the ground state of the chromophore may start to deplete. This will cause saturation effects and the excitation will no longer depend on the light intensity to the power of two. When saturation occurs, the tissue will be exposed to more light than needed. Thus saturation should be avoided, which limits the excitation power that should be used for two-

photon excitation. In turbid media, however, the scattering decreases the intensity so much that saturation effects are not likely to be present.

Another limiting factor is plasma formation, which occurs when the electromagnetic field is very strong and depends on the peak intensity and the pulse width [34]. The intensity threshold for plasma formation is in the range of some hundreds of gigawatts per square centimetre to some terawatts per square centimetre. At these intensities intracellular optical breakdown and plasma formation can occur, resulting in intense white luminescence and severe morphological damage, such as cell fragmentation [42].

4.3.3. Pulse-length dependence of photodamage

In two-photon imaging, the time average power, P_{ave} , has been considered as the main limiting factor [43]. Hence, the pulse width should be shortened to maximise the following equation (2.12):

$$\langle R(t) \rangle \approx \frac{4n}{ph^2 w^2} g_p Cd \frac{\langle P(t) \rangle^2}{ftl} \quad (4.7)$$

If the pulse repetition frequency, f , is kept constant then the two-photon excitation rate can be expressed as

$$\langle R(t) \rangle \propto \frac{\langle P(t) \rangle^2}{t}. \quad (4.8)$$

The use of shorter pulses has only been considered to be limited by the spectral width of the pulse. For a given average power a mode-locked laser can boost the signal by a factor 10^5 if the objective is compensated for dispersion. Moreover, the repetition rate has been considered not to exceed the inverse lifetime of the dyes. An appropriate repetition rate should then be around 125 MHz for typical fluorescence lifetimes of 0.5–8 ns [44].

The reason why P_{ave} has been taken as a limiting factor is because the photodamage was believed to be of a linear nature, like heating (of water) through linear absorption and optical trapping. However, if high order effects limit the excitation intensity, such as the unwanted excitation of chromophores, ultrashort pulses do not bring any advantages. Further on, if the limiting effects display a cubic or high-order dependence, shorter pulses are a disadvantage.

This pulse length dependence of the cell damage has been studied in multiphoton microscopy. The results from this area can be helpful in photodynamic therapy as well. The cell damage has been studied by König *et al.* [42, 45] and they found that the damage follows the two-photon P_{ave}^2 / t relation (see equation 4.7 and 4.8). Hence, the damage decreases with increasing pulse length. When König, So *et al.* [45] studied the autofluorescence in the mitochondria owing to the presence of fluorescent coenzymes, they found that the threshold for cell damage is somewhere around 10^{11} W/cm² corresponding to 10^{31} photons/cm²s for a laser with 80 MHz PRF and 150 fs pulse length.

Fisher *et al.* [13] summarised various publications about the pulse-length dependence of the photodamage in the diagram in figure 4.4. However, the thresholds given in this diagram might be

higher than the actual values, which is seen when putting the just mentioned value of König *et. al.* in the diagram (10^{11} W/cm², 150 fs).

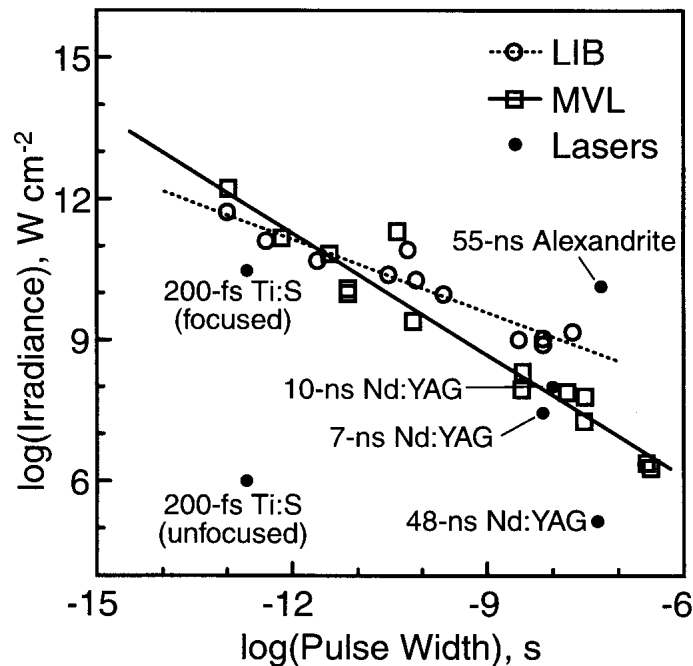


Figure 4.4 Comparison of laser pulse properties relative to laser-induced damage threshold (LIB) and minimum visible lesion threshold (MVL). Least-squares fit lines for LIB (dashed line) and MVL (solid line) are also shown. (From reference [13].)

The use of picosecond pulses in two-photon imaging was studied by Bewersdorf and Hell [44]. In their experiment they used a Nd:YVO₄ laser that has 7.1 ps long pulses and a repetition frequency of 200 MHz or 400 MHz (two lasers). The temporal gap between the pulses was then in the same order as the fluorescence lifetime of the dye used but saturation effects played only a minor role in the experiment. Their conclusion was that it is possible to provide two-photon images, when using lower pulse intensity, longer pulses and higher repetition rate than the standard Ti:Sapphire laser has. However, they thought that it is probably difficult to achieve good results in applications, where up to 300 mW of average power of 100–300 fs are required.

Experiments with CW-lasers in two-photon imaging have also been performed. Hell *et al.* [46] studied the UV-absorbing nuclear stain DAPI. They used a Scanning near-field optical microscopy (SNOM) setup with an uncoated optical fibre drawn to ca 50 nm radius, which served as an efficient probe for both excitation of the sample and collection of the fluorescence. The exposure of CW-laser resulted in morphological changes such as rounding up and shrinkage. Similar phenomena also occur in conventional single-photon UV microscopy. The power of 100–200 mW in CW TPM corresponds to ~1 mW of pulsed excitation. The images generated at these powers are 10 times fainter than those generated in the pulsed mode of 3–4 mW of power. The conclusion drawn by Hell *et al.* [46] was that the use of CW-lasers in two-photon microscopy (TPM) has advantages, compared to the use of pulsed lasers or UV excitation, with regard to system simplicity, maintenance and cost. On the other hand, it will almost not be possible to perform deep imaging with fast far-field CW-TPM in strongly scattering media [47].

5. Experiments

Two main experiments were performed. They were studies of two-photon induced fluorescence and one-photon fluorescence in tissue phantom, respectively. Below the description and analysis of these two experiments, some theoretical calculation considering two-photon excitation in turbid media follows.

5.1. A study of the variation of two-photon induced fluorescence as a function of depth in tissue phantoms

One advantage with TPE in PDT is the possibility to activate sensitizer with wavelengths in the *optical window* of tissue (see section *Two-photon excitation in photodynamic therapy*, chapter 3). In this spectral region tissue has considerably lower (linear) absorption, and the light can propagate deeper. The treatable depth for TPE PDT is mainly determined by scattering (see above, or chapter 6), that therefore limits the depth at which two-photon photodynamic effects can be achieved. Hence it is of great interest to study the efficiency of TPE (accomplished with laser light of suitable wavelength) as a function of depth in turbid media. Remarkably enough very few such studies have been performed (or at least been published), and for experiments down to a depth of the order of millimetres, we are only aware of one study (Ying *et al.* [38]).

The idea of our experiment is to use a small fluorescing ball, corresponding to for example a small tumour doped with photosensitizer, placed in tissue phantom. The fluorescing ball is, in turn, attached on the tip of an optical fibre, guiding the light to a photomultiplier tube. The idea is then to stepwise move the dye ball deeper into the tissue phantom and at every depth optimise the signal by adjusting the focal depth.

This way of detection of two-photon fluorescence in the immediate vicinity of the fluorescing region, deep inside the tissue phantom, is not the same as used by Ying *et al.* in reference [38] (described above), and as far as we know no one has performed such an experiment before!

5.1.1. Setup and materials

The experimental setup is schematically shown in figure 5.1.

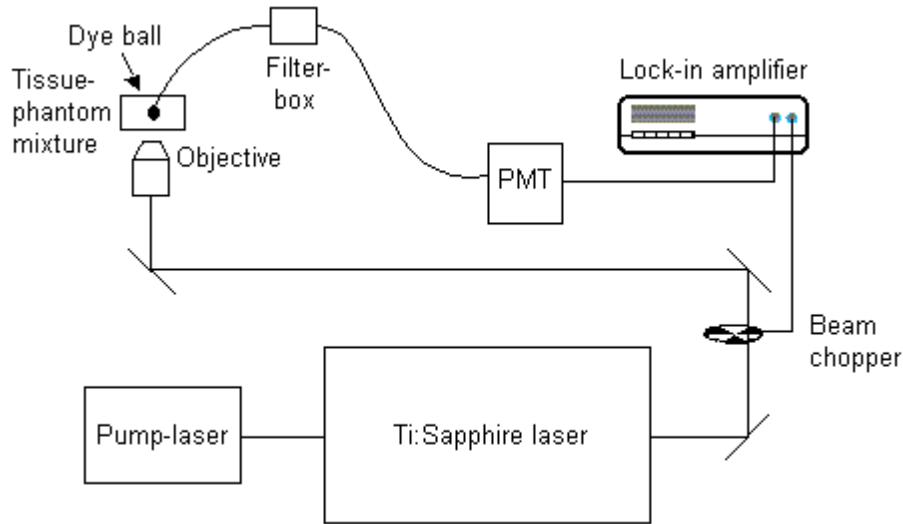


Figure 5.1 Schematics of the experimental setup for the two-photon excitation experiment.

The laser source used is a Kerr-effect self mode-locked titanium-sapphire laser (a “Mira 900” from Coherent), pumped by a continuous wave Nd:YVO₄ crystal (diode-pumped) solid state laser (“Millennia V_s” from Spectra-Physics), giving 5 W power at 532 nm. The Ti:Sapphire laser produces pulses with FWHM of approximately 150 fs, with a pulse repetition frequency of 76 MHz. The wavelength of the laser light is centred at 792 nm (approximately 10 nm broad).

A microscope (Nikon “Inverted Microscope Diaphot 300”) was used to focus the laser beam and to position the focus in three dimensions. Thus only its objective holder, the corresponding focus adjustment, and its stage where used, the later as an “x-y-positioner”. No microscopy was done.

A fluorescence objective with long working distance, approximately ten millimetres, was utilised to focus the laser beam into the tissue phantom solution, placed on the microscope stage. The objective was an Olympus “LMPlanFI” (infinity corrected), with 50 times magnification and a numerical aperture of 0.50.

An optical fibre was used to pick up the signal. It was mounted on an optical fibre holder (on the microscope stage), attached to a micrometer positioner for “z-positioning”. The optical fibre (600 μm in diameter) was placed in an angle of about 30° with respect to the z-axis; the latter defined as straight vertically from the stage. The tip of the fibre had a small fluorescing ball, with a diameter of about 1.5 mm (see below for details on its preparation), attached to it. See detailed view, figure 5.2.

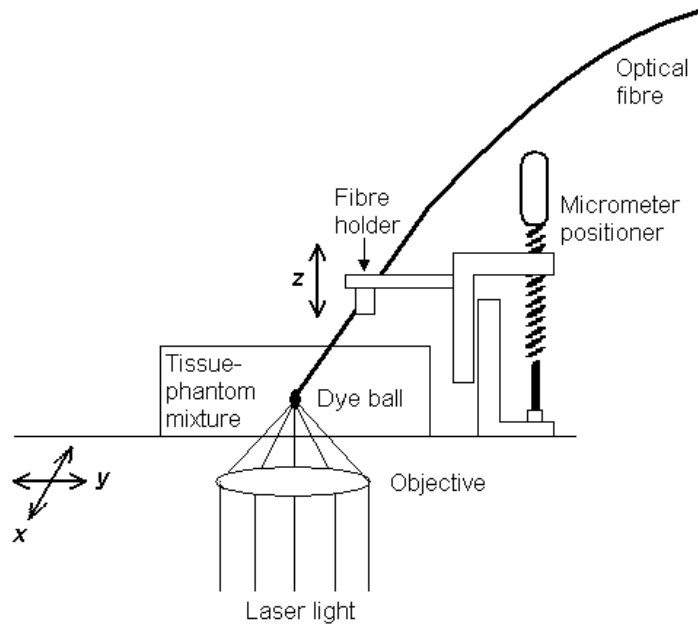


Figure 5.2 Detailed view of the system for positioning of the Rhodamine ball, in the experimental setup.

The fibre guided the fluorescence light to a “filter-box”. This box contained 4 mm Schott BG39 filter, completely blocking out any laser light (transmittance, t , less than $9 \cdot 10^{-5} / \text{mm}$ for the laser wavelength). Only the TPE fluorescence light passed the filter.

From the filter-box another fibre guided the light to a Hamamatsu R928 photomultiplier tube (PMT) built into a light shielding box. This detector was then connected (via a coaxial cable) to the lock-in amplifier (Stanford Research Systems “Model SR830 DSP”). A lock-in reference signal was produced with a mechanical chopper (chopping frequency: $617 \pm 2 \text{ Hz}$). Note that even though dealing with a pulsed laser signal, the high repetition rate, corresponding to a pulse separation of about 13 ns (still one order of magnitude greater than typical decay times of fluorescing dye molecules), implies that some more than sixty thousand pulses pass every chopper opening. Hence it is legitimate to consider the laser beam as being continuous, relative to the “beam chopping”.

The fluorescing ball

The dye Rhodamine B (chloride), also known as Rhodamine 610, (*o*-(6-Diethylamino-3-diethylimino-3H-xanthe-9-yl)benzoic acid, $\text{C}_{28}\text{H}_{31}\text{N}_2\text{O}_3\text{Cl}$), has a strong two-photon absorption cross section for excitation wavelengths around 792 nm ($d \approx 125 \cdot 10^{-50} \text{ cm}^4\text{s}/\text{photon}$ according to Xu and Webb [15]). Hence it was the choice as fluorophore in our experiment. In appendix 3 a one-photon absorption spectrum, a one-photon emission spectrum, and a two-photon fluorescence spectrum of Rhodamine B, are shown.

Some Rhodamine B was solved in ethanol (ethanol solution: approximately 30% ethanol and 70% water), giving a dye molar concentration of approximately 1.15 millimolar (mM). Some “drops” of this solution were mixed together with a little *Epoxy* glue (“Araldit Rapid” from Casco), and then the corresponding hardener, of about the same amount as the glue, was mixed in. Before the mixture had hardened, it was formed to a small ball on the tip of the optical fibre. Thereafter the ball was further overdrawn with Rhodamine solution. Finally the ball was left to harden.

5.1.2. Tissue phantom preparation

In order to make a tissue phantom, a mixture consisting of 5.4% Intralipid infusion liquid (200 mg/ml; from Fresenius Kabi) and 94.6% distilled water was prepared.

Three different Rhodamine B solutions of concentrations ranging from 0.1 to 100 mM were produced, in the same manner as described above. These were diluted ten times when mixed together with Intralipid mixture (giving final dye concentrations ranging from 0.01 to 10 mM). The produced fluorescent tissue phantoms were similar to that used by Xu and Webb in their determination of two-photon excitation cross sections of molecular fluorophores [15]. They used a dye concentration of 0.1 mM.

Before the final experiment some “pre-tests” were performed. From these tests an Intralipid mixture with a dye concentration of approximately 0.1 mM was chosen.

5.1.3. Measurement procedure

The two-photon excited fluorescence signal from three different liquids was studied; “pure” Intralipid mixture, the Intralipid mixture with 0.1 mM Rhodamine B added, and a pure Rhodamine B solution in ethanol (unknown concentration). The liquids were contained in small polystyrene wells with plane bottoms (diameter 34.3 mm; wells specially made for cell growth). The laser light could then be focused through the bottom of the well, into the tissue phantom mixture.

In the experiment the fluorescing ball on the optical fibre was first immersed in the pure Rhodamine solution. The focus of the laser beam was then clearly visible, allowing gross adjustments of the fluorescent ball. Thereafter the ball was taken out from the pure dye solution, by translation along the z-axis only (no change of the x-y-position). Then the 0.1 mM Rhodamine B Intralipid sample was placed over the objective on the microscope stage, and the fluorescing ball was immersed in this phantom (still without any changing of the x-y-position). The ball was positioned on the optical axis of the laser beam so it just touched the bottom of the well. (After that it was only allowed to shift the fibre upwards, not downwards, in order to avoid any hysteresis in the micrometer screw.) The ball was then moved upwards, until it was located 0.50 mm above the well bottom. At this point the detected signal was again optimised; in the z-direction by using the focus adjustment wheel on the microscope; and in x-y-direction by moving the fluorescing ball. The maximum signal was noted. Thereafter the fluorescing ball was moved upward in steps of 0.10 mm (corresponding to an increasing depth of 0.10 mm in the medium). At each step the signal was optimised by adjusting the focus along the optical axis. No adjustments were now done in the x-y-plan. For depths between 0.5–1.40 mm, the time-integrating constant used for the lock-in amplifier was set to 300 ms. At greater depths the time-constant was increased to 10 seconds, because of the weaker signal at these depths.

After completing the measurements, the laser power at the sample (*i.e.* after the focusing objective) was measured to 0.7 mW.

5.1.4. Results

The results of the measurement are shown in figure 5.3a and figure 5.3b (logarithmic “y-axis”). The detected fluorescence signal is shown as a function of depth of the fluorescing ball in the tissue phantom. The setup allowed measurements of the fluorescence between 400 and 600 nm. The peak of the TPE Rhodamine B fluorescence is at 580 nm. This is at the same wavelength as the fluorescence peak in the SPE Rhodamine B spectrum. The depth is given in millimetres and the intensity in arbitrary units. (The unit used is actually the current, in nA, given by the lock-in amplifier.)

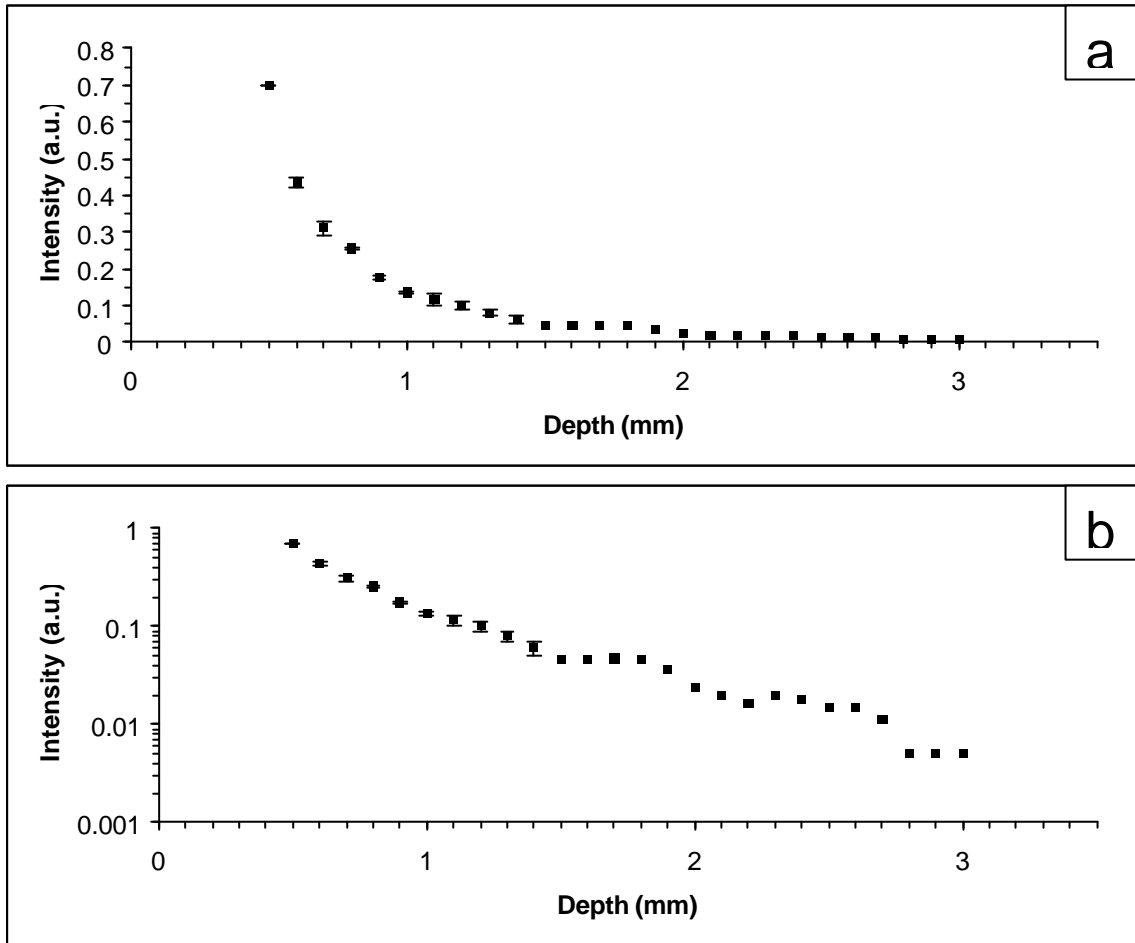


Figure 5.3 Detected TPE induced fluorescence in tissue phantom (Intralipid solution) with Rhodamine B, as a function of the depth of detection. a) Linear intensity scale. b) Logarithmic intensity scale.

The measurement errors of the depth are so small that they fall completely within every dot in the diagram, and therefore no error bars are shown in the “x-direction”. The intensity error bars shown for the points from 0.5 mm to 1.4 mm, illustrate the variation of the read-out value from the lock-in amplifier. The upper and lower bar represents the upper and lower “turning-points”. The arithmetic mean value of these has been taken as the “dot value” in the diagram. For depths below 1.4 mm, the time-integrating constant was increased and hence the signal become less noisy. The corresponding error bars thus completely fell within the diagram dots.

The intensity signal due to other causes than the laser light is less than 0.0005 in the arbitrary unit used. That is at least one order of magnitude lower than the points with the lowest intensity value.

5.2. A study of the variation of single-photon induced fluorescence as a function of depth in tissue phantoms

As a comparison to the TPE-signal variation with depth, a corresponding measurement for single-photon excitation was performed.

5.2.1. Experimental setup

The setup in this experiment was almost identical to the one described above. There were only a few differences. The laser used in this case, was a continuous wave krypton ion laser (“Innova 300” from Coherent), with a laser wavelength at 406.7 nm. The second distinction was that no objective was used. Hence, no focusing took place, and no focus adjustments were necessary. In the filter-box we now placed three 3 mm thick Schott GG435 long pass filter ($t \leq 1 \cdot 10^{-5} / 3 \text{ mm}$ for $\lambda = 406.7 \text{ nm}$), blocking the laser light at 406.7 nm.

During the measurement the laser delivered an output power of 22 mW. To reduce this, filters taking down the power approximately 60 times were placed in the beam path.

5.2.2. Measurement procedure

The optical fibre with the fluorescing ball was positioned in the beam path, above the microscopy stage (no well). The fluorescence was detected, while the signal was optimised by x-y-adjustment of the fibre. The x-y-position was then held fixed during the measurement. The time-integrating constant of the lock-in amplifier was set to 10 s. The Intralipid solution was then placed in position. In this series of measurements we started to measure at a depth of 10 mm, moving towards the laser. The fluorescence signal was measured at lots of locations. The lock-in signals did fluctuate considerably, so for each point of measure, the signal was observed for quite a long time (typically one minute), and the lowest and highest “turning points” were noted, respectively.

5.2.3. Results

The result of the measurement is shown in figure 5.4a and figure 5.4b (logarithmic “y-axis”). The detected signal of one-photon fluorescence is shown as a function of depth of the fluorescing ball in the tissue phantom. Note that the GG435 filters in the filter-box let pass most light above 435 nm. The emission peak of Rhodamine B is around 580 nm.

The depth is given in millimetres and the intensity is the same arbitrary units used above. The measurement errors are so small that they fell completely within every dot in the diagram, therefore no error bars are shown.

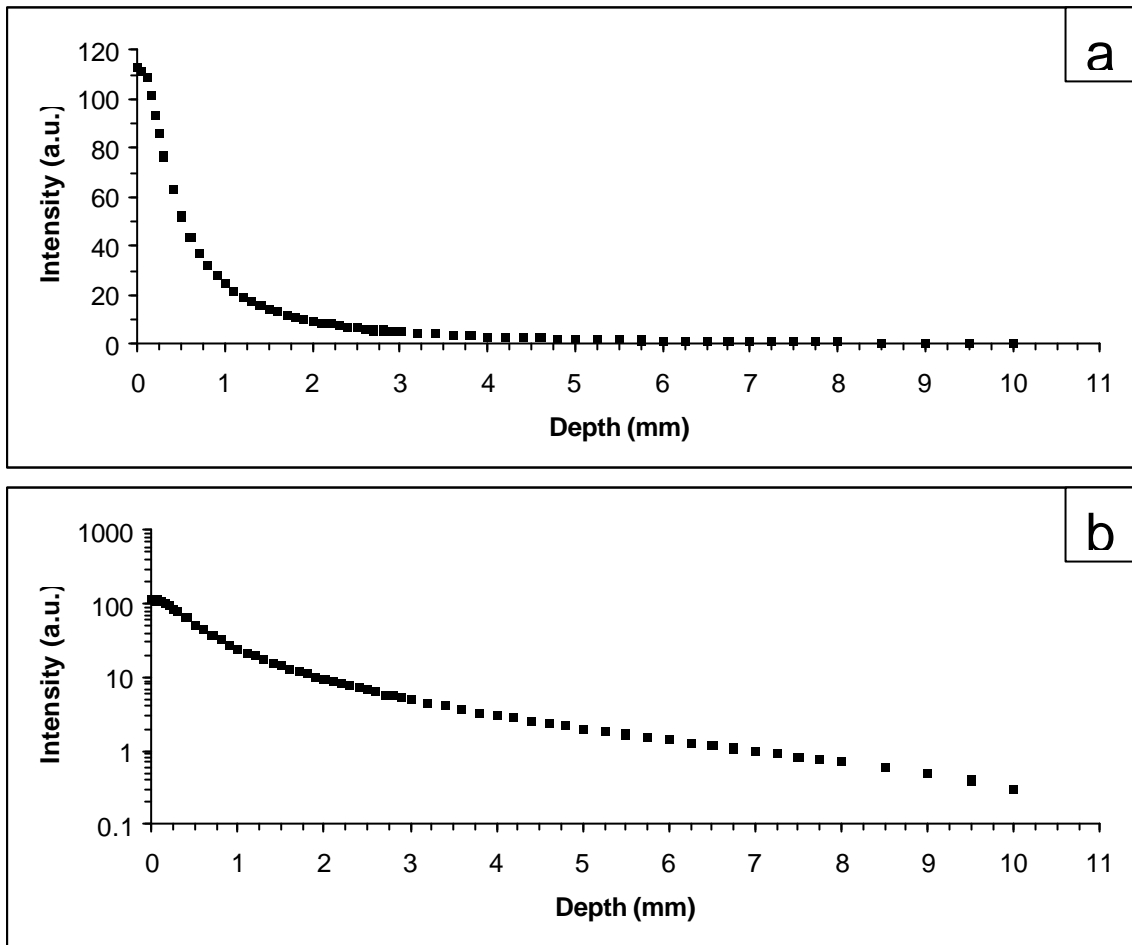


Figure 5.4 Detected single-photon excitation intensity within the Rhodamine B ball in tissue phantom (Intralipid solution), as a function of the ball depth. a) Linear view. b) Logarithmic view.

The intensity signal due to other causes than the laser light is less than 0.0005 in the arbitrary units used. That is at least three orders of magnitude less than the lowest signal detected.

5.3. Measurement of optical constants in the tissue phantom mixtures

The scattering coefficient (μ_s), absorption coefficient (μ_a), and g -factor of the tissue phantoms were measured at wavelengths of 790, 580 and 410 nm, respectively, using an integrating sphere system. The instrument and the measurement procedure are presented in reference [48]. The results of these measurements are shown in table 5.1.

Table 5.1 The measured optical properties of the tissue phantoms at different wavelengths. Note that the values for $\lambda = 410$ nm are uncertain, because two experimental setup parameters were not known for this wavelength, and reasonable guesses had to be applied for those.

Wavelength	Intralipid mixture			Intralipid mixture with Rhodamine B		
	m_t	m_s	g	m_t	m_s	g
790 nm	0.024 mm ⁻¹	2.61 mm ⁻¹	0.67	0.028 mm ⁻¹	2.39 mm ⁻¹	0.69
580 nm	0.024 mm ⁻¹	6.49 mm ⁻¹	0.77	0.077 mm ⁻¹	4.84 mm ⁻¹	0.69
410 nm	0.037 mm ⁻¹	6.11 mm ⁻¹	0.63	0.071 mm ⁻¹	5.00 mm ⁻¹	0.66

5.4. Experimental analysis and discussion

In the following paragraphs the two-photon induced fluorescence intensity versus depth measurements is analyzed. Important for this analysis is that in these experimental cases as well as in most real tissue (for wavelengths in the near-infrared region), scattering is dominating over absorption. A more general discussion about scattering and absorption effects in connection to TPE and TPE PDT is also given below.

5.4.1. Analysis of the two-photon excitation induced curve

The detected two-photon excitation induced fluorescence, as a function of the depth of the dye ball in the tissue phantom is shown in figure 5.3a and 5.3b.

Firstly, we note that TPE fluorescence signals could be obtained both from the ball and from the liquid. The optimisation of the signal at 0.5 mm depth was extremely sensitive to x-y-adjustments, *i.e.* there was a very strong dependence on the relative location of focus. Hence, the inference must be that the detected signal in this position probably was dominated by two-photon fluorescence from the Rhodamine ball.

Secondly, it can be noted (see *Two-photon excitation in turbid media*, chapter 6), that when the focusing depth reaches 4–6 times the length of the scattering mean free path, the two-photon fluorescence near the surface of the sample becomes as high as the one at focus. This number of mean free path lengths was obtained for a numerical aperture of 0.25. In our study a lens with *N.A.* of 0.50 was used, and as discussed in *The optical system*, chapter 4, and in chapter 6 below, a higher *N.A.* will increase this depth. In the experiment the scattering coefficient (at $\lambda = 790$ nm) was measured to 2.39 mm⁻¹. This corresponds to a scattering mean free path length of 0.42 mm, which taken four to six times yields some 1.7 to 2.5 mm.

According to the experimental idea, the thought was to optimise the detected signal by changing focus. If it was true that the two-photon fluorescence at focus was higher than the fluorescence close to the surface, down to a depth of at least 1.7 mm, then the maximum detected signal would be achieved with the fluorescent ball in the focal point, down to a depth some greater than 1.7 mm. (At 1.7 mm the intensity of fluorescence *in the ball* would be as high as the intensity of the fluorescence *at the surface*. However, fluorescent light originating from the surface region

attenuates, while propagating from the surface to the dye ball. Hence, the *detected* signal would be dominated by two-photon fluorescence from the ball down to a greater depth than 1.7 mm.)

Suppose this was true in the actual experiment, and that the fluorescence at the region of detection (*i.e.* at the optical fibre tip), was predominated by fluorescence induced in the ball region, rather than fluorescence at the position of the beam entering the tissue phantom. Thus one can assume, to a first approximation, that the detected signal is proportional to the fluorescence in focus, as far as the depth is less than at least the 1.7 mm mentioned above. Under these conditions it is possible to apply the formula used by Ying, Liu and Alfano [38], describing the intensity distribution, holding for a Gaussian beam, when the linear absorption could be ignored:

$$I(\mathbf{r}, z) = I_0 \left(\frac{w_0}{w(z)} \right)^2 \exp\left(-\frac{2\mathbf{r}^2}{w^2(z)} \right) \exp(-\mathbf{m}_s(z + z_s)) \quad (5.1)$$

The peak intensity at the focal plan, defined by $z = 0$, is symbolised with I_0 ; $w_0 = \sqrt{I_{z_0}/p}$ and $w(z) = w_0 \sqrt{1 + (z/z_0)^2}$, where z_0 (called the *confocal parameter*) is defined as the distance (along the z-axis) from the centre of focus to where the beam waist is $\sqrt{2}$ times the beam waist in the focal plan, w_0 ; z_s is the depth of focus inside the sample. The dependence of the numerical aperture is implicitly included in the parameter z_0 , and hence also in w_0 . The intensity squared, $I^2(0, z)$, along the z-axis, has then the following proportionality condition:

$$I^2(0, z) \propto \frac{1}{\left(1 + \left(\frac{z}{z_0} \right)^2 \right)^2} \exp(-2\mathbf{m}_s(z + z_s)) \quad (5.2)$$

Ignoring the radial distribution; by using \mathbf{r} equal to zero; equation (5.1) can be modified to our situation. Then z has to be set to zero, because the ball was always placed in the focal point (at which $z = 0$). Expression (5.2) then takes the simple form

$$I_{\text{TPF}}(0, z_s) = I^2(0, z_s) \propto e^{-2\mathbf{m}_s z_s}, \quad (5.3)$$

where z_s is the distance between the surface of the medium and the focus point (I_{TPF} is the intensity of the two-photon fluorescence).

The distance z_s can be written as $z_d + z_b$, where z_d is the depth as measured in the experiment, and z_b is the, supposed constant, axial depth *inside* the Rhodamine ball, at which the centre of focus is located. Because the latter parameter is constant, it only contributes with a constant factor in front of equation (5.3), and can therefore be included in the proportionality constant. Hence, we apply the following expression to the mathematical analysis of the measurement:

$$I_{\text{TPF}} \propto e^{-2\mathbf{m}_s z_d} \quad (5.4)$$

Using the scattering coefficient measured with the integrating sphere (for $\lambda = 790$ nm), a least square fit of (5.4) to the measurement series is shown in figure 5.5a and 5.5b. The absolute intensity is the only parameter fitted. The equation fits well for the first three points, but degrades drastically for greater depths. As can be seen in figure 5.7 below, if only including the first points

to the fit, good agreement is obtained down to a depth of 0.8 mm (but not deeper). From this it is inferred that the theoretical model likely is valid down to a depth of perhaps 0.8 mm, but not for greater depths.

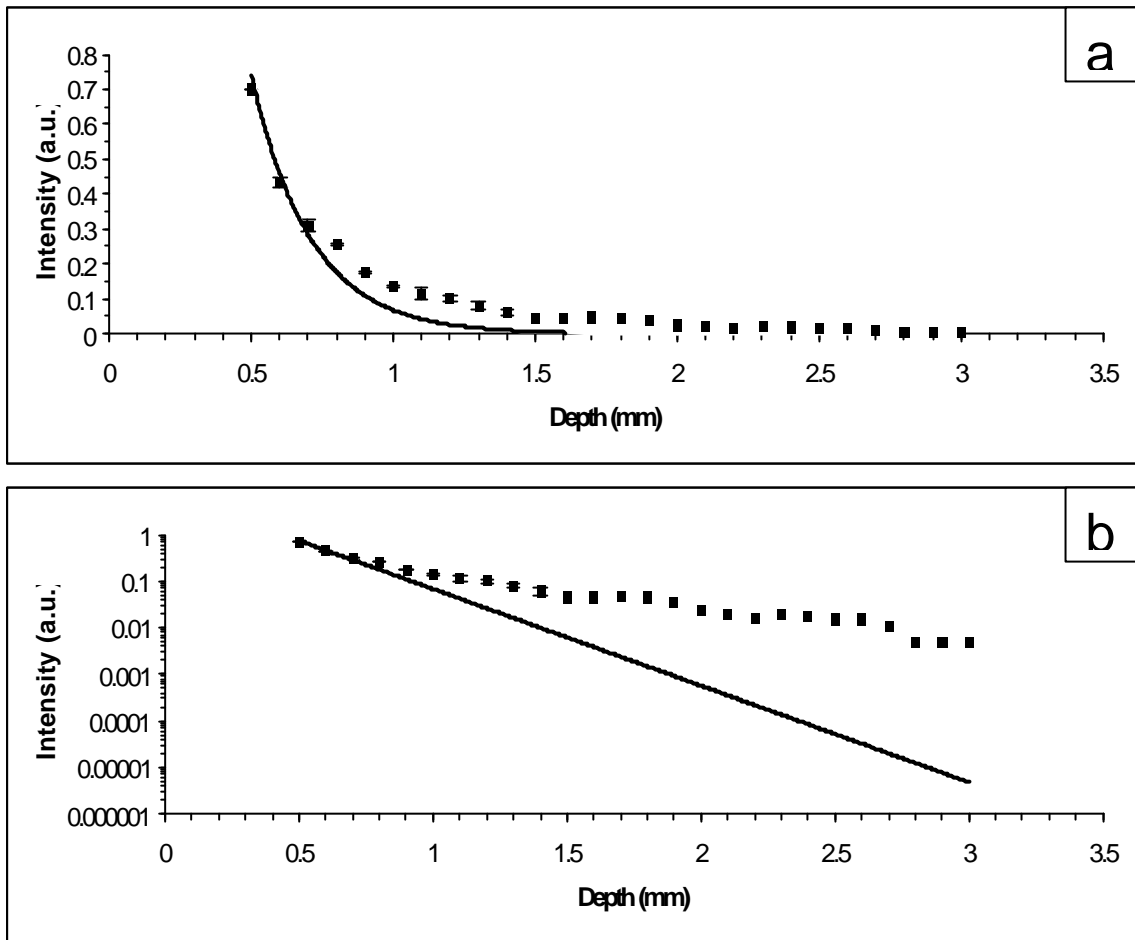


Figure 5.5 An exponential curve corresponding to expression (5.4), with the absolute intensity fitted, is plotted together with the experimental result of the two-photon induced fluorescence measurement. Figure a shows a view with linear intensity scale; figure b shows one with logarithmic scale. Note the good resemblance between experiment and theory close to 0.5 mm.

There are several reasons that could explain this discrepancy for depths below 0.8 millimetres. One explanation could be measurement errors. In the experiment the actual depth of focus was not measured; the goal was just to optimise the signal strength for each position of the fluorescent ball. Hence, it is a possibility that the point of focus was located somewhere else in the phantom, than at the place of the ball. In this situation (5.4) would not be valid. Note also other experimental complications, *e.g.* the dye concentration in the ball is unknown (relative to the concentration in the phantom-mix).

Another likely explanation, is that light originating from two-photon fluorescence in Rhodamine molecules in the phantom-mix (in contrast to the dye ball) closer to the surface, takes over the fluorescence dominance from focus (at the ball), already at a depth of about 0.8 mm. The results by Ying *et al.* indicated that the *total integrated fluorescence* from the region near the surface was greater in the experiment than what could be expected from expression (5.4) for greater depths. Their experimental results also indicated that the total integrated fluorescence from the region near the surface was greater than the one in the focal region. Hence, it would not be so

surprising if the detected fluorescence mainly originates from regions close to the surface, and not from TPE in the dye ball, already at depths beyond 0.8 mm.

A model for the detected fluorescence when the fluorescent ball is positioned deeply inside the medium has not been worked out. Such a model would probably show a rather great complexity with fluorescence contributions both from the ball and the medium. The model has to handle both the light transport to the regions contributing to the fluorescence and from these regions to the optical fibre guiding the light to the detector.

However, one of the simplest attempts to analyse the detected signal for the depths below 0.8 mm, can be tested. That is to approximate the fluorescing region as a point source within a homogenous infinite medium (thereby ignoring every boundary effects), and applying the solution to the diffusion equation* for such geometry. This equation is given by [49]

$$I(r) \propto \varphi(r) = \frac{P\mu_{eff}^2}{4\pi\mu_a} \frac{1}{|\vec{r}|} e^{-\mu_{eff}|\vec{r}|}. \quad (5.5)$$

Here, $I(r)$ is the intensity of the TPE fluorescence as a function of the distance passed in the media (r), and $\varphi(r)$ is the photon fluence rate; P is the power of the TPE fluorescence light. The coefficient μ_{eff} is given by

$$\mu_{eff} = \sqrt{3\mu_a(\mu_a + \mu'_s)}. \quad (5.6)$$

The optical property coefficients are constant (for constant wavelength), so for constant P equation (5.5) can be written as

$$I(r) \propto \frac{1}{|\vec{r}|} e^{-\mu_{eff}|\vec{r}|}. \quad (5.7)$$

It is obvious that the conditions under which this equation normally holds are not quite fulfilled; the fluorescing region is not a point source, but has a finite distribution; the medium is not homogenous, due to that the size of the dye ball is comparable to the distance between the sample surface and the ball itself, and these two media are different (and the optical properties of the ball is in fact unknown); the sample medium is not infinite in size, it rather got a *slab geometry*, or possibly a *semi-infinite geometry*; the distance between the sample surface and the tip of the detecting optical fibre is only a few times greater than the scattering mean free path, and therefore boundary effects probably would affect the recorded signal. Further, the fluorescence consists not only of one wavelength, but rather of a spectral interval ranging from around 400 nm and up (confer diagram A3.3 in appendix 3), with a peak at 580 nm. Hence μ_{eff} is not constant. However, because the formula is so very easy to work with, it is a first choice to apply, when no more appropriate mathematical model exists.

As one more simplification $|\vec{r}|$ (in (5.7)) is set equal to the experimentally measured depth of the ball. The affect of this approximation is reasonably small in the experimental case.

* The diffusion equation is valid when the reduced scattering coefficient $\mu'_s = \mu_s(1 - g) \gg \mu_a$, which is the case in this experiment.

In figure 5.6 one can see a curve of the form

$$I = \text{constant} \cdot \frac{1}{z_d} e^{-m_{\text{eff}} z_d} \quad (5.8)$$

adjusted to the experimental curve (m_{eff} corresponding to $\lambda = 580 \text{ nm}$ has been used, because the fluorescence peak of Rhodamine B is located at this wavelength). As seen, the resemblance of the two curves is not striking, but at greater depths it looks real good. This is a very rough model that is expected to be valid only at great depth in the medium – only at depths where the two-photon fluorescence at focus at the dye ball is out-ruled in the total detected signal. In fact, if the same fit is performed over the depth interval 1.5 to 2.5 mm only (the deepest points have been left out because the detected intensity from these positions were comparable with the background noise), the curves are in very good agreement with each other. (In fact, the fit in figure 2 has been adjusted to the interval of depth between 1.5 and 2.5 mm. The fit has then been extrapolated.) This indicates that at greater depth, corresponding to more than approximately four scattering mean free paths (1.7 mm in this experiment), the signal is dominated by fluorescence originating from near the sample surface. This result is, in fact, similar to other studies, referred to above and in chapter 6.

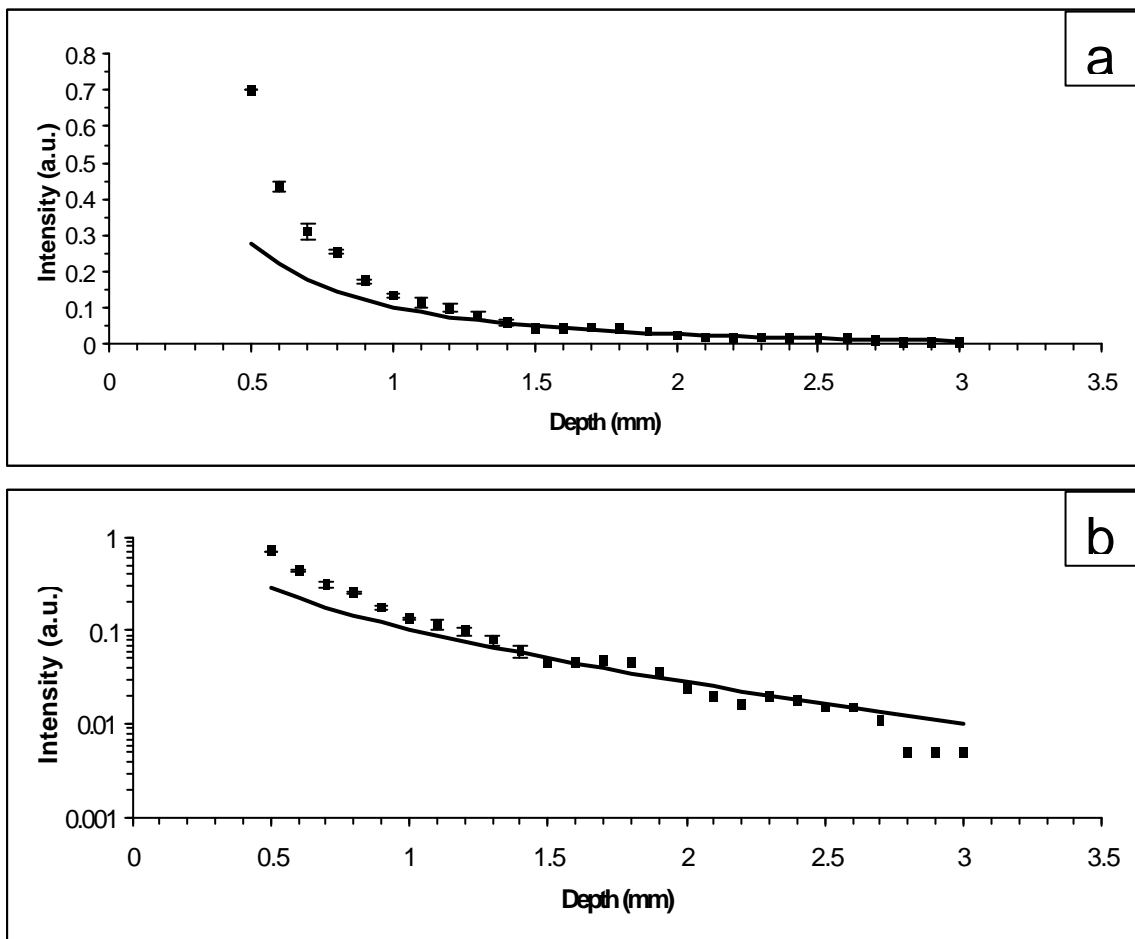


Figure 5.6 The figure shows again the experimentally measured points. Here a solution to the diffusion equation ((5.8)) has been applied, shown as solid curve. The absolute intensity has been used as the only free parameter, in order to perform a least square fit to the depth interval between 1.5 and 2.5 mm, and then extrapolation of this curve to the whole interval (0.5–3.0 mm) has been done. Figure 2a gives a linear “y-axis”, 2b a logarithmic. As seen, the resemblance between the curve and the measured points is good at greater depths, but bad for the most superficial points.

In figure 5.7 both the curve fit of (5.4), for depths between 0.5 and 0.8 mm, and of (5.8), for depths between 1.5 and 2.5 mm, are shown.

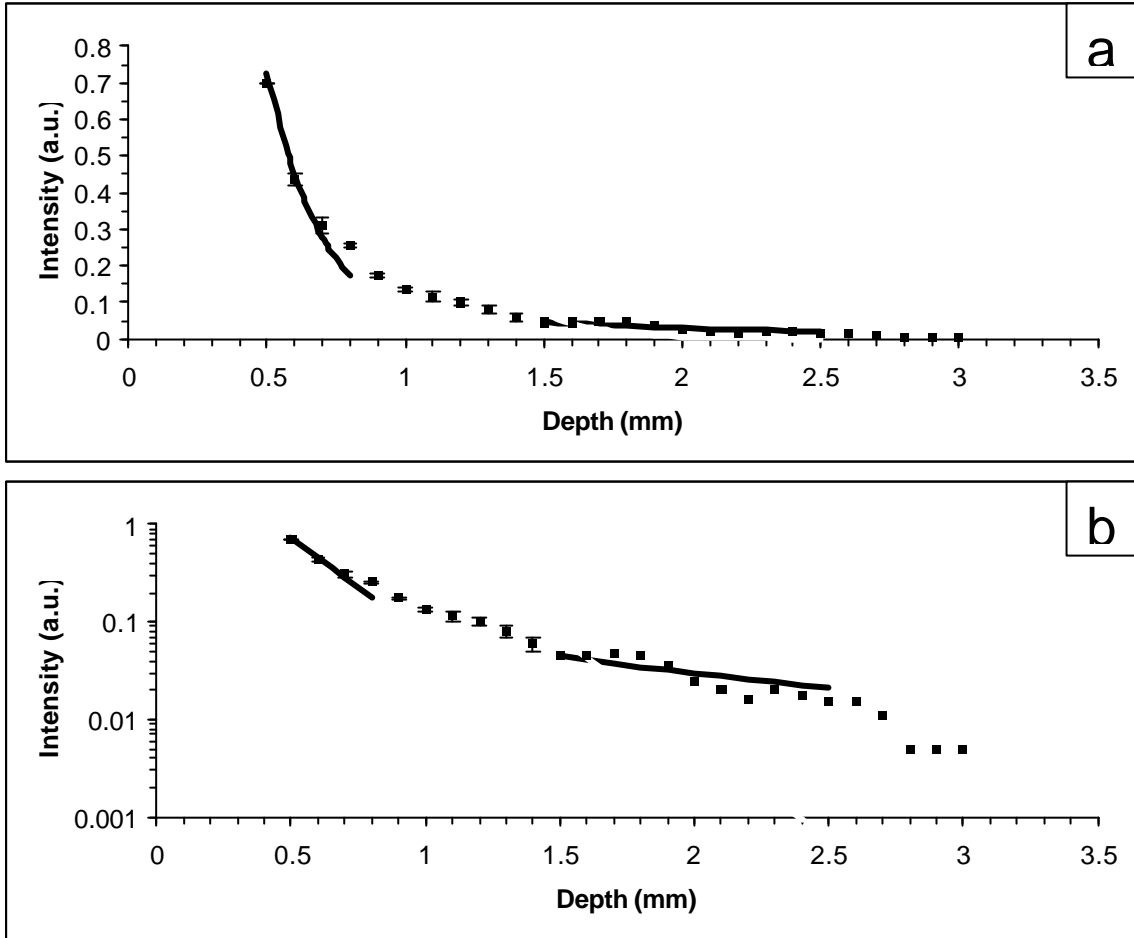


Figure 5.7 This figure shows two different curves. In the interval of depth from 0.5 to 0.8 mm expression (5.4), supposed to hold for TPE in the fluorescing ball, is adapted. In the interval 1.5 to 2.5 mm expression (5.8) is plotted. That expression is supposed to be (roughly) true, if TPF close to the sample surface dominates the detected signal. Note that the two different kind of curves both fits well in their intervals, respectively. Logarithmic intensity is used in the b figure.

Finally, equations (5.4) and (5.8), were combined to one formula according to the following:

$$I = c_1 e^{-2m_s z_d} + c_2 \frac{1}{z_d} e^{-m_{eff} z_d} \quad (5.9)$$

The two constants c_1 and c_2 were used as free parameters in a least squares fit. The result is shown in figure 5.8 and indeed there is a very good match between the curve based on equation (5.9) and the experimental values. However, it is yet not really clear what conclusions can be drawn from this theoretical model, but it supports our belief about that the detected intensity is a combination of fluorescence in the ball and fluorescence from regions close to the sample surface. The adjusted values of the constants in equation (5.9) is 4.49 and 0.18 for c_1 and c_2 , respectively. For further analysis it might be interesting to compare these values to the values of the corresponding constants in figures (5.5) and (5.6), which were 8.09 and 0.36, respectively. However, this has not been performed yet.

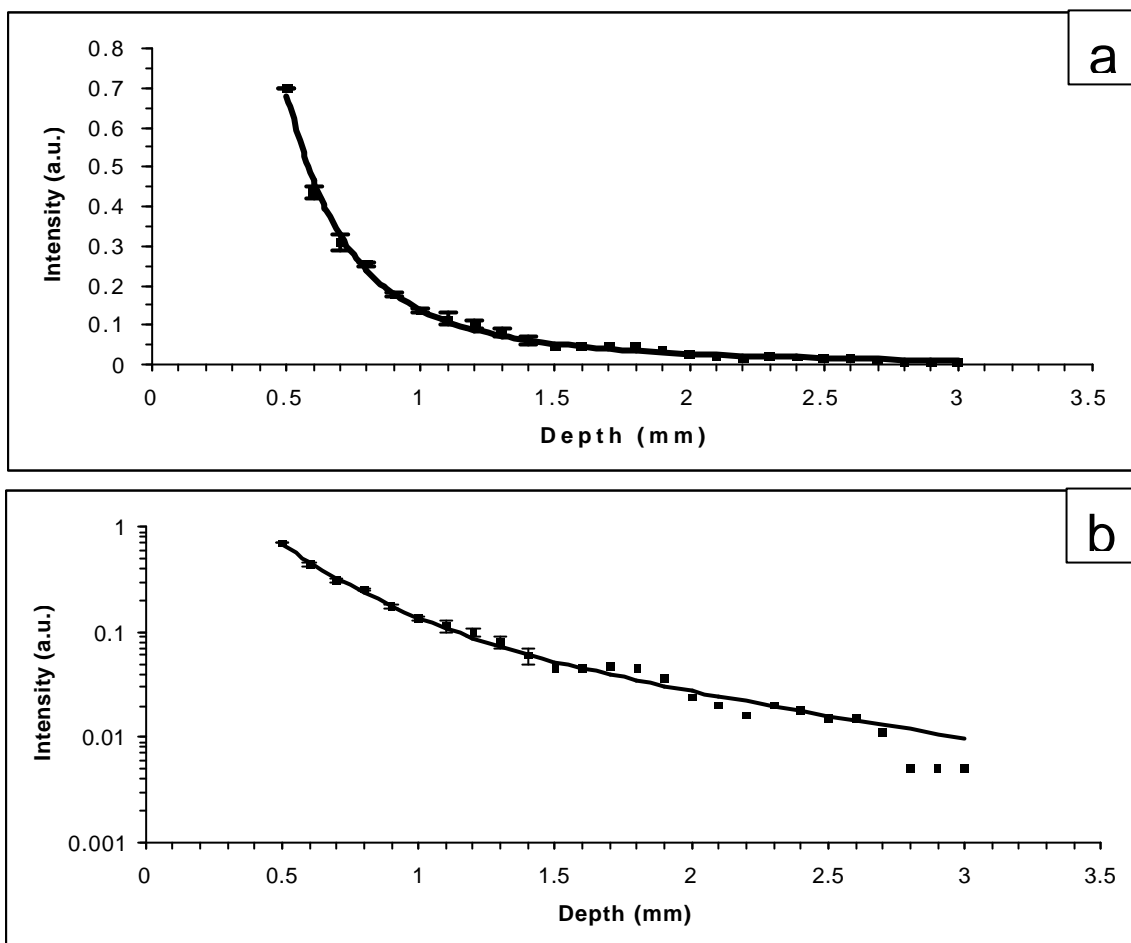


Figure 5.8 The combined expression (5.9) fitted to the measurement series. Linear intensity scale in a, logarithmic intensity scale in b.

In conclusion, we believe that the detected signal is dominated by two-photon fluorescence in the Rhodamine ball, down to a depth of perhaps 10 mm. At greater depths will the fluorescence originating from two-photon excitation close to the surface of the sample take over the dominance.

5.4.2. Analysis of the one-photon excitation curve

It was shown in figure 5.4 how the detected fluorescence in the dye ball varied with depth for single-photon excitation (SPE) at 406.7 nm, varied with depth. We have again tried to fit the solution of the diffusion equation for the simplest possible geometry to this experimental curve. The experimental situation in this case is again quite different from the assumptions necessary for the theoretical derivation. Nor in this case the assumption of a point source is especially good; the source is a relatively broad (approximately) Gaussian laser beam entering the sample boundary. The medium is not infinite either. The experimental geometry is the one of a slab, or approximately of a semi-infinity here too. Opposite to the other experiment, in this one the light source is outside the medium.

In figures 5.8a and 5.8b, the measured signal has again been plotted (linear and logarithmic view, respectively), now excluding the points within the first three millimetres, nearest the surfaces of the sample (the two “slab boundaries”), in order to avoid boundary effects. A least square fit to

the experimental curve, using the diffusion equation solution (5.8), is also shown. The values for m_u and m_s (0.037 and 6.11 inverse millimetres, respectively) were independently obtained from the integrating sphere measurement (for $I = 410$ nm). The absolute intensity was the only fitted parameter. As seen from the figure there is a quite good, but far from perfect, resemblance between theory and experiment. The discrepancy might be due to that the theoretical formula (5.8) is not valid, or to the fact that for the fit $|\vec{r}|$ has been set equal to the depth of the top of the ball, not to the distance from the surface to the focus point *within* the ball. It might also depend on some experimental artefacts. For example, the optical properties used in the fit are somewhat uncertain. This is because two experimental setup parameters of the integrating sphere system used are unknown for so short wavelengths as 406.7 nm. Therefore some assumptions have been applied to achieve approximate values of the optical quantities. There are reasons to believe that especially one of these two parameter value guesses is more or less erroneous. If so, it is pretty likely that the obtain values of m_u and m_s is greater than they should be. This is believed to contribute to the discrepancy between the measured and the fitted curve. Anyway, the important thing is that the solution to the diffusion equation (5.5) (or equation (5.8)) does provide a quite good comparison to the experiment, and hence can be used as a very simple approximate model for the same.

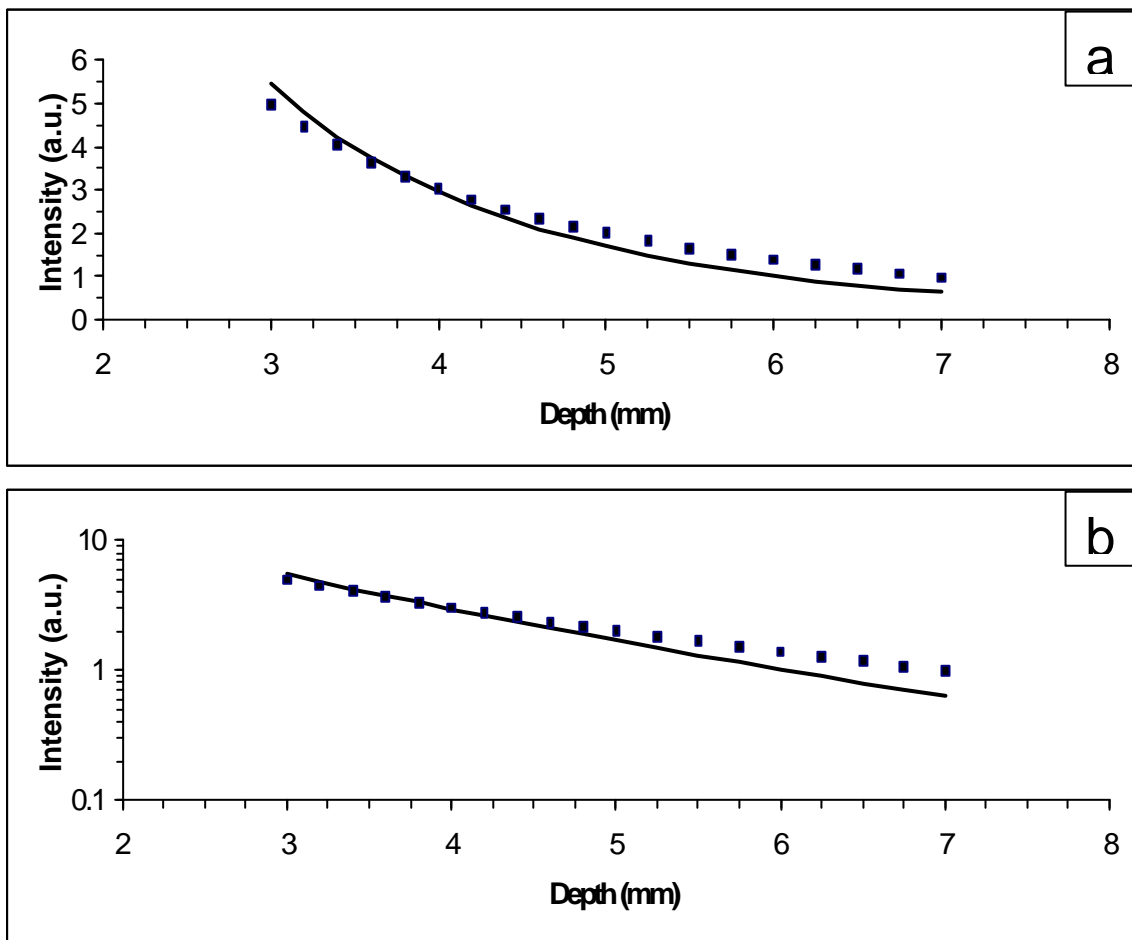


Figure 5.9 A solution to the diffusion equation ((5.8)) has been adjusted to the one-photon excitation points by means of a least square fit with the absolute intensity as the only fit parameter. Linear and logarithmic scale in a and b, respectively.

Interesting to note from this analysis, is that a curve based on the diffusion equation of the more complex geometry of a point source illuminating a semi-infinite homogenous medium (see reference [49]), assuming only detection along the z-axis (*i.e.* r is set to zero), also was plotted versus the measured points. That curve showed in fact *less* good fitting to the measurement, than the one for an infinite medium did. However, the interpretation of this is not clear.

Because the two described experiments have lots of differences, it is not so easy to make concluding comparisons of them. The most striking observation, when looking at the intensity versus depth diagram of the two measurements, is perhaps the high intensity detected in the single-photon case. Even at a depth of 10 mm, the signal was very strong. However, in real tissue the absorption at about 400 nm is very strong, rapidly attenuating the signal. In order to do a measurement at this wavelength, with more realistic tissue phantom, absorber has to be mixed into the phantom. One conclusion can, however, be made: SPE fluorescence varies with depth roughly as $\exp(-\text{constant} \cdot \text{depth})$, rather than $\exp(-2 \cdot \text{constant} \cdot \text{depth})$ as TPE fluorescence does. (This is an indication of the intensity-squared dependency in TPE, in contrast to the linear intensity dependency in SPE.)

5.4.3. Measurement errors

The possible errors in measuring the depths are small. There is an uncertainty in the z-coordinate of a few hundred parts of a millimetre, in the position when the fluorescing ball just touched the bottom of the well. However, if the definition of zero depth is shifted somewhat from the real location, it just contributes with a small constant z-factor to every measure point. The same holds for any hysteresis effect in the micrometer screw, when changing the direction of motion. Except for the precision in the setting of the zero-level, the precision of the depth in the other measured points is limited by the precision of the scale on the micrometer screw, which is less than 5 μm .

One problem with the measurements on two-photon signal was that the detected signal was extremely sensitive to x-y-adjustments of the fluorescing ball, when the fluorescence was generated in the ball. For example this was the situation in the Rhodamine solution used for spatial calibration, and also close to the well bottom in the tissue phantom mixture. The microscope stage is made for as small x-y-adjustments as is required for moving around a small microscope sample. However, the sensitivity needed for us to optimise the detected signal in the x-y-plan was not accessible. Even a so slight turning on the stage adjustment wheels, that one hardly could feel it during the adjustment, made a very big difference in signal level. This is of course due to the tiny focal spot. This resulted in that optimisation in the x-y-plan was accomplished only ones, at the first point of the measurement. Then no adjustments in this sense were performed (focus adjustments only in the z-direction). Consequently, here is a source of error. It is possible that an x-y-change of location of the dye ball at the points deeper into the tissue phantom would have given raise to a much stronger detected intensity.

Another problem associated with the ball position, is that the focus depth was not actually measured. It was assumed that the highest signal should be reached, when the focal point was at the dye ball. However, at greater depths, this was probably not true. There is a suspicion that the focal point is positioned at lower depths than the ball, when measuring at greater depths.

The time-integrating constant on the lock-in amplifier where set to 300 ms for the measurements at depths between 0.5 and 1.4 mm in the two-photon fluorescence experiment, and to 10 s for the rest of the points in this measurement as well as for all points in the one-photon study. Because

the signal varied rather much, the long integration time improved the signal-to-noise considerably. The total recording time becomes, however, long for the 10 s integration time setting (much longer than ten seconds). Hence some of the points measured for such a time-constant might have been measured too early, before the signal really settled down. (There was a greater risk for this latter error in the two-photon measurement, than in the one-photon measurement, because the former were performed under time strain on the experimentalists.)

The read-out value from the lock-in amplifier did at some occasions behave somewhat peculiar. The cause of this is not known, but it is believed to have origin in either instrumental defects (most probable), or in some lack in the measurement procedure. However, this peculiarity was minimised by keeping the PMT gain as low as possible (close to the minimum gain necessary for the PMT to give any out-put signal), but it would probably have been a technical advantage if a higher PMT gain could be used.

The polystyrene wells used to contain the samples, are not high quality equipment for the purpose in the experiments. Its optical properties affect the focusing and the boundary conditions in unknown ways.

There are possibly also some other unwanted affects in the measurement. One is the possibility of linear single-photon excitation at 790 nm. However, Rhodamine B has very low absorption in this near-infrared part of the spectrum, and therefore such effects are not believed to be of importance. Another one is that if the dye concentration is too high, saturation effects might be introduced. The concentration of Rhodamine B in the tissue phantom mixture was of the same order as used by Xu and Webb in their determination of two-photon excitation cross sections of this dye (in reference [15]), and for that measure they had tested the concentration in order to find one without any saturation. Hence, there were probably no saturation effects in our phantom mixture. However, the concentration in the fluorescing ball is unknown. This may only be of importance when the ball is close to the surface, as the intensity falls off quickly at depth.

5.4.4. Experimental improvements

What can be done in order to improve this measurement on two-photon fluorescence? First of all it is worth noting that the performed study was in fact not considered as a *real* experiment. After a long time of trouble shooting the experiment finally begun to work. However, at that time the resources for the study were running out, and these measurements were performed in a great lack of time, mainly to see if we could find any indicator of something interesting, worth further studies.

The filter combinations used must be revised. At the same time as the laser wavelength have to be efficiently blocked, a minimum loss of intensity is needed at the fluorescence wavelengths. A good choice may be to use a band pass filter, which only let the fluorescence peak wavelength pass. Even better would be a broader band pass filter allowing more of the broadband to pass. As noted above it is also necessary to measure with a long time-integrating constant on the lock-in amplifier, and for the experimentalists to have quite a lot of time for the procedure, so the read-out from the amplifier has time to really settle down before read off.

A CCD camera connected to a spectrometer would be an alternative to the use of a PMT in combination with a lock-in amplifier, is a CCD camera. This would also have the advantage that the whole wavelength spectrum can be detected simultaneously. Consequently it would also reduce the problem with the filter combination.

It is also important to improve the x-y-translation stage of the fluorescing ball. A setup with possibility of micrometer adjustments (or at least tens of micrometers; as is the case with most micrometer screws) seems to be required.

The laser light intensity in the sample, and the efficiency in coupling the fluorescence light to the detector should be increased, in order to get a stronger fluorescence signal. (Note, however, that saturation effects in the sample should be avoided. This could of course be achieved by using a more powerful laser source (for example by raising the pump laser power). The laser must also keep a stable at a high out-put power, without loosing its mode-lock. Ti:Sapphire lasers are in general very stable, but some improvement might be obtained by cooling the titanium-sapphire crystal (this was not the case in the experiment). Actually, the day the measurement were carried out was one of the hottest this summer, and the temperature in the lab room was so high so the laser maximum power did decrease and finally also its capability of mode-locking were lost (of course after the measurement procedure). Further measurements are therefore recommended to be performed at more normal conditions.

Another improvement would be to decrease the number of guiding mirrors between the laser and the sample, and the one used should preferably be dichroids (in our setup there were some gold-mirrors). One could also consider the use of a pulse compressor, to attain shorter pulses with higher peak intensities. Further, an objective lens with higher numerical aperture might also give a more intense signal. At last, when the collected light passes the filter-box, one order of magnitude is lost in intensity without any filters inside the box. Hence the box should be replaced by a more appropriate construction.

In order to avoid the complexity of the mix of two-photon fluorescence, from the dye ball and from the surrounding solution, future experiments should preferably be conducted with no fluorescing dye mixed into the phantom.

As an alternative to the method used here; with constant scattering coefficient in the sample, and varying depths; one can keep the depth constant, and alter the concentration of the scatterer in the sample. In both cases the intensity is, in fact, measured as a function of the number of scattering mean free path lengths through the sample medium. This was the approach applied by Ying *et al.* in [38].

5.5. Theoretical calculation of the TPE in turbid media

An approximation of the TPE excitation in turbid media is obtained by using equation (5.1) (from reference [38]), which combines the Gaussian intensity distribution and Beer-Lambert's law. The following intensity distributions have been calculated by using the approximation

$$z_0 = \frac{I}{p \cdot (N.A.)^2}. \quad (5.10)$$

The results are shown below.

5.5.1. Variations of the scattering coefficient

In the four pictures in figure 5.10 the scattering coefficient is increased from 0/mm to 12/mm with the step of 4/mm, corresponding to 0, 4, 8, 12 scattering mean free path lengths SMFPL, because the focal distance is 1 mm. The numerical aperture is kept constant in these calculations. In figure 5.11 the corresponding axial (along the z-axis) distributions are shown.

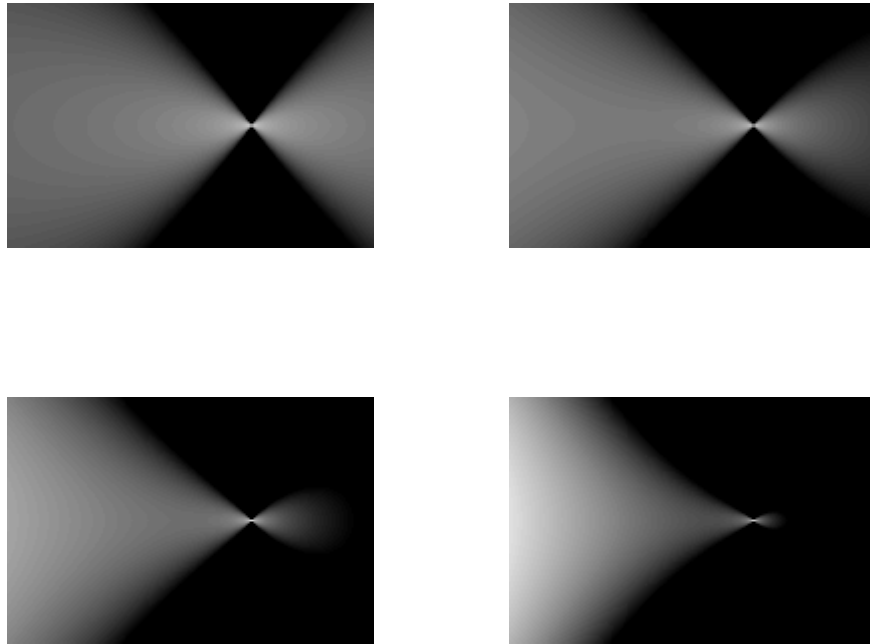


Figure 5.10 The TPE distribution in a turbid medium with focus at 0, 4, 8, and 12 scattering mean free path lengths (SMFPL). The intensity of the TPE is in arbitrary units and is displayed in logarithmic scale. In the upper left picture there is no scattering, whereas the bottom right picture has strongest scattering.

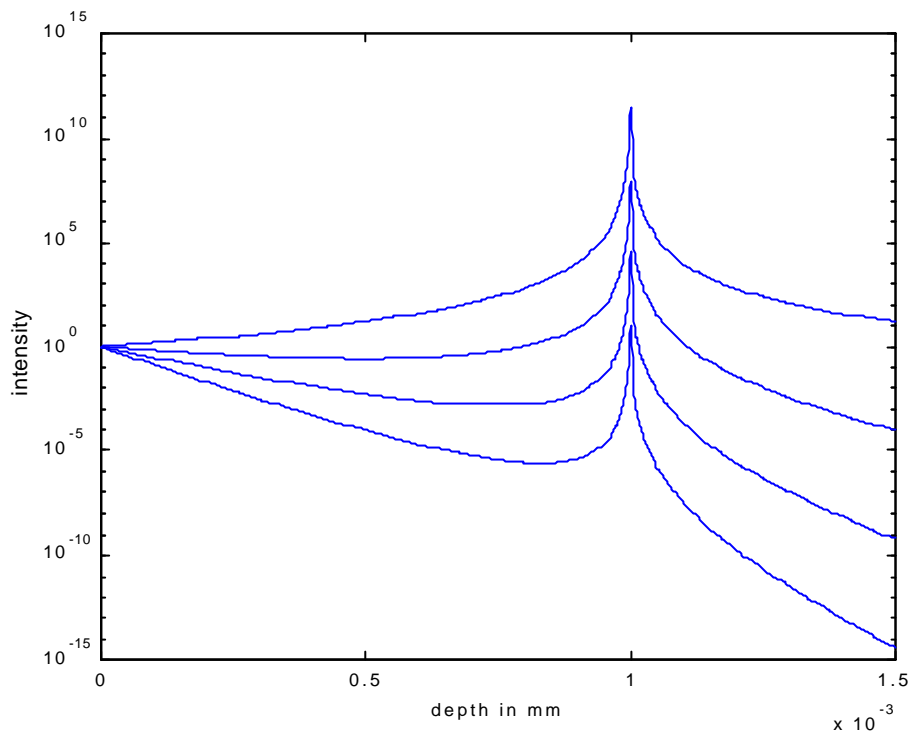


Figure 5.11 The intensity (arbitrary units) along the z-axis, for a focus depth corresponding to 0, 4, 8, and 12 SMFPL. The most upper curve corresponds to a focus depth of 0 SMFPL, the lowest to 12 SMFPL. Logarithmic intensity scale.

5.5.2. Variations of the numerical aperture

In figure 5.12 the intensity distribution is given for various numerical aperture of 0.25, 0.50, and 0.75. The scattering coefficient is kept constant to 10/mm. In figure 5.13 the corresponding axial (along the z-axis) distributions are shown.

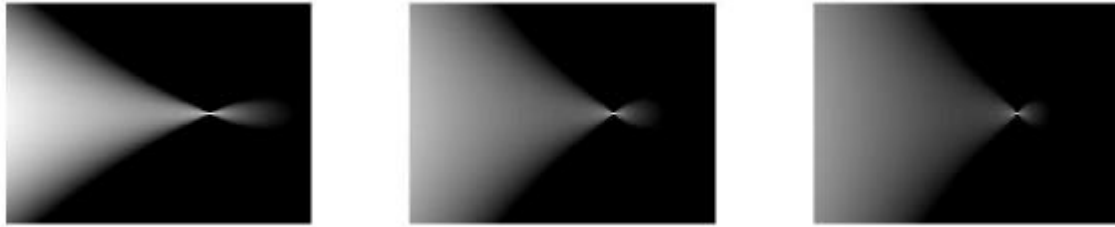


Figure 5.12 TPE distribution in a turbid medium with a scattering coefficient of 10/mm, for a numerical aperture of 0.25, 0.50, and 0.75, respectively (from the left to the right). The intensity of the TPE is in arbitrary units and is displayed in logarithmic scale.

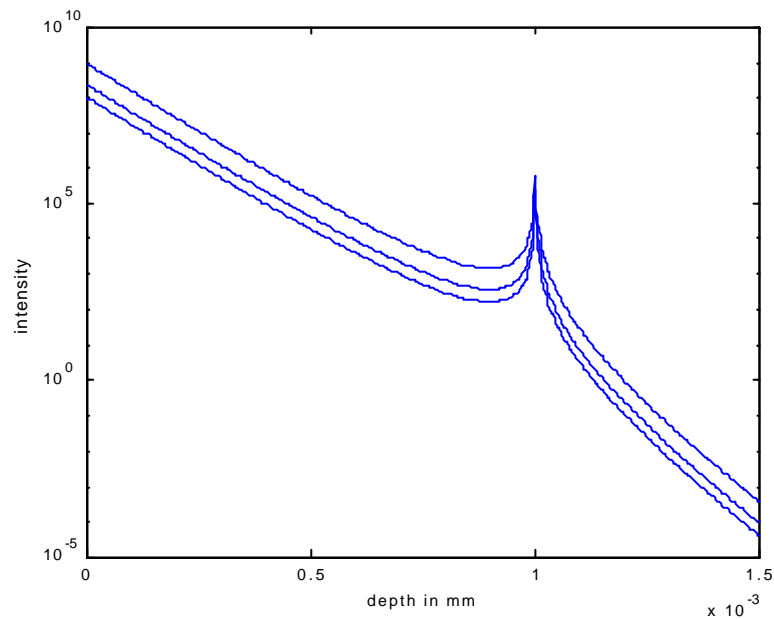


Figure 5.13 The intensity along the z-axis for numerical apertures of 0.25, 0.50, and 0.75, where the numerical aperture 0.75 gives the lowest intensity at the surface. The intensity is given in arbitrary units and logarithmic scale.

6. Discussion and conclusion

6.1. Two-photon excitation in turbid media

A few papers describing studies of two-photon fluorescence induced in scattering media, have been published (*e.g.* references [37-40, 50]). Most of them are directed towards two-photon fluorescence microscopy. The axial depth in the studied samples, has been limited to within an order of magnitude of 100 μm . For PDT purposes, at least for tumour treatment, one order of magnitude higher (minimum) is required (see below). One study considering depths up to some millimetres has been reported by Ying, Liu and Alfano [38].

The effect of absorption is negligible in comparison to scattering for tissue in the near infrared region – or in technical terms: the absorption coefficient, m_a , is much smaller than the scattering coefficient, m_s . Therefore, when studying for example TPE distributions caused by NIR radiation in tissue, it is not the linear one-photon absorption that sets the limits, scattering effects determinates the distributions.

6.1.1. Ballistic versus non-ballistic photons in TPE

In some papers about two-photon excitation experiments, one can read that only ballistic photons contribute to TPE in the focal region (*e.g.* in reference [31]) because of the loss of spatial and temporal coherence when scattered. This can be miss-interpreted as if the scattered photons are completely forbidden to contribute to TPE, as if perfect coherence is a requirement – that is, however, not true! It is, however, true that two-photon fluorescence is strongly dependent on the coherence (see for example reference [10] or [15]).

When focusing a NIR laser beam into a sample of turbid media, it is mainly the ballistic photons that will contribute to the TPE. This is because the high photon flux needed to obtain TPE is mainly achieved in the focal region, where the ballistic photons are dominating. Hence, the diffuse light will usually not contribute much to the TPE, unless the intensity is so extremely high, that focusing is not necessary.

6.1.2. The g -factor influence on scattered photons in TPE

As described in chapter 4 the g -value of a scattering medium can influence the number of photons reaching the focal volume, thus contributing to TPE [37]. According to the results of Dunn *et al.*, a g -value of 0.95 or more might yield a large number of such photons, while for lower g -values the number of these photons contributing to TPE in the focal volume, is almost independent of the anisotropi factor (*i.e.* the g -value). In their experiment, Dunn *et al.* simulated the TPE signal for a laser beam focussed at a depth of 02 mm (see chapter 4 for details). However, at least for photodynamic *tumour* therapy purposes, the effective depth must often necessarily be much greater than in Dunn's *et al.* simulation, and we believe that their result can probably not be linearly extrapolated to greater depths.

In addition, most types of tissue have a lower g -value between 0.7 and 0.95 [36]. Therefore, in this paper only ballistic photons will be considered to contribute to two-photon excitation (in focus), and the anisotropy factor g will thus not be important.

6.1.3. The dependence of polarization for TPE in turbid media

In appendix 1, it is noted that the two-photon cross section on average, in a sample of randomly oriented molecules (which can often be assumed to be the case in tissue-like media), can be expressed as $A + B \cos^2 \mathbf{q}_{1,2}$. The angle represents the one between the directions of polarisation (supposed linear) of the two absorbed photons; A and B are constants dependent on molecular parameters. Hence, it is relevant to consider how this polarisation dependency might influence TPE in focus.

If the constant A dominates over B , this dependency can be neglected (it always holds that $A = |A| \geq |B|$). Further, when focusing the beam of linearly polarised light, the deviation of the beam path also changes the polarization direction*. This deviation depends on the $N.A.$ of the focusing objective. This might perhaps affect how the focal TPE-signal depends on the numerical aperture, due to the polarization dependency.

However, the polarization dependency on TPA is here believed to be insignificant, because no consideration of the polarisation has been taken in articles about theoretical studies of TPE in turbid media, referred to in this report (as well as no one else we have read). Only the squared intensity dependency has been taken into account. This indicates that it is common to ignore the influence of polarization, and consequently, in this report, the affect of polarization will be assumed to have no significant importance in TPE PDT.

6.1.4. The significance of the numerical aperture in TPE PDT

The numerical aperture ($N.A.$) of a lens determines how tightly it is focusing, and therefore the size of the focal volume. A high $N.A.$ means a tight focus and a small focal volume. Hence, for a high $N.A.$ the intensity in focus becomes high, but the spatial distribution of the same is more concentrated. This implies that for a high $N.A.$, the two-photon fluorescence is stronger in focus than for a low one, but for the latter there is instead fluorescence from a larger region. In fact, according to the theoretical analysis presented in *The two-photon excitation rate*, in chapter 2 (in turn based on reference [15]), the *total* fluorescence (when assuming TPE merely in the focal region) might be approximately independent of the numerical aperture, while the maximum fluorescence (in the centre of the focal volume) anyway correlates to the $N.A.$.

In a study by Gan and Gu [39], Monte Carlo simulations based on Mie scattering theory and geometrical optics were considered for TPE (see below). They studied the influence of the numerical aperture for a focusing depth corresponding to a distance of four times the *scattering mean free path length* (SMFPL). According to their results the TPE peak at focus becomes higher and also narrower for the higher numerical apertures (just as expected from the reasoning above). At the same time the region of maximum fluorescence moves from the surface of the sample, towards the focus. (At $N.A. = 0.5$ the signal maximum close to the surface was approximately as big as the one at focus.

* The direction of polarization is orthogonal to the travelling path, defined as parallel to the direction of the electric field.

For PDT purposes, when focusing at relatively great depths, a weak TPE usually needs to be considered. Therefore, it might be preferable to use objectives/lenses with high numerical aperture, in order to strengthen the TPE. However, this is at the cost of a smaller focal volume, possible to “treat” at every moment. Further, for as high scattering as it is in most tissue-types, there would be TPE close to the sample surface, rather than in focus. This can be minimised by using optics with as high $N.A.$ as possible, because the intensity distribution is spread out over a bigger cross section area, except for close to the focus. This is also good in order to reduce damaging TPE-effects in tissue between its surface and the region where the PDT is desired to take place. However, as discussed by Dunn *et al.* [37], a higher numerical aperture implies a greater difference in photon paths through the sample (supposing ballistic photons), between photons passing the centre of the lens, and those passing close to the edge of the lens. Therefore, it is not necessarily true that maximum TPE rate is achieved with highest $N.A.$.

As noted above, the polarization dependency might also vary with the numerical aperture.

6.1.5. Gaussian beam of ballistic photons

According to the discussion above, the two-photon excitation (in focus) in turbid media can be approximated to solely depend on the intensity of the ballistic photons. The intensity of ballistic photons depends on the scattering and absorption coefficient and is given by the Beer-Lambertian law [51]. Under the assumption that the linear absorption could be ignored, Ying *et al.* [38] evaluated their experimental results using equation 5.1 above:

$$I(\mathbf{r}, z) = I_0 \left(\frac{w_0}{w(z)} \right)^2 \exp\left(-\frac{2\mathbf{r}^2}{w^2(z)}\right) \exp(-\mathbf{m}_s(z + z_s)) \quad (6.1)$$

The intensity squared, $I^2(0, z)$, along the z -axis, has then the proportionality condition displayed in expression 5.2 above:

$$I^2(0, z) \propto \frac{1}{\left(1 + \left(\frac{z}{z_0}\right)^2\right)^2} \exp(-2\mathbf{m}_s(z + z_s)) \quad (6.2)$$

In their paper (reference [38]) they plotted this function for a z -range corresponding to their measurements (from 0 to approximately 27 mm), and compared it with the experimental results. The plots did show a good *qualitative* agreement between theory and experiments, indicating a quite good validity of this very simple model. For instance, the two-photon fluorescence (TPF) intensity at the focal point decreases exponentially as the scattering strength of the sample media increases, whereas the TPF near the surface remains relatively constant; also, the local fluorescence maximum around focus moves towards the surface when the scattering coefficient is increased. Note, however, that their experimental results showed a relatively higher intensity close to the surface of the sample, than predicted by the theoretical model.

Our experiment on two-photon induced fluorescence was not possible to evaluate quantitatively, but qualitatively it gives support to the results by Ying *et al.* [38]. The results of our experiment indicates that the intensity at greater depths, inside a turbid medium sample, is dominated by diffuse light originating from two-photon fluorescence close to the sample surface. This is in

accordance with Yings *et al.* results, as well as the Monte Carlo simulations performed by Gan and Gu [39].

The fact that the fluorescence maximum moves towards the surface, can be understood from (6.2). Taking the derivative and solving for zero, gives the following expression for the intensity peak position (z_{\max}):

$$z_{\max} = -l_s + \sqrt{l_s^2 - z_0^2}, \quad (6.3)$$

where $l_s = 1/\mathbf{m}_s$ is the scattering mean free path of the media. When \mathbf{m}_s increases, l_s decreases and the position of the maximum moves towards the surface. (Maybe \mathbf{m}_s reaches a value such that the square root in (6.3) becomes imaginary, then this corresponds to that the maximum have moved to the surface.)

At depths corresponding to 4–6 times the mean scattering the intensity in the peak has decreased to the level near the surface for a numerical aperture of 0.25 [39]. This is shown experimentally, by other researchers MC-simulations ([37, 40]), and theoretically by the formula above. Therefore equation (6.1) (or (6.2)) can be used as a guideline for how deep into the tissue it is possible to achieve TPE. For higher numerical apertures than 0.25, the depth will be greater, which is shown above in examples of the TPE distribution in turbid media. Note, however, that in our experiment, the selectivity of two-photon excitation was lost at less depth than 4–6 SMFPL (rather at two or three), but the reasons for this lower value are probably due to experimental artefacts.

6.2. Photodamage

In multiphoton microscopy there is a certain window of useful excitation intensities. This window has a lower limit set by the minimum intensity required to achieve two-photon excitation and an upper limit where the light intensity induce cell damage by mainly two-photon absorption. There are no exact values of these limits or thresholds but the lower limit is somewhere in the range of MW/cm² to GW/cm² and the upper limit is somewhere around 100 GW. These values are for the peak power in the focal region.

More interesting is, however, the range of mean powers that can be used. König *et al.* [32] found in their experiments on Chinese hamster ovary (CHO) cells that there is a relatively narrow window of mean power covering only one order of magnitude ($P_{50}/P_{\min} = 10$) [32]. There P_{50} is the mean power, where 50% of the CHO failed normal cell division, and P_{\min} is the minimum mean power required to achieve a detectable two-photon fluorescence signal. The ratio was approximately the same for both 240 fs and 2.2 ps pulses but because the P_{ave}^2/t relationship of TPE the picoseconds pulses required 3 times greater mean power.

The use of two-photon excitation in photodynamic therapy should, in consistency with multiphoton microscopy, also be safe to in a certain optical window or a special range of peak intensities. However, compared to microscopy, the tissue in PDT contains some additional absorbers, namely the blood and the photosensitiser. The haemoglobin in blood has strong linear absorption in the wavelength region of 300–700 nm. Hence, the absorption of haem is a major limitation in linear PDT. If the non-linear absorption of haem is significantly higher than other absorbers in tissue, the

haem might also be a limiting factor in TPE PDT, limiting the maximum peak power in focus that could be delivered to healthy tissue. The blood is, however, moving and the same volume of blood will not be exposed by the focus of the laser beam for a very long time. Besides, to the best of our knowledge, no biological damage caused by two-photon absorption in blood has been reported. As a consequence of this a higher non-linear absorption in blood might not induce more biological damage than in surrounding tissue for a given intensity. Therefore the threshold for biological damage induced by two-photon absorption of haem will be considered to be of the same order as the other chromophores in the tissue.

Regarding the absorption of the photosensitiser outside the tumour, PpIX will once again work as an example. The concentration of the photosensitiser, PpIX, is after a few hours of accumulation about 2–5 times higher in tumour than in the surrounding healthy tissue. Hence, one might think that the photochemical reaction that induces cell damage should also be 2–5 times more frequent in the tumour than in the surroundings, which is not much. The cell killing efficiency for PDT is, however, at least ten times higher in the tumour than in healthy tissue. This discrepancy is probably mainly due to fact that the tumour cells are more likely to have a double DNA break and their repair efficiency thus is lower. This effect is the same as seen in radiotherapy, where the surviving rate for cancer cells is about 20–40% of that of healthy cells for a given dose. In photodynamic therapy, the cell killing in the tumour is also governed by other effects; like, higher oxygen concentration, and micro localisation of the photosensitiser. We will not further speculate on the discrepancy between sensitivity of tumour and normal tissue, as we do not know the precise photobiological damage induced by absorption (linear or nonlinear) of PpIX. Moreover, we will assume that this discussion is valid also for other photosensitiser candidates in two-photon excitation PDT.

Now, the lower intensity limit for multiphoton microscopy was set to the intensity needed to achieve a detectable TPE signal. In TPE PDT the lower threshold should be the minimum intensity required to achieving a PDT effect in the tumour. The upper intensity limit in TPE PDT would be the intensities where unwanted induced cell damage occurs, in this case – outside the tumour. The unwanted cell damage outside the tumour is caused by multiphoton excitation of chromophores (including the photosensitiser); plasma formation; and optical breakdowns. According to the discussion above, the induced damage caused by TPE is of the same order for all chromophores in the tissue, including haem. Hence, the upper intensity limit outside the tumour will be considered to be the same as for multiphoton microscopy. The values of the threshold for induced cell damage by multiphoton absorption vary with the pulse width. Therefore no precise value can be given, but the diagram in figure 4.4 can be used as a guideline. The thresholds for plasma formation and dielectric (optical) breakdown for water are higher than that of multiphoton absorption, hence the threshold of multiphoton absorption will be the main limiting factor. However, in cases where multiphoton absorption of other chromophores than the photosensitiser is not a problem, plasma formation and optical breakdown will be a limiting factor. The saturation effects should also be mentioned, but due to the limitations of scattering in TPE, this will not be considered to play a major role in TPE PDT.

The excitation of chromophores can cause cell death in the same way as photosensitisers do but with the difference that they are not highly localised in the tumour. However, in some tumours there are significantly higher concentrations of special chromophores, which will then work as natural photosensitisers [31].

6.3. Two-photon excitation in photodynamic therapy

According to the discussion above, the maximum depth of TPE in PDT is limited by the loss of selectivity in turbid media. In other words, after a depth of about 4–6 times the photon scattering mean free path length (SMFPL), the two-photon absorption outside focus (predominately close to the surface) is higher than the TPA in the focus (for $N.A. = 0.25$). Higher laser intensity would then only slightly increase the treatment depth but significantly increase the photodynamic damage close to the surface. If the increase of the photodynamic effect in superficial tissue is not a limiting factor, a higher laser power could increase the treatment depth. Otherwise, higher laser power will not improve the maximum treatment depth in TPE PDT.

A higher $N.A.$ does not considerably increase the depth at which the selectivity is lost. If, for example, the $N.A.$ is increased from 0.25 to 0.75, the maximum theoretical depth would be $2 \ln(0.75/0.25)$ scattering mean free path lengths more than for $N.A. = 0.25$, *i.e.* approximately 6–8 times the SMFPL.

The maximum depth of 4–6 scattering mean free path lengths (SMFPL) corresponds to about 0.5 mm. In tissue that has a scattering coefficient of 10/mm, 8 times the SMFPL corresponds to 0.8 mm. This can be compared to single-photon PDT, which has an effective depth of about 3 mm. Consequently; two-photon excitation with light in the tissue optical window does not increase the treatment depth in PDT.

König *et al.* [32] studied the PDT performance of Photofrin and PpIX under two-photon excitation. They scanned the beam from a Ti:Sapphire laser over a sample area of $160 \mu\text{m} \times 160 \mu\text{m}$, right at the surface, using 2 mW mean power. The result showed that the exposed sensitiser-labelled CHO cells had decreased their cloning efficiency to 50% after 13 scans for Photofrin and 24 scans for PpIX, which corresponds to applied energies of about 10 mJ and 19 mJ per cell. The time needed for one scanning is about 15 seconds. Consequently it takes 6 minutes to treat an area (one single layer of cells) of 0.03 mm^2 . (However, Hill reports in reference [52], that it might be possible to treat eye melanomas with approximately 100 times higher speed.) This time could of course be decreased by increasing the average power. If this experiment would have been performed at a 4 SMFPL (still with a Ti:Sapphire laser) approximately a mean power of 6 W should have been needed at the surface to achieve mean power of 2 mW in focus. The laser power needed to achieve the same absorbed dose by two-photon excitation would be different for lasers with other parameters. Theoretical calculations for how the laser power changes by altering the pulse width and pulse repetition frequency are given in table 6.1.

Table 6.1 Theoretical calculations of laser powers for some typical laser parameters.

wavelength	780 nm	1064 nm	800 nm
pulse width	200 fs	2 ps	1 ns
pulse repetition frequency	76 MHz	400 MHz	100 MHz
average power	6 W	5 W	500 W
peak power	400 kW	63 kW	5 kW
peak intensity in focus	190 GW /cm ²	30 GW /cm ²	2 GW /cm ²

The powers are obtained from the assumption that the TPE PDT effect is proportional to the two-photon excitation rate equation. As seen in the table, the powers are very high, but as mentioned above, the two-photon cross section of PpIX is very low. If the two-photon cross section of the photosensitiser would be 100 times larger, the power needed would decrease by the same factor. However, the numbers indicated in the table are only a rough approximations and the PDT effect might not be the same for all cases above. Therefore, experiments *in vivo* must be performed, in order to achieve the optimal therapeutic ratio, where the damage to the tumour is a maximum and the damage to the normal tissue is a minimum. If the therapeutic ratio of PDT is not affected by variations in pulse width (for pulses shorter than picoseconds, maybe also nanoseconds), longer pulses are preferred because then simpler optics can be used, like fibres. Optimisation of the laser pulse shape (the pulse spectrum) can also increase the TPE ratio. The high power required achieving a photodynamic process at 4 SMFPL will probably be limited by heating, caused by linear absorption. Hence, heating will be a limiting factor for TPE in PDT even though this is not a limiting factor in multiphoton microscopy. Plasma formation and optical breakdowns should not be a problem as long as the selectivity is maintained, because then the peak intensity at the surface should not be higher than the peak intensity in focus.

The photodynamic reaction has been reported to be the same for TPE of the photosensitisers as that for SPE [22, 32], hence, TPE PDT is a possibility. However, photosensitisers with larger two-photon cross sections could increase the therapeutic ratio and the selectivity, hence also the maximum treatment depth.

The selectivity is, however, the main advantage of TPE over SPE in PDT. This could be helpful in for example treatment of Barret's esophagus, malign melanoma in the eye, and age-related macular degeneration. For this to become a clinical reality, further research is required.

6.4 Conclusion

In conclusion, the maximum depth of two-photon excitation in PDT is limited by scattering; cell death, caused by multiphoton absorption of other chromophores than the photosensitiser; and heating. The high intensity required can also cause plasma formation and optical breakdown at the tissue surface. Turbid media, like tissue, causes the two-photon excitation in focus to degrade so much that the two-photon absorption rate in the superficial tissue is higher than the absorption rate in the focus at relatively small depths, which also was observed in our experiment. This means that the selectivity, obtained by focusing, disappears after 4–8 scattering mean free path lengths. The maximum treatment depth is, hence, less than for single-photon excitation in PDT. The multiphoton absorption of other chromophores than the photosensitiser that occur in focus or close to the surface limit the peak power that can be used in TPE PDT. (The average power is limited by linear heating.) Even though these limitations, TPE in PDT may be useful, where extra selectivity is needed, *e.g.* in treatment of malign melanoma in the eye. However, larger volumes will be harder to treat, because of the time needed to scan the laser beam over the entire volume.

7. Acknowledgements

This work would not have been accomplished without the help and support of persons at the Division of Atomic Physics.

First of all, we would like to thank our supervisor Prof. Stefan Andersson-Engels for guiding us throughout this work. Further, we also would like to thank Anders Persson and Stefan Kröll. Finally, we want to thank all people in the Medical Group, especially Johannes Swartling, Christoffer Abrahamsson, and Tommy Sjögren.

8. References

1. M.J. Wirth and H.O. Fatunmbi, Very high detectability in two-photon spectroscopy, *Anal. Chem.* **62**, 973-976 (1990).
2. R.H. Pantell and H.E. Puthoff, *fundamentals of Quantum Electronics*, (John Wiley & Sons, 1969).
3. M. Göppert-Mayer, Über Elementarakte mit zwei Quantensprüngen, *Annalen der Physik* **9**, 273-294 (1931). German.
4. V. Hughes and L. Grabner, The Radiofrequency Spectrum of Rb^{85}F and Rb^{87}F by the Electric Resonance Method, *Phys. Rev.* **79**, 314-322 (1950).
5. W. Kaiser and C.G.B. Garrett, Two-photon Excitation in $\text{CaF}_2:\text{Eu}^{2+}$, *Phys. Rev. Lett.* **7**, 229-231 (1961).
6. W. Demtröder, *Laser Spectroscopy*, (Springer-Verlag, 1981).
7. S. Svanberg, *Atomic and Molecular Spectroscopy – Basic Aspects and Practical Applications*, (Springer Verlag, Heidelberg, Germany, 2001).
8. W.K. Bischel, P.J. Kelly and C.K. Rhodes, High-resolution Doppler-free two-photon spectroscopic studies of molecules. I. The ν_3 bands of $^{12}\text{CH}_3\text{F}$, *Phys. Rev. A* **13**, 1817-1828 (1976).
9. Multiphoton Fluorescence Microscopy – Introduction. <http://www.micro.magnet.fsu.edu/primer/techniques/fluorescence/multiphoton/multiphotonintro.html> (2001).
10. M.A. Albota, C. Xu and W.W. Webb, Two-photon fluorescence excitation cross sections of biomolecular probes from 690 nm to 960 nm, *Appl. Opt.* **37**, 7352-7356 (1998).
11. A.P. Thorne, U. Litzén and S. Johansson, *Spectrophysics – Principles and Applications*, (1997).
12. E.A. Wachter, W.P. Partridge, W.G. Fisher, C. Dees and M.G. Petersen, Simultaneous two-photon excitation of photodynamic therapy agents, in *SPIE*, vol. **3269**, 68-75 (1998).
13. W.G. Fisher, W.P. Partridge, Jr., C. Dees and E.A. Wachter, Simultaneous two-photon activation of type-I photodynamic therapy agents, *Photochem. Photobiol.* **66**, 141-155 (1997).
14. K. Teuchner, W. Freyer, D. Leupold, A. Volkmer, D.J.S. Birch, P. Altmeyer, M. Stücker and K. Hoffmann, Femtosecond Two-photon Excited Fluorescence of Melanin, *Photochem. Photobiol.* **70**, 146-151 (1999).
15. C. Xu and W.W. Webb, Measurements of two-photon excitation cross sections of molecular fluorophores with data from 690 to 1050 nm, *J. Opt. Soc. Am. B* **13**, 481-491 (1996).

16. W.G. Fisher, E.A. Wachter, F.E. Lytle, M. Armas and C. Seaton, Source-corrected two-photon excited fluorescence measurements between 700 and 880 nm, *Appl. Spectr.* **52**, 536-545 (1998).
17. H.J. Koester, D. Baur, R. Uhl and S.W. Hell, Ca²⁺ Fluorescence Imaging with Pico- and Femtosecond Two-Photon Excitation: Signal and Photodamage, *Biophys. J.* **77**, 2226-2236 (1999).
18. C. af Klinteberg, On the use of light for the characterization and treatment of malignant tumours, Dissertation thesis, Lund Institute of Technology, Lund, Sweden (1999).
19. K. König, H. Schneckenburger, A. Rück and R. Steiner, *In vivo* photoproduct formation during PDT with ALA-induced endogenous porphyrins, *J. Photochem. Photobiol. B* **18**, 287-290 (1993).
20. G.S. Cox and D.G. Whitten, Mechanisms for the photooxidation of protoporphyrin IX in solution, *J. Am. Chem. Soc.* **104**, 516-521 (1982).
21. J.M. Wessels, R. Sroka, P. Heil and H.K. Seidlitz, Photodegradation of protoporphyrin-dimethylester in solution and in organized environments, *Int. J. Radiat. Biol.* **64**, 475-484 (1993).
22. R.L. Goyan and D.T. Cramb, Near-infrared two-photon excitation of protoporphyrin IX: photodynamics and photoproduct generation, *Photochem. Photobiol.* **72**, 821-827 (2000).
23. H.H. Inhoffen, H. Brockmann and K.-M. and Bliesener, Further knowledge of chlorophyll and of hemin, XXX. Photoporphyrins and their transformation into spirigraphis- and isospirigraphis-porphyrin, *Liebsigs Ann. Chem.* 173-185 (1969).
24. E.F. Gudgin Dickson and R. Pottier, On the role of protoporphyrin IX photoproducts in photodynamic therapy, *J. Photochem. Photobiol. B* **29**, 91-93 (1995).
25. Q. Peng, T. Warloe, K. Berg, J. Moan, M. Kongshaug, K.-E. Giercksky and J.M. Nesland, 5-aminolevulinic acid-based photodynamic therapy: Clinical research and future challenges, *Cancer* **79**, 2282-2308 (1997).
26. J.C. Finlay, D.L. Conover, E.L. Hull and T.H. Foster, Porphyrin bleaching and PDT-induced spectral changes are irradiance dependent in ALA-sensitized normal rat skin in vivo, *Photochem. Photobiol.* **73**, 54-63 (2001).
27. S. Bagdonas, L.W. Ma, V. Iani, R. Rotomskis, P. Juzenas and J. Moan, Phototransformations of 5-aminolevulinic acid-induced protoporphyrin IX in vitro: a spectroscopic study, *Photochem. Photobiol.* **72**, 186-192 (2000).
28. D.J. Robinson, H.S. de Bruijn, N. van der Veen, M.R. Stringer, S.B. Brown and W.M. Star, Protoporphyrin IX fluorescence photobleaching during ALA-mediated photodynamic therapy of UVB-induced tumors in hairless mouse skin, *Photochem. Photobiol.* **69**, 61-70 (1999).

29. D.J. Robinson, H.S. de Bruijn, N. van der Veen, M.R. Stringer, S.B. Brown and W.M. Star, Fluorescence photobleaching of ALA-induced protoporphyrin IX during photodynamic therapy of normal hairless mouse skin: The effect of light dose and irradiance and the resulting biological effect, *Photochem. Photobiol.* **67**, 140-149 (1998).
30. J.D. Bhawalkar, N.D. Kumar, C.-F. Zhao and P.N. Prasad, Two-photon photodynamic therapy, *J. Clin. Laser Med. Surg.* **15**, 201-204 (1997).
31. E.A. Wachter, M.G. Petersen and C. Dees, Photodynamic therapy with ultrafast lasers, in *Commercial and biomedical applications of ultrafast lasers*, Proc. SPIE vol. **3616**, 66-74 (1999).
32. K. König, I. Riemann and P. Fischer, Photodynamic therapy by nonresonant two-photon excitation, in *Conference on optical methods for tumor treatment and detection: Mechanism and techniques in photodynamic therapy VIII*, Proc. SPIE vol. **3592**, 43-49 (1999).
33. S.J. Madsen, C.-H.C. Sun, B.J. Tromberg, V.P. Wallace and H. Hirschberg, Photodynamic therapy of human glioma spheroids using 5-aminolevulinic acid, *Photochem. Photobiol.* **72**, 128-134 (2000).
34. S. Andersson-Engels, I. Rokahr and J. Carlsson, Time- and wavelength-resolved spectroscopy in two-photon excited fluorescence microscopy, *J. Microsc.* **176**, 195-203 (1994).
35. M. Öbrink, Study of two-photon excited fluorescence microscopy for spectroscopic studies of tissue, Master's thesis, Lund Institute of Technology, Lund, Sweden (1995).
36. W.-F. Cheong, Summary of optical properties, in *Optical-Thermal Response of Laser-Irradiated Tissue*, eds. A.J. Welch and M.J.C. van Gemert, pp. 275-303 (Plenum Press, New York, 1995).
37. A. Dunn, V.P. Wallace, M.L. Coleno, M.W. Berns and B. Tromberg, Influence of optical properties on two-photon fluorescence imaging in turbid samples, *Appl. Opt.* **39**, 1194-1201 (2000).
38. J. Ying, F. Liu and R.R. Alfano, Spatial distribution of two-photon-excited fluorescence in scattering media, *Appl. Opt.* **38**, 224-229 (1999).
39. X. Gan and M. Gu, Spatial distribution of single-photon and two-photon fluorescence light in scattering media: Monte Carlo simulation, *Appl. Opt.* **39**, 1575-1579 (2000).
40. C.M. Blanca and C. Saloma, Monte carlo analysis of two-photon fluorescence imaging through a scattering medium, *Appl. Opt.* **37**, 8092-8102 (1998).
41. A. Schönle and S.W. Hell, Heating by absorption in the focus of an objective lens, *Opt. Lett.* **23**, 325-327 (1998).
42. K. König, T.W. Becker, P. Fischer, I. Riemann and K.-J. Halhuber, Pulse-length dependence of cellular response to intense near-infrared laser pulses in multiphoton microscopes, *Opt. Lett.* **24**, 113-115 (1999).

43. W. Denk, D.W. Piston and W.W. Webb, Two-photon molecular excitation in laser-scanning microscopy, in *Handbook of biological confocal microscopy*, ed. J.B. Pawley, pp. 445-458 (Plenum Press, New York, 1995).
44. J. Bewersdorf and S.W. Hell, Picosecond pulsed two-photon imaging with repetition rates of 200 and 400 MHz, *J. Microsc.* **191**, 28-38 (1998).
45. K. König, P.T.C. So, W.W. Mantulin and E. Gratton, Cellular response to near-infrared femtosecond laser pulses in two-photon microscopes, *Opt. Lett.* **22**, 135-136 (1997).
46. S.W. Hell, M. Booth, S. Wilms, C.M. Schnetter, A.K. Kirsch, D.J. Arndt-Jovin and T.M. Jovin, Two-photon near- and far-field fluorescence microscopy with continuous-wave excitation, *Opt. Lett.* **23**, 1238-1240 (1998).
47. W. Denk and K. Svoboda, Photon upmanship: Why multiphoton imaging is more than a gimmick, *Neuron* **18**, 351-357 (1997).
48. J. Swartling, C. af Klinteberg, J.S. Dam, T. Johansson, J. Roth and S. Andersson-Engels, Comparison of spatially and temporally resolved diffuse reflectance measurement systems for determination of biomedical optical properties at 785 nm. In press (2001).
49. S. Andersson-Engels. Light diffusion in turbid media. <http://kurslab-atom.fysik.lth.se/FED4Medopt/> (2001).
50. A. Dunn, V.P. Wallace, M.L. Coleno, P.T.C. So and B. Tromberg, Study of the spatial point spread function with depth in two-photon microscopy, in *Three-dimensional and multidimensional microscopy: Image acquisition and processing VI*, Proc. SPIE vol. **3605**, 112-119 (2001).
51. Measurements of optical properties – the integrating sphere set up. <http://kurslab-atom.fysik.lth.se/FED4Medopt/> (2001).
52. P. Hill, Multiphoton excitation eradicates eye cancers, *Opto & Laser Europe* 29-31 (2000).

Appendix 1 – Theoretical derivations of two-photon absorption properties

An approximate, but detailed, quantum-mechanical derivation of the two-photon transition probability rate and absorption cross section, in the special case of a monochromatic light field, is given.

Two-photon transition probability

Second order time-dependent perturbation theory is used to derive an approximate expression for the two-photon transition probability for the situation when only one wavelength is involved. This is, of course, not really realistic compared to the quite broad, mode-locked laser pulses used in our experiments, but the goal with this section is just to show a qualitative approach of the theoretical background. The procedure follows mainly the one in reference [1] (which in turn follow closely that of Maria Göppert-Mayer [2]), except from the fact that it specialises to the situation of two *non*-equal wavelengths. The present derivation is more detailed and therefore more suited for they with only basic knowledge in quantum mechanics. Another similar, but a little more general, derivation can be found in, for example, [3].

The Hamiltonian can be written as the sum of the unperturbed Hamiltonian (\mathcal{H}_0) and the interaction Hamiltonian (\mathcal{H}'): $\mathcal{H} = \mathcal{H}_0 + \mathcal{H}'$. We further suppose the external field is weak enough to be treated as a perturbation. We also presume there are no energy levels in the molecule possible to reach via a single photon excitation from the ground state. Consequently there is a situation of second order events, and the first order transition probability is zero.

Now following the customary procedure of perturbation theory [4] the quantum mechanical amplitude of the k :th eigenstate, $c_k(t)$, a time t after the perturbation has been turned on, is expanded in a power series. For time-dependent perturbations the well-known recursive expression ([1, 5])

$$\frac{d}{dt} (c_k^{(s)}(t)) = \frac{1}{i\hbar} \sum_n \langle k | \mathcal{H}' | n \rangle c_n^{(s-1)}(t) e^{i\omega_{kn}t} \quad (\text{A1.1})$$

can be used. (In [4] the equivalent Dyson integral series expression is given.) The summation is over all eigenstates n and ω_{kn} is the frequency corresponding to a transition from the n :th to the k :th energy eigenstate.

If the system initially is in the ground state, $|g\rangle$, *i.e.* $c_k(0) = \delta_{kg}$, it follows that $c_k^{(s)}(0) = 0$ for all $s \geq 1$ (because $c_k(0) \equiv c_k^{(0)}(0)$). Consequently the first-order derivative expression are immediately identified as:

$$\frac{d}{dt} (c_k^{(1)}(t)) = \frac{1}{i\hbar} \langle k | \mathcal{H}' | g \rangle e^{i\omega_{kg}t} \quad (\text{A1.2})$$

To integrate this, it is necessary to introduce the explicit time-dependence of the Hamiltonian. Since there is a harmonic radiation field,

$$\mathcal{H}' = \tilde{\mathcal{H}}' \cos \omega t = \frac{1}{2} \tilde{\mathcal{H}}' (e^{-i\omega t} + e^{i\omega t}), \quad (\text{A1.3})$$

where $\tilde{\mathcal{U}}'$ is time-independent. ω is here nothing else than the (supposed constant) light frequency. Putting equation (A1.3) in the right hand side of equation (A1.2) and integrating it gives:

$$\frac{1}{2i\hbar} \langle k | \tilde{\mathcal{U}}' | g \rangle \int \left(e^{i(\omega_{kg} - \omega)t} + e^{i(\omega_{kg} + \omega)t} \right) dt = -\frac{1}{2\hbar} \langle k | \tilde{\mathcal{U}}' | g \rangle \left(\frac{e^{i(\omega_{kg} - \omega)t}}{\omega_{kg} - \omega} + \frac{e^{i(\omega_{kg} + \omega)t}}{\omega_{kg} + \omega} \right) + \text{constant} \quad (\text{A1.4})$$

Taking the initial value $c_k^{(1)}(0) = 0$ in consideration the result becomes

$$c_k^{(1)}(t) = -\frac{1}{2\hbar} \langle k | \tilde{\mathcal{U}}' | g \rangle \left(\frac{e^{i(\omega_{kg} - \omega)t} - 1}{\omega_{kg} - \omega} + \frac{e^{i(\omega_{kg} + \omega)t} - 1}{\omega_{kg} + \omega} \right). \quad (\text{A1.5})$$

Now it is time to bring the result one step further, and use this first-order expression, equation (A1.5), to reach the second-order amplitude of our final state $|f\rangle$. From the recursion formula (A1.1) we have

$$\frac{d}{dt} (c_f^{(2)}(t)) = \frac{1}{i\hbar} \sum_k \langle f | \mathcal{U}' | k \rangle c_k^{(1)}(t) e^{i\omega_{fk}t}. \quad (\text{A1.6})$$

Substituting equation (A1.3) for \mathcal{U}' , and inserting equation (A1.5) for $c_k^{(1)}(t)$, into the right hand side of equation (A1.6), gives

$$\begin{aligned} & -\frac{1}{4i\hbar^2} \sum_k \langle f | \tilde{\mathcal{U}}' | k \rangle \langle k | \tilde{\mathcal{U}}' | g \rangle \left(e^{-i\omega t} + e^{i\omega t} \right) \left(\frac{e^{i(\omega_{kg} - \omega)t} - 1}{\omega_{kg} - \omega} + \frac{e^{i(\omega_{kg} + \omega)t} - 1}{\omega_{kg} + \omega} \right) e^{i\omega_{fk}t} = \\ & = -\frac{1}{4i\hbar^2} \sum_k \langle f | \tilde{\mathcal{U}}' | k \rangle \langle k | \tilde{\mathcal{U}}' | g \rangle \times \\ & \left(\frac{e^{i(\omega_{fg} - 2\omega)t}}{\omega_{kg} - \omega} - \frac{e^{i(\omega_{fk} - \omega)t}}{\omega_{kg} - \omega} + \frac{e^{i\omega_{fg}t}}{\omega_{kg} + \omega} - \frac{e^{i(\omega_{fk} - \omega)t}}{\omega_{kg} + \omega} + \frac{e^{i\omega_{fg}t}}{\omega_{kg} - \omega} - \frac{e^{i(\omega_{fk} + \omega)t}}{\omega_{kg} - \omega} + \frac{e^{i(\omega_{fg} + 2\omega)t}}{\omega_{kg} + \omega} - \frac{e^{i(\omega_{fk} + \omega)t}}{\omega_{kg} + \omega} \right). \quad (\text{A1.7}) \end{aligned}$$

Note that $\omega_{fk} + \omega_{kg} = \omega_{fg}$, for every k . To get a more manageable expression after the integration, it is now necessary to make some approximations. The primitive function (with respect to t) to each of the terms inside the parentheses in equation (A1.7) contains a ratio, which denominator is the product of the corresponding denominator in (A1.7) and the corresponding exponential frequency factor (neglecting the imaginary constant). By taking the summation over k of every such integrated term, one sees that the completely dominating terms in every of these summations, as well as in the total sum, would be those with two very small factors in the denominator. As a consequence of the assumption that no single-photon excitations are allowed, the angular frequency ω_{kg} is never really close to ω . For the same reason the value of ω_{fk} is never especially near ω . The difference $(\omega_{fg} - 2\omega)$ is always close to zero, and $(\omega_{kg} - \omega)$ is much smaller than $(\omega_{kg} + \omega)$ for some k , and smaller for all. Hence, in this rough approximate derivation, the first term inside the parentheses of equation (A1.7) will be considered to dominate

the integrated expression. Ignoring the rest of the terms and performing the integration yields the following:

$$c_f^{(2)}(t) \approx \frac{1}{4\hbar^2} \sum_k \langle f | \mathcal{D}' | k \rangle \langle k | \mathcal{D}' | g \rangle \frac{e^{i(\omega_{fg}-2\omega)t} - 1}{(\omega_{fg} - 2\omega)(\omega_{kg} - \omega)}, \quad (\text{A1.8})$$

where the initial value been applied for finding the integration constant. We have finally found an expression for the second-ordered amplitude term of the final state!

The probability of finding the system in the final state after a time t is thus the absolute value of the amplitude squared. But because there is a “semi-continuum” of close laying energy eigenstates, rather than *one* highly localised discrete state the *total* transition probability is reached when integrating the squared amplitude over the vicinity of twice the photon energy above the ground state. In terms of the density of states, the total probability for a two-photon absorption to have taken place is:

$$P_{\text{TPA}}(t) \approx \int |c_f^{(2)}(t)|^2 \rho(E_{fg}) dE_{fg} \quad (\text{A1.9})$$

Note that this of course says nothing about later deexcitation. To proceed, first observe that

$$\begin{aligned} |e^{i(\omega_{fg}-2\omega)t} - 1|^2 &= (e^{i(\omega_{fg}-2\omega)t} - 1)(e^{-i(\omega_{fg}-2\omega)t} - 1) = 2 - (e^{-i(\omega_{fg}-2\omega)t} + e^{i(\omega_{fg}-2\omega)t}) = \\ &= 2(1 - \cos(\omega_{fg} - 2\omega)t) = 4 \sin^2 \frac{(\omega_{fg} - 2\omega)t}{2} \quad \Rightarrow \quad \uparrow \\ & \quad \text{equation (A1.8)} \end{aligned} \quad (\text{A1.10})$$

$$\begin{aligned} |c_f^{(2)}(t)|^2 &\approx \frac{1}{4} \frac{\sin^2 \frac{(\omega_{fg} - 2\omega)t}{2}}{(\hbar\omega_{fg} - 2\hbar\omega)^2} \left| \sum_k \frac{\langle f | \mathcal{D}' | k \rangle \langle k | \mathcal{D}' | g \rangle}{(\hbar\omega_{kg} - \hbar\omega)} \right|^2 = \\ &= \frac{1}{4} \frac{\sin^2 \frac{(E_{fg} - 2E)t}{2\hbar}}{(E_{fg} - 2E)^2} \left| \sum_k \frac{\langle f | \mathcal{D}' | k \rangle \langle k | \mathcal{D}' | g \rangle}{(E_{kg} - E)} \right|^2. \end{aligned} \quad (\text{A1.11})$$

For times much longer than the width of the density of state*, one can approximate t as infinite. Then rewriting the “sinus-factor” in (A1.11) as

$$\frac{\sin^2 \frac{(E_{fg} - 2E)t}{2\hbar}}{(E_{fg} - 2E)^2} = \frac{\pi t}{4\hbar^2} \frac{1}{\pi} \frac{\sin^2 \frac{(E_{fg} - 2E)t}{2\hbar}}{t(E_{fg} - 2E)^2}, \quad (\text{A1.12})$$

* The *full width at half maximum*, FWHM, for the natural broadening (in frequency units) of a spectroscopic transition, is given by [7] (page 171) or [10] (page 44), $\Delta\nu = 1/2\pi\tau$, where τ is the *mean lifetime* of the corresponding state. It is rather common to speak of the *width* as a time, actually referring to the mean time τ . The density of states distribution (in frequency or energy units) is very broad, and hence the thought mean time becomes very small.

and using the identity ([4, 5])

$$\lim_{t \rightarrow \infty} \frac{1}{\pi} \frac{\sin^2 tx}{tx^2} = \delta(x), \quad (\text{A1.13})$$

one has

$$\lim_{t \rightarrow \infty} \frac{1}{\pi} \frac{\sin^2 \frac{(E_{fg} - 2E)t}{2\hbar}}{(E_{fg} - 2E)^2 t} = \delta\left(\frac{E_{fg} - 2E}{2\hbar}\right) = 2\hbar \delta(E_{fg} - 2E). \quad (\text{A1.14})$$

Accordingly, combining equations (A1.11) and (A1.12), inserting the results into equations (A1.9), and finally letting t go to infinity gives

$$P_{\text{TPA}}(t) \approx \frac{\pi t}{8\hbar} \int \delta(E_{fg} - 2E) \left| \sum_k \frac{\langle f | \tilde{\mathcal{U}}' | k \rangle \langle k | \tilde{\mathcal{U}}' | g \rangle}{(E_{kg} - E)} \right|^2 \rho(E_{fg}) dE_{fg}. \quad (\text{A1.15})$$

Thanks to the Dirac delta function this integral has approximately the same value even when it is evaluated over all E_{fg} , and the result becomes*

$$P_{\text{TPA}}(t) \approx \frac{\pi t}{8\hbar} \left| \sum_k \frac{\langle f | \tilde{\mathcal{U}}' | k \rangle \langle k | \tilde{\mathcal{U}}' | g \rangle}{(E_{kg} - E)} \right|^2 \rho(E_{fg}), \quad (\text{A1.16})$$

where, for simplicity, the fact that $2E \approx E_{fg}$ has been used.

However, the total probability is not particularly interesting, but the transition probability *rate* is! That is the probability per unit time, or

$$W_{\text{TPA}} = \frac{dP_{\text{TPA}}}{dt} \approx \frac{\pi}{8\hbar} \left| \sum_k \frac{\langle f | \tilde{\mathcal{U}}' | k \rangle \langle k | \tilde{\mathcal{U}}' | g \rangle}{(E_{kg} - E)} \right|^2 \rho(E_{fg}). \quad (\text{A1.17})$$

* $\int_{-\infty}^{+\infty} \delta(x - x_0) f(x) dx = f(x_0) \Rightarrow \int_{-\infty}^{+\infty} \delta(E_{fg} - 2E) f(E_{fg}) dE_{fg} = f(2E)$

Electric dipole approximation of the Hamiltonian

We now need to find an expression for the Hamiltonian. If it is assumed that electric dipole is the main contributor to the transitions, one can write the perturbing Hamiltonian as $\tilde{\mathcal{H}}' \approx \vec{E} \cdot \vec{\mu}$. \vec{E} is the electric field of the incoming radiation, and $\vec{\mu} = -e\vec{r}$ is the electric dipole moment of the electrons (in many electron atoms one actually has to take the sum over all electrons), with origin in the nucleus for the one atom case. (Note that while dealing with quantum mechanics these quantities are of course operators rather than usual vectors!) Neglecting higher order multipoles, the \vec{E} - field (for plane waves) can be written as (e.g. [1])

$$\vec{E} = |\vec{E}| \hat{\epsilon} e^{i(\vec{k} \cdot \vec{r} - \omega t)}, \quad (\text{A1.18})$$

where $\hat{\epsilon}$ is the polarization direction vector and \vec{k} is the wave vector. For atoms with a small size compared to the wavelength of the surrounding electromagnetic field – as is the common experimental case – it is reasonable to use the *electric dipole approximation*, and approximate the exponential in equations (A1.18) to 1.

Hence the matrix elements in expression (A1.17) can be rewritten as

$$\langle f | \tilde{\mathcal{H}}' | k \rangle \langle k | \tilde{\mathcal{H}}' | g \rangle \approx \langle f | \vec{E} \cdot \vec{\mu} | k \rangle \langle k | \vec{E} \cdot \vec{\mu} | g \rangle \approx |\vec{E}|^2 e^2 \langle f | \hat{\epsilon} \cdot \vec{r} | k \rangle \langle k | \hat{\epsilon} \cdot \vec{r} | g \rangle. \quad (\text{A1.19})$$

Using the intensity (or *flux*) definition $I = c\epsilon |\vec{E}|^2$ * (for example [6], page 221; or [7], page 143), where c is the speed of light in vacuum and ϵ the electric permittivity (not to confuse with the polarization direction vector) of the medium, equations (A1.19) can instead be written in terms of the intensity. The final expression for the two-photon transition probability rate, W_{TPA} , hence becomes

$$W_{\text{TPA}} \approx \frac{\pi e^4}{8\hbar c^2 \epsilon^2} I^2 \left| \sum_k \frac{\langle f | \hat{\epsilon} \cdot \vec{r} | k \rangle \langle k | \hat{\epsilon} \cdot \vec{r} | g \rangle}{E_{kg} - E} \right|^2 \rho(E_{fg}). \quad (\text{A1.20})$$

If the energy E is substituted by $\hbar\omega$, the reduced Planck constant (\hbar) can be taken out from the last two factors of expression (A1.20). From the squared matrix summation \hbar -bar squared fall out in the denominator. Close to the final state of the transition, the density of state function, $\rho(E_{fg})$, transform like the Dirac delta function. Accordingly, $\rho(E_{fg}) = \rho(\hbar\omega_{fg}) = \rho(\omega_{fg})/\hbar$, and equation (A1.20) expressed in terms of the angular frequency, instead of energy, takes the form

$$W_{\text{TPA}} \approx \frac{\pi e^4}{8\hbar^4 c^2 \epsilon^2} I^2 \left| \sum_k \frac{\langle f | \hat{\epsilon} \cdot \vec{r} | k \rangle \langle k | \hat{\epsilon} \cdot \vec{r} | g \rangle}{\omega_{kg} - \omega} \right|^2 \rho(\omega_{fg}). \quad (\text{A1.21})$$

The density of states, $\rho(\omega_{fg})$, is nothing but just the line-shape function $g(\omega_{fg})$, or, to be more precise, $g(2\omega)$! When dealing with a single molecule, a Lorentzian line profile function should be

* This is actually the expression holding for unpolarized light, which is not really the case for laser radiation, but for our purpose in this derivation the expression is sufficiently accurate.

used; in the situation of an assembly of molecules, it is appropriate to replace it with a Gaussian one*.

As is easily seen, W_{TPA} is proportional to the intensity *squared*, as opposed to the linear dependency of ordinary single-photon absorption! It also depends on the polarization of the light.

Two-photon absorption cross section

Cross section is, loosely speaking, a measure of the probability for an event to occur. In the case of two-photon absorption the following reasoning holds. If P_{abs} is the absorbed power, V is the volume, and N_V the number of molecules per unit of volume, then is

$$\frac{P_{\text{abs}}}{V} / N_V = \frac{P_{\text{abs}}}{VN_V} = P_{\text{abs,mol}} \quad (\text{A1.22})$$

the absorbed power per molecule (on average). Instead of power it can be written in terms of energy:

$$P_{\text{abs,mol}} = \frac{E_{\text{abs,mol}}}{t} \quad (\text{A1.23})$$

However, the absorbed energy per molecule is nothing but the absorbed energy per “event”, that is $2\hbar\omega$, times the number of “events” per time, *i.e.* the transition rate W_{TPA} , hence

$$P_{\text{abs,mol}} = 2\hbar\omega W_{\text{TPA}}. \quad (\text{A1.24})$$

Now the cross section can be defined as the ratio of the absorbed power per molecule ($P_{\text{abs,mol}}$), and the incident *flux*** , I (or intensity in this case):

$$\sigma_{\text{TPA}} = \frac{2\hbar\omega W_{\text{TPA}}}{I} \quad (\text{A1.25})$$

Together with equations (A1.21) (and the sentence following the same), we have

$$\sigma_{\text{TPA}} \approx \frac{\pi e^4}{4\hbar^3 c^2 \epsilon^2} g(2\omega) \left| \sum_k \frac{\langle f | \hat{\epsilon} \cdot \vec{r} | k \rangle \langle k | \hat{\epsilon} \cdot \vec{r} | g \rangle}{\omega_{kg} - \omega} \right|^2 \omega I. \quad (\text{A1.26})$$

Hence the absorption cross section (of course assuming no saturation effects) is *proportional* to the intensity, but also to the frequency! It also depends on the polarization. In practise it is inconvenient to work with a cross section dependent on the intensity. Therefore it is common to define the *two-photon cross section* δ . This quantity is defined by the ratio of σ_{TPA} in expression (A1.26), and the photon flux, expressed as the number of photons (the symbol “#” means “the number of”) per unit area and unit time:

* For a sample of molecules, a dependency on the molecular velocity can also be seen [1, 11]. If the wave vectors of the two light waves, in a two-photon excitation like that, are opposite but equal in length, the line profile becomes pure Lorentzian and one can obtain so called *Doppler-free two-photon spectroscopy*.

** The general definition of *flux* is $I = \frac{P}{A}$, where A is the area of the incident surface (*e.g.* [7]).

$$\delta \equiv \sigma_{\text{TPA}} \left/ \frac{\# \text{ photons}}{At} \right. = \frac{At\sigma_{\text{TPA}}}{\# \text{ photons}} = \frac{At\sigma_{\text{TPA}}}{E/\hbar\omega} = \frac{\hbar\omega At\sigma_{\text{TPA}}}{E} = \frac{\hbar\omega\sigma_{\text{TPA}}}{I} \approx$$

$$\approx \frac{\pi e^4}{4\hbar^2 c^2 \epsilon^2} \omega^2 g(2\omega) \left| \sum_k \frac{\langle f | \hat{\epsilon} \cdot \vec{r} | k \rangle \langle k | \hat{\epsilon} \cdot \vec{r} | g \rangle}{\omega_{kg} - \omega} \right|^2 \quad (\text{A1.27})$$

The dimension of δ is *area times time times area squared*, and is usually expressed in $\text{cm}^4\text{s}/(\text{number of photons})$.

Some discussion about two-photon absorption of scattered photons

The expressions for the two-photon transition probability rate (A1.21) and the absorption cross section (A1.26), derived above, are derived for the case of simultaneous absorption of two photons with the same (linear) polarization direction. Now, suppose two scattered photons (still with the same frequency) reaches the atom. Because they scattered, they (probably) have different directions of their polarization and propagation vectors. This can be taken into account for, if first writing the interaction Hamiltonian, \mathcal{H}' , in (A1.3) as

$$\mathcal{H}' = \tilde{\mathcal{H}}' \cos\omega t = (\tilde{\mathcal{H}}'_1 + \tilde{\mathcal{H}}'_2) \cos\omega t. \quad (\text{A1.28})$$

The two Hamiltonians represents two (possibly) different electromagnetic fields. Then modifying (A1.18) in the following way

$$\begin{cases} \vec{E}_1 = |\vec{E}_1| \hat{\epsilon}_1 e^{i(\vec{k}_1 \cdot \vec{r} - \omega t)} \\ \vec{E}_2 = |\vec{E}_2| \hat{\epsilon}_2 e^{i(\vec{k}_2 \cdot \vec{r} - \omega t)} \end{cases}, \quad (\text{A1.29})$$

where the two electric fields corresponds to the two Hamiltonians in expression (A1.28), respectively, a more general two-photon transition probability rate can be derived. The calculations are straight forward, as above, and the final result for the two-photon transition probability rate becomes

$$W_{\text{TPA}} \approx \frac{\pi e^4}{8\hbar^2 c^2 \epsilon^2} g(2\omega) \left| \sum_k \frac{\langle f | \hat{\epsilon}_1 \cdot \vec{r} | k \rangle \langle k | \hat{\epsilon}_2 \cdot \vec{r} | g \rangle + \langle f | \hat{\epsilon}_2 \cdot \vec{r} | k \rangle \langle k | \hat{\epsilon}_1 \cdot \vec{r} | g \rangle}{E_{kg} - E} \right|^2 I_1 I_2, \quad (\text{A1.30})$$

where I_1 and I_2 represents the intensities of the two electric fields, respectively.

Let us take a closer look at the matrix summation in (A1.30). Replacing the energy difference E_{kg} in the denominator, with some kind of mean value E_m , the whole denominator can be put outside the summation. A quantitative value of E_m is of no great importance; it is enough to conclude that $(E_m - E)$ should be of the same order, or at least an order close to that of $(E_{fg} - E)$. Thanks to this manoeuvre it becomes possible to use the closure condition, and simplify the expression:

$$\left| \sum_k \frac{\langle f | \hat{\epsilon}_1 \cdot \vec{r} | k \rangle \langle k | \hat{\epsilon}_2 \cdot \vec{r} | g \rangle + \langle f | \hat{\epsilon}_2 \cdot \vec{r} | k \rangle \langle k | \hat{\epsilon}_1 \cdot \vec{r} | g \rangle}{E_{kg} - E} \right|^2 \approx$$

$$\begin{aligned}
&\approx \frac{1}{(E_m - E)^2} \left| \sum_k (\langle f | \hat{\epsilon}_1 \cdot \vec{r} | k \rangle \langle k | \hat{\epsilon}_2 \cdot \vec{r} | g \rangle + \langle f | \hat{\epsilon}_2 \cdot \vec{r} | k \rangle \langle k | \hat{\epsilon}_1 \cdot \vec{r} | g \rangle) \right|^2 = \\
&= \frac{1}{(E_m - E)^2} \left| \sum_k \langle f | \hat{\epsilon}_1 \cdot \vec{r} | k \rangle \langle k | \hat{\epsilon}_2 \cdot \vec{r} | g \rangle + \sum_k \langle f | \hat{\epsilon}_2 \cdot \vec{r} | k \rangle \langle k | \hat{\epsilon}_1 \cdot \vec{r} | g \rangle \right|^2 = \\
&= \frac{1}{(E_m - E)^2} \left| \langle f | (\hat{\epsilon}_1 \cdot \vec{r})(\hat{\epsilon}_2 \cdot \vec{r}) | g \rangle + \langle f | (\hat{\epsilon}_2 \cdot \vec{r})(\hat{\epsilon}_1 \cdot \vec{r}) | g \rangle \right|^2 = \\
&= \frac{4}{(E_m - E)^2} \left| \langle f | (\hat{\epsilon}_1 \cdot \vec{r})(\hat{\epsilon}_2 \cdot \vec{r}) | g \rangle \right|^2 \tag{A1.31}
\end{aligned}$$

Converting the matrix expression in (A1.31), from Dirac notation, to wave function notation, one finds

$$\frac{4}{(E_m - E)^2} \left| \int \Psi_f^*(\hat{\epsilon}_1 \cdot \vec{r})(\hat{\epsilon}_2 \cdot \vec{r}) \Psi_g d^3\vec{r} \right|^2. \tag{A1.32}$$

Hence (A1.30) can be written as

$$W_{\text{TPA}} \approx \frac{\pi e^4}{2\hbar^2 c^2 \epsilon^2} g(2\omega) \left| \int \Psi_f^*(\hat{\epsilon}_1 \cdot \vec{r})(\hat{\epsilon}_2 \cdot \vec{r}) \Psi_g d^3\vec{r} \right|^2 \frac{I_1 I_2}{(E_m - E)^2}, \tag{A1.33}$$

and one sees that the two-photon absorption rate, W_{TPA} , to a rough approximation, follows a proportionality condition:

$$W_{\text{TPA}} \propto I_1 I_2 \left| \int \Psi_f^*(\hat{\epsilon}_1 \cdot \vec{r})(\hat{\epsilon}_2 \cdot \vec{r}) \Psi_g d^3\vec{r} \right|^2 \tag{A1.34}$$

Apparently, it is necessary to know the wave functions of the ground state and the final state, in order to explicitly calculate the polarization dependency of the TPA transition rate. This is of course impossible for complex molecules. However, in a try to get a sense of how it might look, the easiest possible example can be analysed, that of a hydrogenic atom/ion. Imagine a two-photon electric dipole transition, for simplicity assuming only linearly polarized light to be involved, from the ground state of a hydrogen atom, to the first higher state fulfilling the selection rules for such excitation. That is a transition from the state denoted by $\{n, l, m_l\} = \{1, 0, 0\}$, to the state $\{2, 0, 0\}$. Calculating the integral expression in (A1.34) for the corresponding wave functions leads to:

$$\left| \int \Psi_f^*(\hat{\epsilon}_1 \cdot \vec{r})(\hat{\epsilon}_2 \cdot \vec{r}) \Psi_g d^3\vec{r} \right|^2 = a_0^4 |(-C)\hat{\epsilon}_1 \cdot \hat{\epsilon}_2|^2 = a_0^4 C^2 \cos^2 \theta_{1,2}, \tag{A1.35}$$

where a_0 is the Bohr radius, C a numerical constant with a value of approximately 0.99, and $\theta_{1,2}$ the angle between the polarization directions of the two photons. One reason to the very simplicity of equation (A1.35), is that the hydrogenic wave function of states with the azimuthal quantum number, l , equal to zero, is angularly independent (the spherical harmonics are constant).

Instead calculating the integral in equation (A1.33), for a transition from $\{1, 0, 0\}$ to $\{3, 2, 0\}$ provides:

$$\left| \int \Psi_f^*(\hat{\varepsilon}_1 \cdot \vec{r})(\hat{\varepsilon}_2 \cdot \vec{r}) \Psi_g d^3\vec{r} \right|^2 = a_0^4 \left| (-\tilde{C})(\hat{\varepsilon}_1 \cdot \hat{\varepsilon}_2 + \varepsilon_1^{(z)} \varepsilon_2^{(z)}) \right|^2 = a_0^4 \tilde{C}^2 (\cos\theta_{1,2} + \varepsilon_1^{(z)} \varepsilon_2^{(z)})^2 \quad (\text{A1.36})$$

Here \tilde{C} is a constant with a numerical value of approximately 0.26, and $\varepsilon_1^{(z)}$ and $\varepsilon_2^{(z)}$ are the “z-coordinates” of $\hat{\varepsilon}_1$ and $\hat{\varepsilon}_2$, respectively. As one sees, the expression becomes more complicated.

The interesting thing is, however, the term $\cos^2\theta_{1,2}$ showing up again. Therefore one could guess that this is a common feature, and that it always is possible to write the integral-expression (actually its absolute value squared) involving the polarization dependency, in the form of a second-degree cosine polynomial:

$$C_2 \cos^2\theta_{1,2} + C_1 \cos\theta_{1,2} + C_0, \quad (\text{A1.37})$$

where the constants C_i depends on the specific molecular state, but also on the polarization correspondence.

Changing over to cross section again, when there are two electric fields, some modifications are needed. In the second footnote on page A1-6, the flux was defined as $I = P/A$ (where P is power and A area). Introducing n_1 and n_2 as the *number of photons* of the (possibly) different polarizations, respectively, the total flux can be written as

$$I = \frac{P}{A} = \frac{E}{tA} = \frac{\hbar\omega n_1 + \hbar\omega n_2}{tA} = \frac{\hbar\omega n_1}{tA} + \frac{\hbar\omega n_2}{tA} = \frac{E_1}{tA} + \frac{E_2}{tA} = I_1 + I_2. \quad (\text{A1.38})$$

This implies that I should be replaced by $I_1 + I_2$ in (A1.25).

If supposing the guess preceding (A1.37) is true, the expression for the cross section now will take the form (use (A1.25), (A1.33), (A1.37) and (A1.38))

$$\begin{aligned} \sigma_{\text{TPA}} &\approx \frac{\pi e^4}{\hbar^3 c^2 \varepsilon^2} g(2\omega) \frac{\omega}{(\omega_m - \omega)^2} \frac{I_1 I_2}{I_1 + I_2} (C_2 \cos^2\theta_{1,2} + C_1 \cos\theta_{1,2} + C_0) \propto \\ &\propto \frac{I_1 I_2}{I_1 + I_2} (C_2 \cos^2\theta_{1,2} + C_1 \cos\theta_{1,2} + C_0) \propto C_0 + C_1 \cos\theta_{1,2} + C_2 \cos^2\theta_{1,2}. \quad (\text{A1.39}) \end{aligned}$$

In fact, in the late 1960's, Monson and McClain showed that in a sample of randomly oriented molecules, as is the case in a gas or a liquid, the *averaged* mean value of the cross section (the polarization dependency regarded) for an absorption of two linearly polarized photons, had the form

$$\langle \sigma_{\text{TPA}} \rangle = A + B \cos^2\theta_{1,2}, \quad (\text{A1.40})$$

where A and B are constants depending on molecular parameters [8] ([9] gives further generalisations). A has the property of always being positive. B can be either positive or negative, but if negative, it always holds that $A \geq |B|$, or in other words, $A + B$ is always positive. The conclusion of this is that if the constant A dominates over B , then the effect of different polarization directions can be ignored.

Very brief about the situation of more than two different fields

Assume there are three or more different fields, which can cooperate to induce a two-photon transition. If so, every pair-combination of the fields is capable to combine to an absorption event. In this case one has to calculate the transition probability rate for every pair-combination, and then use that to determine the cross section for just this combination of fields. After doing that, it is no more complicated than taking the arithmetic mean value of all these “partial cross sections”, in order to find the total average one. If i and k are index labels corresponding to the different fields, and n is the number of fields, then the total *mean cross section* becomes

$$\sigma_{\text{TPA};\text{tot}} = \frac{\sum_{k \neq i} \sigma_{\text{TPA};i,k}}{\binom{n}{2}} = \frac{2}{n(n-1)} \sum_{k \neq i} \sigma_{\text{TPA};i,k} . \quad (\text{A1.41})$$

References

1. W.K. Bischel, P.J. Kelly and C.K. Rhodes, High-resolution Doppler-free two-photon spectroscopic studies of molecules. I. The ν_3 bands of $^{12}\text{CH}_3\text{F}$, *Phys. Rev. A* **13**, 1817-1828 (1976).
2. M. Göppert-Mayer, Über Elementarakte mit zwei Quantensprüngen, *Annalen der Physik* **9**, 273-294 (1931).
3. V.I. Bredikhin, M.D. Galanin and V.N. Genkin, Two-photon absorption and spectroscopy, *Sov. Phys. Usp* **16**, 299-321 (1973).
4. J.J. Sakurai, *Modern Quantum Mechanics*, (Addison-Wesley, 1995).
5. O. Svelto, *Principles of Lasers*, (Plenum, 1998).
6. H.-U. Bengtsson, *Bengtsson om klassisk fysik*, (Gleerups, 1995). Swedish.
7. A.P. Thorne, U. Litzén and S. Johansson, *Spectrophysics – Principles and Applications*, (1997).
8. P.R. Monson and W.M. McClain, Polarization dependence of the two-photon absorption of tumbling molecules with application to liquid 1-chloronaphthalene and benzene, *The Journal of Chemical Physics* **53**, 29-37 (1970).
9. W.M. McClain, Excited state symmetry assignment through polarized two-photon absorption studies of fluids, *The Journal of Chemical Physics* **55**, 2789-2796 (1970).
10. S. Svanberg, *Atomic and Molecular Spectroscopy – Basic Aspects and Practical Applications*, (Springer Verlag, Heidelberg, Germany, 2001).
11. W. Demtröder, *Laser Spectroscopy*, (Springer-Verlag, 1981).

Appendix 2 – Tissue optics

Tissue optics describes the light propagation in tissue. When light propagates through tissue, it can be either scattered or absorbed. These interactions are strongly wavelength dependent.

Absorption

The light absorption in tissue depends on the absorption spectra of the molecules present and is thus very wavelength dependent. Molecules, absorbing light (especially in the visible region) are called chromophores. The most important tissue chromophores, in the visible and near-infrared wavelength regions, are haemoglobin and water. Another important chromophore is melanin, small pigments in skin and eye. The absorption of melanin decreases monotonically with increasing wavelength.

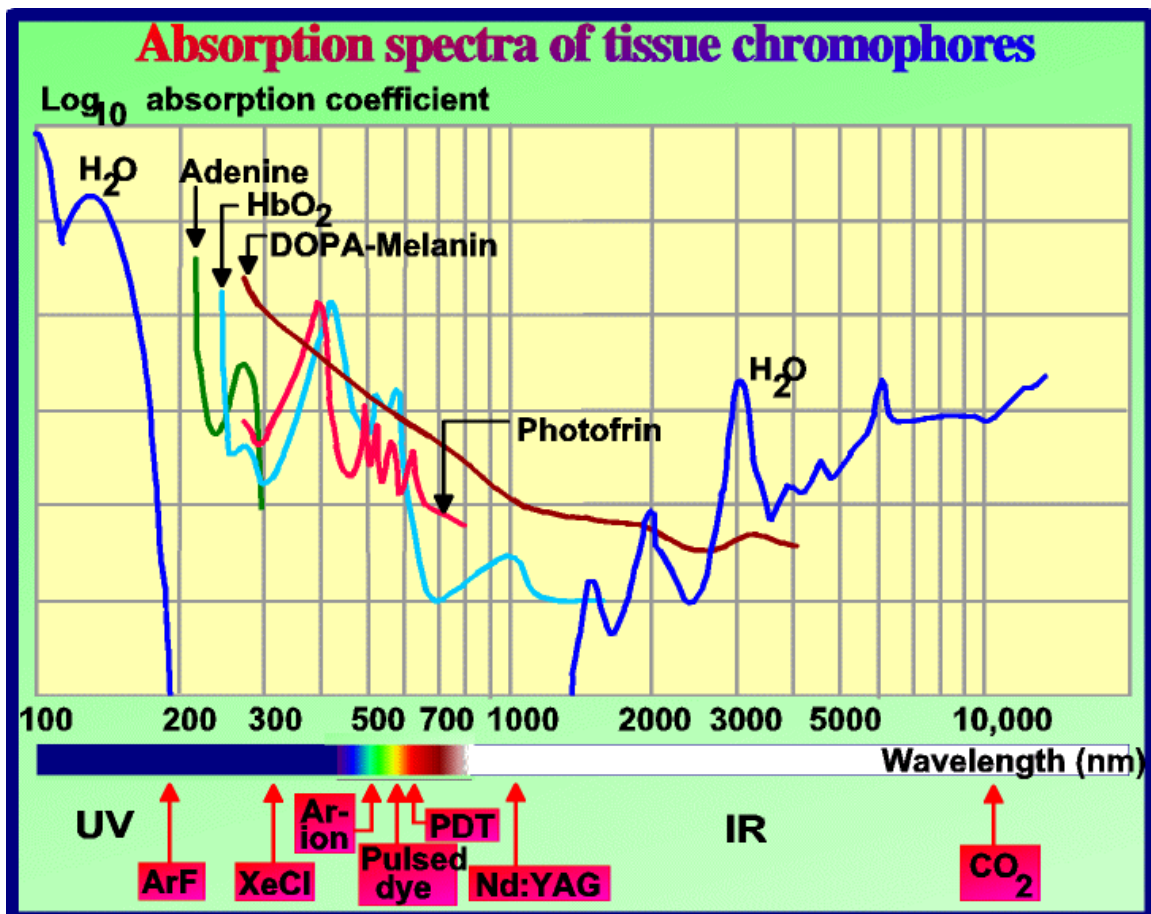


Figure A2.1 Absorption spectra of tissue chromophores.

A typical absorption spectrum of tissue is shown in figure A2.1. The absorption coefficient drops by almost two orders of magnitude when it goes from 400 nm to 700 nm. The region between 700 nm and 1300 nm is known as the optical window of tissue, due to the low absorption.

In order to describe the tissue absorption the absorption coefficient, μ_a , is used, which is defined as the probability for absorption per unit length. The light absorbed by the tissue can induce a temperature increase, or re-emitted as fluorescence, or contribute to photochemical reactions.

Scattering

There are two main groups of scattering processes; elastic and inelastic processes. For photon energies from UV to NIR, elastic scattering is strongly dominating. The elastic scattering, by particles with a size much smaller than the wavelength of the light, is called Rayleigh scattering. Interactions with larger particles are described by Mie theory. For both types of interactions, the scattering has a strong wavelength dependence, which varies as λ^{-4} for Rayleigh events and approximately as λ^{-2} for larger particles. Consequently, blue light is more scattered than red light.

Scattering is also described by the probability of a scattering event per unit length. The sum of the absorption coefficient and the scattering coefficient (μ_s) yields the total attenuation coefficient (μ_t), which describe the probability of all light-tissue interactions per unit path length of a propagating photon:

$$\mu_t = \mu_a + \mu_s \quad (\text{A2.1})$$

The scattering angle from a single scattering event has a probability distribution or phase function described by the anisotropy factor, g . The value of g is equal to the expectation value of $\langle \cos \theta \rangle$, where θ is the scattering angle, ranges from -1 to $+1$. The value -1 and $+1$ corresponds to total backscattering and total forward scattering, respectively. Isotropic scattering is represented by $g = 0$. Tissue is strongly forward scattering with g -values between 0.7 and 0.95 [1].

In the therapeutic window, the light distribution in tissue is often modeled by using the reduced scattering coefficient, μ'_s ,

$$\mu'_s = (1 - g)\mu_s. \quad (\text{A2.2})$$

This coefficient describes the inverse of the average distance a photon travels before the scattering can be regarded as isotropic. Then, the effective mean free path between interaction events in a strongly scattering media is described by the inverse of the linear transport coefficient

$$\mu_{tr} = \mu_a + (1 - g)\mu_s = \mu_a + \mu'_s. \quad (\text{A2.3})$$

Typical values of the optical properties for tissues in the therapeutic window are [2]:

$$\begin{aligned} g &= 0.8 - 0.95 \\ \mu_a &= 50 - 150 / \text{cm} \quad (\text{at } 800 \text{ nm}) \\ \mu_s &= 0.05 / \text{cm} \quad (\text{at } 800 \text{ nm}) \end{aligned}$$

References

1. W.-F. Cheong, Summary of optical properties, in *Optical-Thermal Response of Laser-Irradiated Tissue*, eds. A.J. Welch and M.J.C. van Gemert, pp. 275-303 (Plenum Press, New York, 1995).
2. A. Dunn, V.P. Wallace, M.L. Coleno, P.T.C. So and B. Tromberg, Study of the spatial point spread function with depth in two-photon microscopy, in *Three-dimensional and multidimensional microscopy: Image acquisition and processing VI*, Proc. SPIE vol. **3605**, 112-119 (2001).

Appendix 3 – Spectra of Rhodamine B

Shown below are the single-photon absorption spectrum and fluorescence spectrum, of the fluorophore Rhodamine B [1], used as dye in the experiments described above.

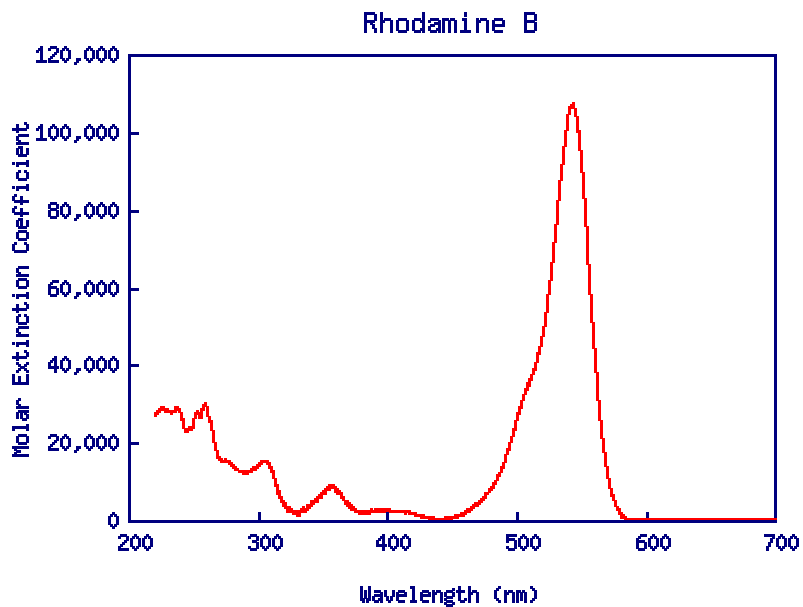


Figure A3.1 The single-photon absorption spectrum of Rhodamine B (solved in ethanol; concentration unknown). Note that the relative (one-photon) absorption is, in fact, low around 400 nm (*i.e.* half the wavelength of two-photon excitation wavelengths) compared to the absorption peak at 543 nm.

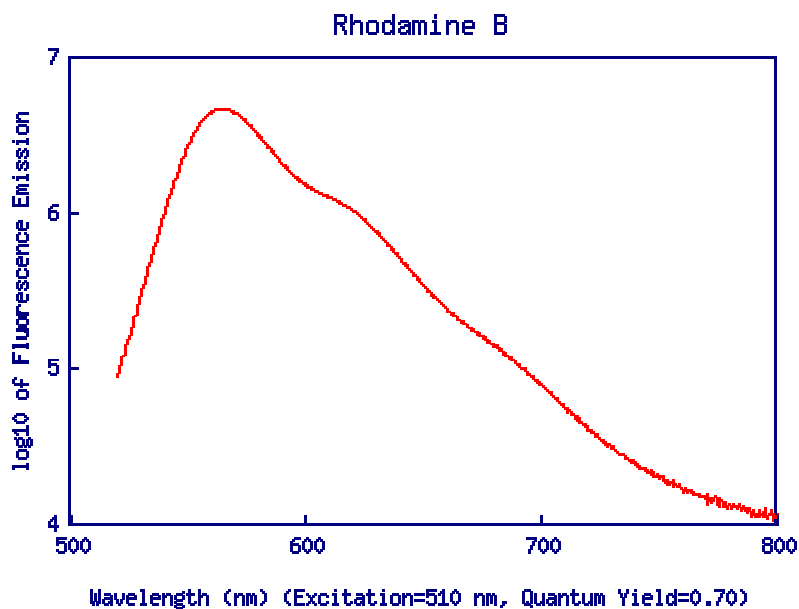


Figure A3.2 Fluorescence spectrum of Rhodamine B (in ethanol; concentration unknown). The emission peak is located around 580 nm.

Shown below is the fluorescence spectrum originating from two-photon excitation in a solution of Rhodamine B in a mixture of ethanol and distilled water (approximately 30% ethanol and 70% water). The spectrum has been measured with a spectrometer and a CCD camera. As for one-photon excitation mode (figure A3.2 above), the fluorescence peak at 580 nm is obvious. However, the width of the peak is more narrow than the one in figure A3.2, which shows fluorescence following one-photon excitation.

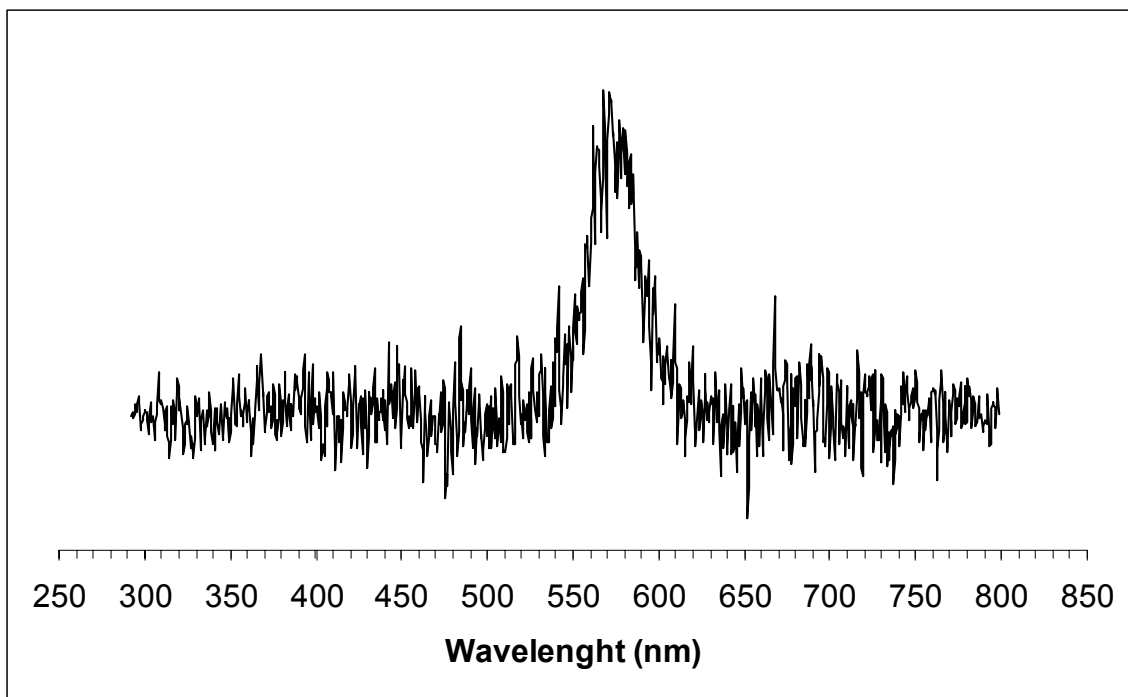


Figure A3.3 Measured fluorescence spectrum originating from two-photon excitation of Rhodamine B solution (unknown concentration). An isolated peak is seen around 580 nm.

References

1. Rhodamine B. <http://omlc.org/spectra/PhotochemCAD/html/rhodamineB.html> (2001).

Appendix 4 – Basics of Monte Carlo simulations

Monte Carlo (MC) simulation is a frequently used technique to describe photon propagation in tissue. The simulation is based on random walk of photons in an absorbing and scattering medium. Each photon that is injected into the tissue is traced through all its scattering events until it exits the tissue or is terminated through absorption. Physical parameters, such as time-of-flight, path, and absorption position can be logged during the simulation. A large number of photons then give a statistical distribution of the parameters studied. The advantages of the simulation are that there are no limitations in tissue geometry or homogeneity and that the diffusion theory does not have to be valid. The main drawback is that long computation time is needed, especially for high scattering or absorption, and for long distances.

A Monte Carlo code made by Wang and Jacques [1], that treats the steady state case for a multi-layered medium can be found on a public computer domain.

References

1. L. Wang and S.L. Jacques, Monte Carlo modeling of light transport in multi-layered tissues in standard C, (Laser Biology Research Laboratory, M. D. Anderson Cancer Center, University of Texas, Houston, Texas 1992).

